

# Pacific Northwest National Laboratory

Operated by Battelle for the  
U.S. Department of Energy

## Retrieval Process Development and Enhancements Waste Simulant Compositions and Defensibility

M. R. Powell  
G. R. Golcar  
J. G. H. Geeting

RECEIVED  
NOV 10 1997  
OSTI

September 1997

Prepared for the U. S. Department of Energy  
under Contract DE-AC06-76RLO 1830

## DISCLAIMER

This report was prepared as an account of work sponsored by an agency of the United States Government. Neither the United States Government nor any agency thereof, nor Battelle Memorial Institute, nor any of their employees, makes any warranty, expressed or implied, or assumes any legal liability or responsibility for the accuracy, completeness, or usefulness of any information, apparatus, product, or process disclosed, or represents that its use would not infringe privately owned rights. Reference herein to any specific commercial product, process, or service by trade name, trademark, manufacturer, or otherwise does not necessarily constitute or imply its endorsement, recommendation, or favoring by the United States Government or any agency thereof, or Battelle Memorial Institute. The views and opinions of authors expressed herein do not necessarily state or reflect those of the United States Government or any agency thereof.

PACIFIC NORTHWEST NATIONAL LABORATORY  
*operated by*  
BATTELLE  
*for the*  
UNITED STATES DEPARTMENT OF ENERGY  
*under Contract DE-AC06-76RLO 1830*

Printed in the United States of America

Available to DOE and DOE contractors from the  
Office of Scientific and Technical Information, P.O. Box 62, Oak Ridge, TN 37831;  
prices available from (615) 576-8401.

Available to the public from the National Technical Information Service,  
U.S. Department of Commerce, 5285 Port Royal Rd., Springfield, VA 22161



This document was printed on recycled paper.

PNNL-11685  
UC-721

**Retrieval Process Development and Enhancements  
Waste Simulant Compositions and Defensibility**

M. R. Powell  
G. R. Golcar  
J.G.H. Geeting

September 1997

DISTRIBUTION OF THIS DOCUMENT IS UNLIMITED 

Prepared for the U.S. Department of Energy  
under Contract DE-AC06-76RLO 1830

**MASTER**

Pacific Northwest National Laboratory  
Richland, Washington 99352

**DISCLAIMER**

**Portions of this document may be illegible  
in electronic image products. Images are  
produced from the best available original  
document.**

## Summary

The purpose of this report is to document the physical waste simulant development efforts of the EM-50 Tanks Focus Area at the Hanford Site. Waste simulants are used in the testing and development of waste treatment and handling processes because performing such tests using actual tank waste is hazardous and prohibitively expensive. This document addresses the simulant development work that supports the testing of waste retrieval processes using simulants that mimic certain key physical properties of the tank waste. Development and testing of chemical simulants are described elsewhere (Elmore et al. 1992; LaFemina 1995).

This work was funded through the EM-50 Tanks Focus Area as part of the Retrieval Process Development and Enhancements (RPD&E) Project at the Pacific Northwest National Laboratory (PNNL). The mission of RPD&E is to understand retrieval processes, including emerging and existing processes, gather performance data on those processes, and relate the data to specific tank problems to provide end users with the requisite technical bases to make retrieval and closure decisions.

Physical simulants are prepared using relatively nonhazardous and inexpensive materials rather than the chemicals known to be in tank waste. Consequently, only some of the waste properties are matched by the simulant. Deciding which properties need to be matched and which do not requires a detailed knowledge of the physics of the process to be tested using the simulant. Developing this knowledge requires reviews of available literature, consultation with experts, and parametric tests. Once the relevant properties are identified, waste characterization data are reviewed to establish the target ranges for each property. Simulants are then developed that possess the desired ranges of properties.

Because simulants are designed with a specific retrieval process in mind, a simulant that is appropriate for testing one process might be inappropriate for another. For example, hard saltcake simulants prepared from potassium-magnesium sulfate were designed specifically for the testing of high-pressure waterjet scarifiers (Hatchell et al. 1996). The mechanical strength and porosity of this simulant can be related to waste characterization data. Other properties such as dissolution rate, solubility, and thermal conductivity were judged to be irrelevant and were not matched, so it is inappropriate to use the potassium-magnesium sulfate simulants to test processes for which these other properties are relevant.

Compromises are often required to develop simulant compositions used for testing. Not all the relevant physical and chemical property measurements have been made on waste samples, so estimates and assumptions must sometimes be made. Where possible, these assumptions are made conservatively so that process testing is more likely to result in over-designed than under-designed equipment. The need to test at large scale often requires that large quantities (tons) of simulants be prepared. In such cases it is often required that nonhazardous, nonregulated materials be used to protect personnel and meet cost constraints.

Simulants for tank waste sludge, hardpan, saltcake, supernate, and slurry have been developed and used for testing. The compositions and properties of many of these simulants are given in this document along with preparation instructions for each. Where the relevant waste characterization data are available, a comparison between the waste and the simulants is also provided. It is hoped that future testing and simulant development efforts at all the Department of Energy waste sites can benefit from the compilation of these data.

In addition to the simulant composition and property data, two simulant testing programs are described. First, a variety of hard saltcake simulants were subjected to the cutting action of high-pressure waterjets. Correlations between the saltcake simulant properties and the depth of waterjet cut were developed. These data are used to help identify the relevant physical properties for the design of hard saltcake simulants for the testing of high-pressure waterjet-based retrieval processes. Second, the dissolution rates of several different salt species were measured. These tests provide a defensible basis for the development of soluble saltcake simulants. By adjusting the solvent concentration, the dissolution rate for a nonhazardous saltcake simulant (e.g., sodium chloride) can be made to approximate that of a hazardous saltcake (e.g., sodium nitrate and nitrite). The correlations for saltcake cutting and the salt dissolution data are given in this report.

# Contents

Summary .....	iii
Nomenclature .....	x
1.0 Introduction .....	1.1
1.1 Chemical versus Physical Simulants .....	1.1
1.2 Simulant Development Strategy .....	1.1
1.3 Purpose of Document .....	1.4
2.0 Simulant Descriptions .....	2.1
2.1 Sludge Simulants .....	2.1
2.1.1 Relevant Properties for Sludge Retrieval .....	2.1
2.1.2 Kaolin Clay Simulants .....	2.4
2.1.3 Bentonite Clay in Water .....	2.12
2.1.4 Bentonite/BaSO <sub>4</sub> Sludge Simulants .....	2.15
2.1.5 Kaolin/Bentonite Sludge Simulants .....	2.15
2.1.6 Kaolin/Plaster Sludge Simulants .....	2.16
2.1.7 Kaolin/Ludox® Sludge Simulants .....	2.19
2.1.8 Silica/Soda Ash Sludge Simulants .....	2.22
2.2 Hardpan Waste Simulants .....	2.26
2.2.1 Relevant Properties for Hardpan/Dried Sludge .....	2.26
2.2.2 Hardpan Simulant and Waste Property Comparison .....	2.26
2.2.3. Kaolin/Plaster Hardpan Simulants .....	2.30
2.3 Saltcake Waste Simulants .....	2.32
2.3.1 Relevant Properties for Saltcake Retrieval .....	2.32
2.3.2 Saltcake Simulant and Waste Property Comparison .....	2.33
2.3.3 Hard Saltcake Simulants (K-Mag) .....	2.37
2.3.4 Soft Saltcake Simulants .....	2.40
2.4 Supernatant Liquid and Slurry Simulants .....	2.40
2.5 Miscellaneous Waste Simulants .....	2.42
2.5.1 ORNL Tank Gunite Simulant .....	2.42
2.5.2 Savannah River Site Tank 19 Zeolite Heel Simulant .....	2.43
2.5.3 Tar-Like Substance Simulant Development for INEEL End-Effector Testing .....	2.46
3.0 Simulant Preparation and Characterization .....	3.1
3.1 Simulant Preparation Procedures .....	3.1
3.1.1 Insensitive Simulants .....	3.1
3.1.2 Sensitive Simulants .....	3.3
3.2 Characterization Procedures .....	3.3
3.2.1 Shear Strength .....	3.3
3.2.2 Compressive Strength .....	3.5
3.2.3 Tensile Strength .....	3.5

3.2.4 Simulant Material Suppliers .....	3.11
4.0 Hard Saltcake Waterjet Cutting Tests .....	4.1
4.1 Introduction .....	4.1
4.2 Background .....	4.1
4.3 Experimental Design .....	4.2
4.4 Saltcake Sensitivity Testing Results and Analysis .....	4.8
4.5 Conclusions .....	4.19
5.0 Salt Crystal Dissolution Studies .....	5.1
5.1 Background .....	5.1
5.2 Experimental Apparatus .....	5.5
5.3 Assumptions and Approximations .....	5.5
5.4 Results .....	5.5
5.4.1 Evaluation of Rate Controlling Step .....	5.5
5.4.2 Evaluation of Rate Constant and Mass Transfer Coefficient .....	5.6
5.4.3 Least Squares Regression of Data from Central Composite Design .....	5.11
5.4.4 Temperature Effects .....	5.11
5.5 Application of Results .....	5.16
6.0 Conclusions .....	6.1
7.0 References .....	7.1
Appendix A: Development of a Simulant for SRS Tank 19 Zeolite Heel .....	A.1
A.1 Summary .....	A.1
A.2 Discussion .....	A.2
A.3 References .....	A.10

## Figures

1.1. Simulant Development Strategy Logic Diagram .....	1.3
2.1. Waterjet Pressure Required for Sluicing vs. Shear Strength .....	2.3
2.2. Particle Size Distribution for NCAW Core Sample #2 .....	2.5
2.3. Particle Size Distribution for Kaolin Clay .....	2.5
2.4. Plot Showing Range of Sludge Shear Strengths .....	2.7
2.5. Kaolin Shear Strength vs. wt% Kaolin .....	2.8
2.6. Kaolin Slurry Rheology Data .....	2.8
2.7. Split-Cell Tensile Strength vs. Shear Strength .....	2.9
2.8. Histogram of Sludge Sample Densities .....	2.11
2.9. Bentonite Shear Strength vs. wt% Bentonite .....	2.13
2.10. Particle Size Distribution for Bentonite Clay .....	2.14
2.11. Strength Gain over Time as a Function of Ludox Content .....	2.21
2.12. Brinkmann Particle Size Distribution for Min-U-Sil® 30 Silica .....	2.23
2.13. Shear Strength vs. Temperature for Silica/Soda Ash and 101-SY Sludge .....	2.24
2.14. Silica/Soda Ash Shear Strength Development with Time .....	2.25
2.15. Photograph of Chalk Shear Strength Tester .....	2.29
2.16. Shear Strength vs. Time for 40% Plaster Hardpan Simulant .....	2.31
2.17. Hard Saltcake Simulant (K-Mag) Compressive Strengths .....	2.38
2.18. K-Mag Porosity vs. Concentration .....	2.39
2.19. K-Mag Average Pore Diameter vs. Concentration .....	2.39
2.20. Compressive Strength of Salt/Plaster Simulants .....	2.41
2.21. Microscope Photograph of Aggregate .....	2.44
2.22. Aggregate Size Distribution for ORNL Gunitite Simulants .....	2.45
2.23. Compressive Strength of ORNL Gunitite Simulant vs. Time .....	2.45
3.1. Littleford Paste Mixer at PNNL .....	3.2
3.2. Rolling-Drum Concrete Mixer .....	3.4
3.3. Haake M5 with Shear Vane .....	3.6
3.4. Compressive Strength Testing of a K-Mag Simulant .....	3.7
3.5. Sludge Tensometer .....	3.8
3.6. Sludge Sample Undergoing Vertical Extrusion Tensile Strength Test .....	3.9
3.7. Brazilian Tensile Test on a K-Mag Simulant Sample .....	3.10
4.1. Saltcake Simulant Blocks used for Waterjet Sensitivity Tests .....	4.3
4.2. Waterjet Testing of Saltcake Simulants .....	4.5
4.3. Saltcake Simulant Blocks Following Waterjet Testing .....	4.7
4.4. Side View of Waterjet Cuts in a Block of Saltcake Simulant .....	4.7
4.5. Effect of Waterjet Pressure on Depth of Cut .....	4.10
4.6. Effect of Nozzle Diameter on Depth of Cut .....	4.13
4.7. Computed $k$ Values for Simulants .....	4.16
4.8. Computed $f(x)$ Values for Each Simulant .....	4.17
4.9. Comparison of Predicted and Measured $C_d$ Values (all simulants) .....	4.18
4.10. Comparison of Predicted and Measured $C_d$ Values for $D_n^{1.5}$ .....	4.18
5.1. Mass Transfer Coefficient for a Free-Falling Particle as a Function of Particle Diameter .....	5.4
5.2. Rate Limiting Step Dependence for Dissolution of NaCl .....	5.7
5.3. Rate Limiting Step Dependence for Dissolution of $\text{Na}_2\text{CO}_3 \cdot 10\text{H}_2\text{O}$ .....	5.7

5.4. Rate Limiting Step Dependence for Dissolution of $\text{NaNO}_2$ .....	5.8
5.5. Rate Limiting Step Dependence for Dissolution of $\text{NaNO}_3$ .....	5.8
5.6. $\text{NaCl}$ Dissolution Rate Data .....	5.9
5.7. $\text{Na}_2\text{CO}_3 \cdot \text{H}_2\text{O}$ Dissolution Rate Data .....	5.10
5.8. True and Apparent Activation Energies .....	5.12
5.9. $\text{NaCl}$ Arrhenius Plot .....	5.13
5.10. $\text{NaNO}_2$ Arrhenius Plot .....	5.14
5.11. $\text{NaNO}_3$ Arrhenius Plot .....	5.15

## Tables

2.1. Composition of ORNL Gunite Tank Sludge Simulant .....	2.10
2.2. Kaolin/Bentonite Sludge Simulant Properties .....	2.16
2.3. Properties of Kaolin/Plaster Sludge Simulants .....	2.18
2.4. Composition of ORNL OHF Tank Sludge Simulant .....	2.19
2.5. Kaolin/Ludox Sludge Simulant Properties .....	2.22
2.6. Silica/Soda Ash Simulant Composition .....	2.25
2.7. Kaolin/Plaster Hardpan Simulant Compositions and Properties .....	2.30
2.8. Hard Saltcake Simulant (K-Mag) Compositions and Properties .....	2.37
2.9. Soft Saltcake Simulant Compositions and Properties .....	2.40
3.1. Simulant Material Specifications .....	3.11
4.1. Saltcake Sensitivity Testing Simulant Compositions .....	4.4
4.2. Saltcake Sensitivity Testing Parameters .....	4.6
4.3. Waterjet Cut Depth Data .....	4.9
5.1. Comparison of Mass Transfer Coefficients as Determined by Equations 5.8 and 5.9 .....	5.4
5.2. Summary of Reaction Rate Constants and Average Mass Transfer Coefficient .....	5.6
5.3. Selected Physical Constants .....	5.11
5.4. Parameter Estimates for Determining the Apparent Rate Constant .....	5.11
5.5. Apparent Activation Energy and Frequency Factors .....	5.16
5.6. Verification of Dissolution Rate Predictions .....	5.17
5.7. Verification of Dissolution Time Ratio Prediction .....	5.18
A.1. Tank 19 Residual Solids Data .....	A.3
A.2. Tank 19 Zeolite Simulant Recipes .....	A.9

## Nomenclature

$a$	parameter for kaolin/Ludox <sup>®</sup> simulant composition calculations
$C_b$	concentration of dissolved salt in the bulk solution
$C_d$	depth of cut into saltcake simulant by high-pressure waterjet
$C_s$	concentration of dissolved salt at the particle surface
$C_p$	moles calcium per liter of Tank 19 zeolite simulant
CSEE	Confined Sluicing End Effector
$d$	salt particle diameter
$D$	diffusion coefficient
$D_n$	diameter of high-pressure waterjet nozzle
$D_v$	diameter of shear vane
$f(x)$	effect of variations in saltcake simulant properties on waterjet cut depth
$H_v$	height of shear vane
INEEL	Idaho National Engineering and Environmental Laboratory
$k$	standoff dependence constant (Section 4.0); salt dissolution rate constant (Section 5.0)
$k_0$	apparent salt dissolution rate constant
$k_m$	salt dissolution mass transfer coefficient
$M_{salt}$	molecular weight of salt
$N$	moles of salt
$P_j$	pressure of high-pressure waterjet at the nozzle exit
PNNL	Pacific Northwest National Laboratory
$r$	particle radius
$t$	time
$t_d$	salt particle dissolution time
$T_{peak}$	peak torque on shear vane during shear strength measurement
$v$	fluid velocity
$W_k$	weight fraction kaolin clay
$W_p$	weight fraction plaster of Paris
$W_s$	weight fraction sand
$W_w$	weight fraction water
$x_b$	weight percent bentonite clay
$x_{barite}$	weight percent barium sulfate
$x_k$	weight percent kaolin clay
$x_L$	weight percent Ludox <sup>®</sup> HS-30
$x_{NaCl}$	weight percent sodium chloride
$x_p$	weight percent plaster
$x_w$	weight percent water
$\nu$	kinematic viscosity
$\rho$	density
$\rho_{salt}$	salt crystal density
$\sigma$	standoff distance between waterjet nozzle and saltcake simulant
$\tau_s$	shear strength
$\phi_z$	volume fraction sand or zeolite

## 1.0 Introduction

Millions of gallons of radioactive waste resides in underground tanks at U.S. Department of Energy (DOE) sites. The waste was generated primarily by the processing of nuclear fuel elements to remove fissile radionuclides for use in atomic weapons. Plans call for the waste to be removed from the tanks and processed to create immobile waste forms which will be stored to prevent release to the environment.

The consistency of the waste ranges from liquid, to slurry, to sticky sludge, to hard saltcake. A variety of waste retrieval and processing methods are being evaluated and implemented. Because tests often cannot feasibly be conducted using waste samples, simulants are used to test candidate waste retrieval, handling, and processing methods.

### 1.1 Chemical versus Physical Simulants

Two general types of simulants are used for testing: chemical simulants and physical simulants. Chemical simulants are used when it is necessary to mimic certain chemical properties of the waste. These simulants are usually prepared by following a series of chemical additions and procedures that approximate those used to originally create the waste with the exception that radioactive materials are not used. Chemical simulants are needed to evaluate processes such as vitrification and certain separations. When the chemistry of the waste affects process performance, chemical simulants are typically used. Chemical simulants are expensive to produce and dispose, and, in most cases, hazardous. Thus, they are used only when other testing methods are inadequate.

Physical simulants are used when the waste's chemical properties are of little or no relevance. In such cases, it is the physical properties of the waste that must be matched by the simulant. It is true that many physical properties depend on chemical properties, so it is important to know the waste physical properties under the chemical conditions that are relevant to the process being tested. Physical properties also can depend on the history of the waste, which can affect particle sizes/shapes as well as other factors. Consequently, chemical simulants do not always (or even often) exhibit the appropriate range of physical properties because the history of the tank waste and the chemical simulants differ significantly (e.g., the waste may have been sitting in a tank for decades).

Despite the differences between chemical and physical simulants, they are designed and used in the same way. A careful consideration of the process to be tested is made to decide which chemical and/or physical properties must be matched between the simulant and the waste. This often requires an iterative approach in which experiments are used to identify which properties are most relevant and which can be ignored. The simulant development process is the subject of the next section.

### 1.2 Simulant Development Strategy

Physical simulants are prepared using relatively nonhazardous and inexpensive materials rather than matching the chemical composition of the tank waste. Consequently, only some of the waste properties are matched by the simulant. Deciding which properties need to be matched and which do not requires a detailed knowledge of the physics of whatever process is to be tested using the simulant.

Developing this knowledge requires reviews of available literature, consultation with experts, and parametric tests. Once the relevant properties are identified, waste characterization data are reviewed to establish the target ranges for each relevant property. Simulants are then developed that possess the desired ranges of properties.

The methodology used to develop physical simulants for the testing of waste retrieval processes is illustrated in Figure 1.1 (Golcar et al. 1997). The first step is to identify the retrieval process or processes for which the simulant is to be developed. Because simulants are designed with a specific retrieval process in mind, a simulant that is appropriate for testing one process might be inappropriate for another. For example, hard saltcake simulants prepared from potassium-magnesium sulfate were designed specifically for the testing of high-pressure waterjet scarifiers (Hatchell et al. 1996). The mechanical strength and porosity of this simulant can be related to waste characterization data. Other properties such as its dissolution rate, solubility, and thermal conductivity were not matched, so it is inappropriate to use the potassium-magnesium sulfate simulants to test processes for which these other properties are relevant.

The second step is to identify the waste properties that are expected to determine the process performance. A combination of literature reviews, consultation with experts, and reviews of existing test data is used to develop an understanding of the mechanisms by which the process operates. An understanding of the relevant mechanisms is needed to develop a list of expected key physical properties. If all the relevant mechanisms have been identified and the associated key properties matched between the waste and the simulant, then process tests using the simulant are expected to predict process performance against the tank waste.

An estimated range for the magnitude of each hypothesized key property is needed to establish target ranges for the simulant(s). Waste characterization data obtained from samples and in situ measurements often can be used to establish the target ranges for certain properties (e.g., viscosity, density, and shear strength). However, these data are not available for the waste in many tanks. Further, available data are sometimes unreliable. In such instances, an examination is made of the waste process history, measurements that have been made on wastes thought to be similar, and any available qualitative descriptions of the waste. These data are used to select a suitably conservative range of values for each of the postulated key waste properties.

Simulants are developed with properties that fall within the desired ranges for each key property. Because it is not always practical to match all the key properties simultaneously, compromises are sometimes required. Where possible, compromises are made such that the simulants yield conservative test results. The sensitivity of the process to changes in each of the key properties is then determined using tests designed to approximate specific aspects of the waste retrieval process. The data from these tests provide an indication of the relative importance of each of the key properties. Simulants used for process testing are then designed to match only the most important key properties, if necessary, and not the less important properties.

Process sensitivity testing involves testing the process (or a specific aspect of the process) against a variety of different simulant compositions. If the process performance against all the simulants is adequately correlated with the postulated key properties, then there is improved confidence that all of the

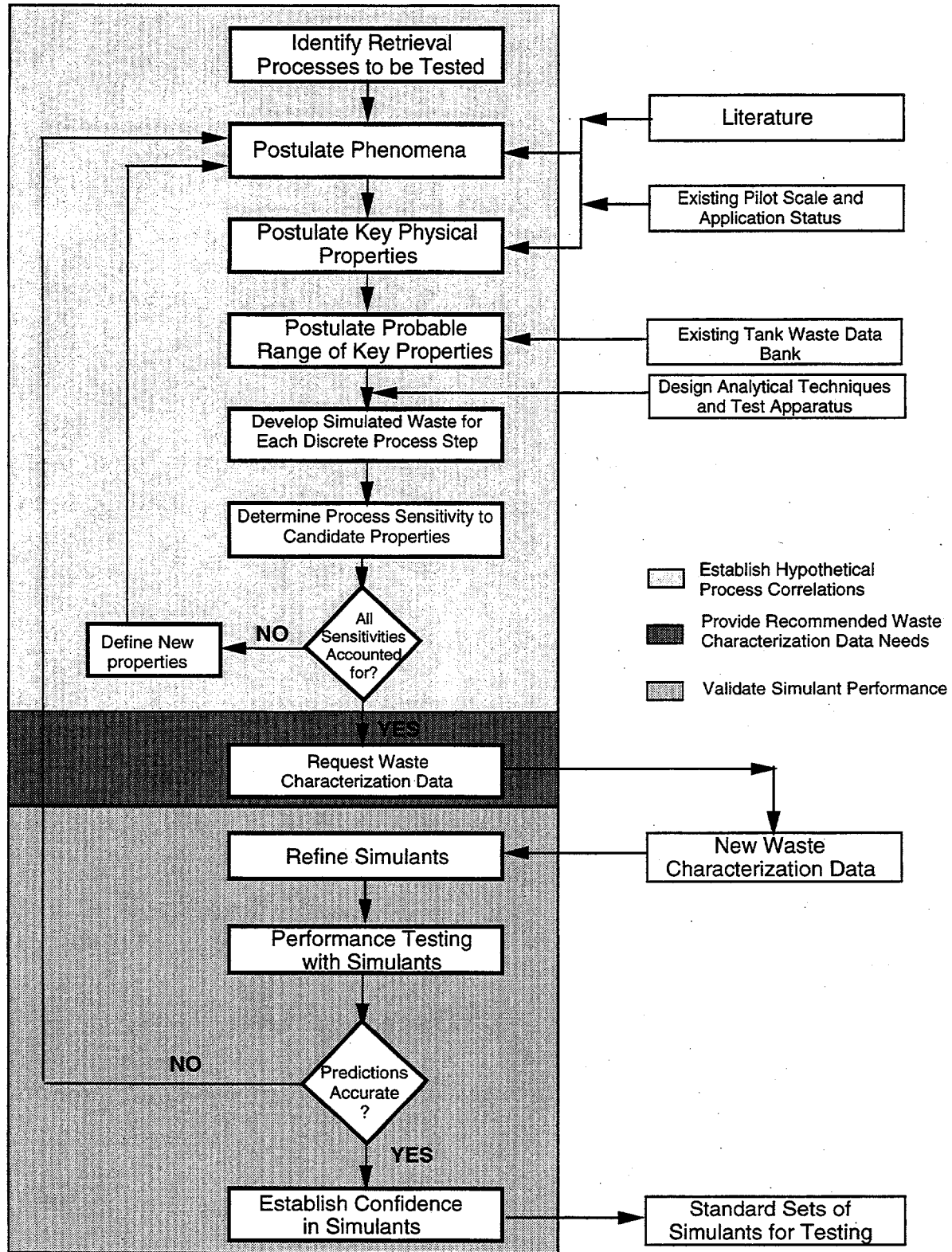


Figure 1.1. Simulant Development Strategy Logic Diagram (from Golcar et al. 1997)

relevant properties have been identified. If it is not adequately correlated, then it is likely that additional or alternative properties must be considered, and a re-examination of the postulated mechanism and relevant properties is required.

Once the key properties have been identified and verified through process sensitivity tests, waste simulants are developed for the purpose of predicting process performance. In some cases, no changes to the simulant compositions are required, and the process sensitivity testing data can be used directly to make process performance predictions. In other cases, additional waste characterization data must be obtained and revised simulant compositions developed before a final set of process performance tests are conducted. If the results of these performance tests are consistent with the process sensitivity tests, then confidence in the validity of the simulants is increased. Alternatively, if the performance tests are not consistent with the sensitivity tests, then a re-examination of the process mechanisms is required to identify any additional candidate key properties.

The final step in the simulant development process is a comparison of the predicted process performance based on simulant testing with the actual process performance against tank waste. If the predictions are verified, then confidence in the validity of the simulants is improved.

### **1.3 Purpose of Document**

A wide variety of waste simulants have been developed and used for testing retrieval processes. Each simulant composition was developed with a specific process in mind. This document lists the compositions of many previously used waste simulants as well as the properties and justification for each. It is hoped that future simulant development efforts will benefit from this collection of simulant recipes.

Because most retrieval operation tests are conducted at relatively large scale, chemical simulants are undesirable. Thus, most of the simulants used for retrieval system testing (i.e., those included in this report) are physical rather than chemical simulants. Others have developed chemical waste simulants (Elmore et al. 1992; LaFemina 1995).

## 2.0 Simulant Descriptions

As described in Section 1.2, an important part of simulant development is the selection of the waste physical properties that will be matched by the simulant. Selection of these properties requires a careful consideration of the retrieval process to be tested. Different processes often require that different simulants be used.

Tank waste can be divided into six general categories. These are: sludge, hardpan, saltcake, supernate, slurry, and miscellaneous. Many of the simulants that have been used for each waste type are described in this section. Because of the large number of different waste simulant recipes that have been used for various test programs, some waste simulant recipes are not included.

### 2.1 Sludge Simulants

The waste properties that are expected to have the greatest influence on the retrieval of sludge are discussed in Section 2.1.1. This is followed in Section 2.1.2 by a listing of many of the sludge simulant compositions which have previously been used and the justification for each.

#### 2.1.1 Relevant Properties for Sludge Retrieval

The sludge properties postulated to be relevant for determining the performance of various candidate waste retrieval technologies are identified in this section. The selection of these properties is based on a combination of testing results and literature reviews. Additional or alternate relevant properties may be selected, based on future testing results.

The key sludge properties for determining the performance of waterjet-based sludge-retrieval methods are thought to be sludge shear strength, sensitivity, cohesiveness, density, and water-absorption rate. Sludge shear strength provides a measure of the capability of the sludge to resist the impinging waterjet. Sludge sensitivity is an indication of the effect of mechanical disruption on the sludge strength. A sludge with a high sensitivity will undergo a drastic decrease in shear strength upon disruption. Cohesiveness<sup>(a)</sup> measures the tendency of the wet sludge to adhere to both itself and to pieces of process equipment. The rate of water absorption affects the rate that the large pieces of dislodged waste disintegrate and form a pumpable slurry. If the sludge contains an appreciable fraction of soluble solids, the solubility and dissolution rate of these solids may be important. In general, it is expected that partially soluble sludge will be retrieved at a greater rate than insoluble sludge, all other properties being equal. Sludge density is important because it influences the rate at which the pieces of dislodged sludge settle either within the tank or within the conveyance line.

---

(a) Cohesiveness is the tendency of a material to stick to other pieces of the same material. The kaolin simulant, for example, is cohesive because separate pieces of kaolin readily stick together. Adhesiveness is the tendency of a material to stick to a different material. In order for a sludge waste to stick to process equipment it must be both adhesive and cohesive. If the waste is only adhesive, then only a thin film would form on the process equipment. If the waste is only cohesive, then not even a film will form. The nature of both the waste and the kaolin simulant make them tend to be *both* adhesive and cohesive.

Tests using a variety of simulants indicate that the sludge-mobilization performance of *submerged-jet*-based retrieval methods (e.g., mixer pumps) is determined primarily by the sludge cohesiveness (Powell et al. 1995). For many sludge-like materials, the maximum expected sludge cohesiveness is a function of the shear strength. The submerged-jet tests also show the importance of partial sludge solubility, but no significant dependence on sludge sensitivity has been found. Sludge sensitivity is expected to be more important for the non-submerged waterjet-retrieval methods.<sup>(a)</sup> Tests using low pressure (< 100 psi) water-in-air jets also imply a strong correlation between shear strength and the jet pressure of incipient mobilization.

To investigate the relationship between low-pressure waterjet sludge mobilization and shear strength, several different sludge simulants were subjected to an impinging water-in-air waterjet. With the jet directed perpendicularly onto the flat sludge simulant surface, the jet flow rate was gradually increased until continuous removal of sludge was observed. The jet flow and pressure required to mobilize the sludge was then correlated with the sludge shear strength.

The data from these tests are plotted in Figure 2.1. The data show that shear strength has a significant effect on the required waterjet pressure. Further, it appears that different simulants can follow different, apparently linear, relationships. The kaolin and bentonite simulant data are reasonably well fit by a line with a slope of 4.0. The kaolin/plaster simulant, however, follows a different line, which has a slope of about 1.2. The kaolin/plaster data are consistent with the results of previous sluicing pressure tests using kaolin/plaster simulant (Powell 1996). The reason for the difference in behavior observed with the kaolin/plaster simulant is not yet known. Regardless, the importance of matching the sludge shear strength when designing sludge simulants is evident.

For high-pressure waterjet applications, the sludge shear strength is not thought to be important for determining whether the waterjet will cause mobilization. The waterjet pressures are orders of magnitude higher than the typical sludge strengths, so rapid penetration of the waterjet into the sludge is expected regardless of sludge shear strength. However, waterjet cutting of hardpan materials, which are thought to have shear strengths in excess of 10 kPa, is likely affected by the hardpan strength.

Shear strength is still thought to be important for high-pressure waterjet applications because the transport of the cut sludge depends strongly on the ability of the waterjets to reduce the size of the dislodged sludge. Stronger sludge resists the slurring action of the waterjets more effectively than does weaker sludge. For this reason, efforts are made to match the sludge shear strength when designing simulants for retrieval processes that use high-pressure waterjets.

---

(a) In mixer-pump-based retrieval systems (submerged waterjet), the dislodged pieces of sludge are broken down into a slurry through the combined action of the mixer pump jet turbulence and travel of the dislodged pieces through the mixer pump volute. The shear stresses imposed on the sludge pieces within the mixer pump are likely much higher than either the disturbed or undisturbed sludge strength. Thus, it is not expected that the decrease in strength of a disrupted sensitive sludge will be of any consequence. In the non-submerged jet applications being considered (e.g., sluicing), the breakup of the dislodged sludge into slurry is performed by the impacting sluice jet turbulence. In this case, the stresses imparted to the dislodged sludge pieces are likely to be much lower. The decrease in sludge strength upon disruption may then accelerate the rate of slurry formation.

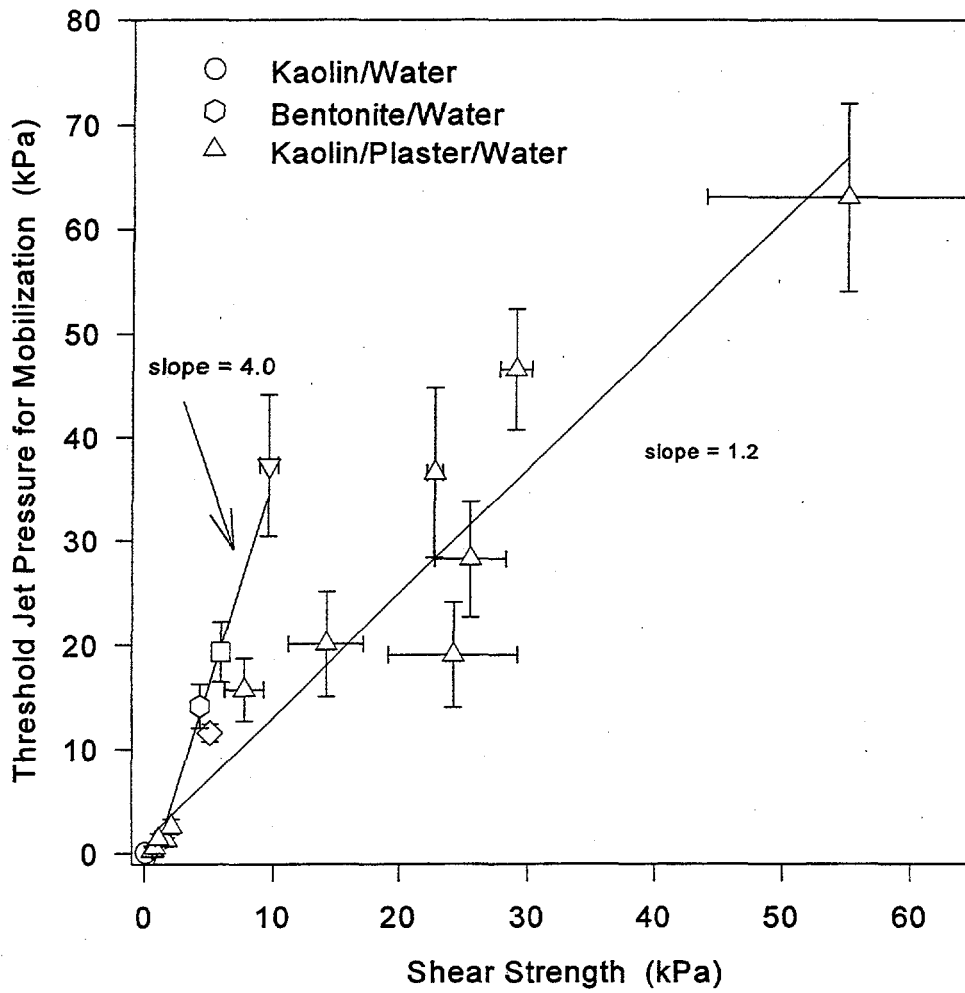


Figure 2.1. Waterjet Pressure Required for Sluicing vs. Shear Strength

Whether the list of postulated key sludge properties given above also applies to non-waterjet-based retrieval techniques is not certain. The exact nature of the candidate retrieval technique must be specified before such a determination can be made. It seems reasonable, however, that for techniques using mechanical cutting/dislodging blades, the sludge shear strength, sensitivity, and cohesiveness would be quite important. Dissolution effects are probably of reduced or negligible importance, depending on the type of conveyance system employed.

With respect to wet sludge-retrieval conveyance system design, the greatest concern is that of conveyance line plugging. Shear strength, cohesiveness, and water-absorption rate are all relevant for conveyance systems. The justification for these key properties is described in Golcar et al. (1997).

The compositions and properties of many of the sludge simulants that have been used for retrieval process testing are given in the following sections. The range of simulants discussed is not intended to encompass all the sludge simulants that have been used at Hanford, but most of the principal physical property simulants are included.

### **2.1.2 Kaolin Clay Simulants**

One of the most often used sludge simulants is a mixture of kaolin clay and water. Kaolin clay is composed of the mineral kaolinite. Kaolinite forms plate-shaped particles with diameters in the 0.3 to 3 micron range and thicknesses in the 0.03 to 1 micron range (Lambe and Whitman 1969). The specific surface area of kaolin clay is typically in the range of 10 to 20 m<sup>2</sup>/g.

There are several properties of kaolin that make it a reasonable simulant for tank sludge. Comparisons of waste properties with those of kaolin/water mixtures are given below.

The particle size distribution of EPK Pulverized kaolin clay has been measured using the same instrument as is used for waste samples and the results are similar (see Figures 2.2 and 2.3<sup>a</sup>). Effects of particle morphology are not addressed by such a comparison, but the plate-like shape of the kaolin particles is expected to render the kaolin conservatively cohesive (i.e., more sticky and difficult to retrieve than the waste).

The kaolin clay shear strength and cohesiveness are thought to be reasonably similar to that of wet tank sludge, based on hot-cell measurements of shear strength and particle size as well as on

---

(a) The particle size distribution data given in Figure 2.2 were taken from Gray, W. J., M. E. Peterson, R. D. Scheele, and J. M. Tingey. 1990. *Characterization of the Second Core Sample of NCAW from DST 101-AZ*. Letter report prepared for Westinghouse Hanford Company by Pacific Northwest Laboratory, Richland, Washington. The Brinkmann particle size analyzer used to collect these data is not sensitive to particles smaller than about 0.5 microns.

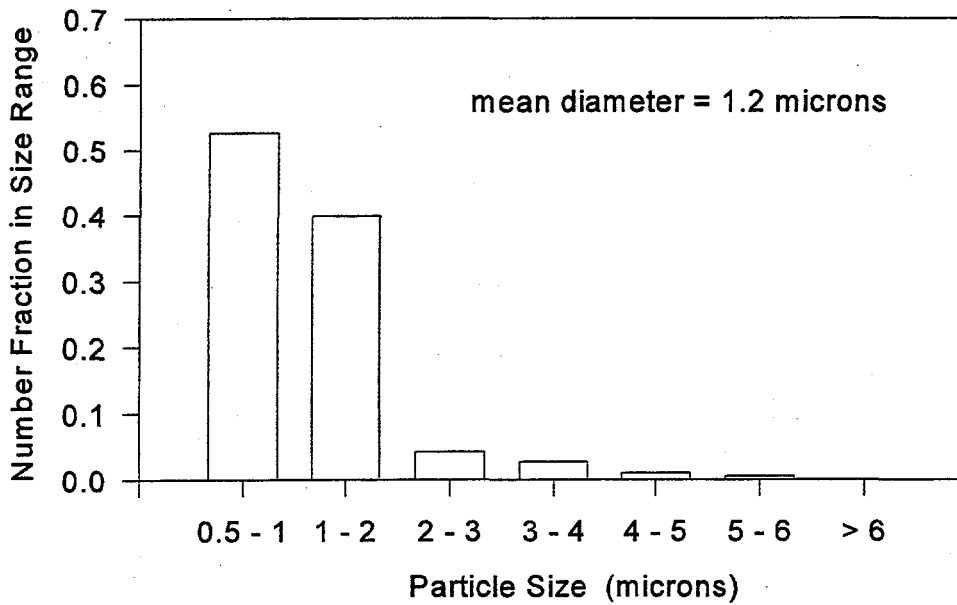


Figure 2.2. Particle Size Distribution for NCAW Core Sample #2

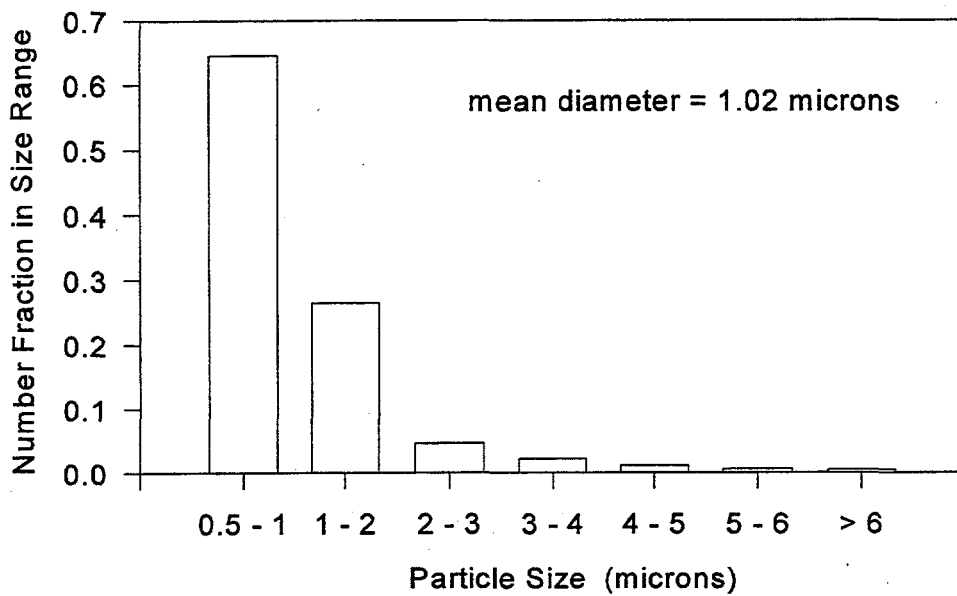


Figure 2.3. Particle Size Distribution for Kaolin Clay (Brinkmann Sample 93-01413)

qualitative descriptions of waste behavior (e.g., "The solids were sticky..."<sup>(a)</sup>). Tank sludge is observed to rinse off of hot-cell spatulas and glassware more readily than the kaolin simulant. This is further evidence that the kaolin simulant is conservatively adhesive.

At a solids concentration of 66 wt% in water, the kaolin simulant shear strength is about 3.5 kPa. The shear strength of sludge samples from various Hanford waste tanks ranges from zero to near 5.0 kPa (Willingham 1994). This is shown in Figure 2.4. Stronger sludge is expected in tanks where the waste has dried and/or reached high temperatures, but this waste type is addressed by the hardpan/dried-sludge simulants in Section 2.2. The dependence of the shear strength of kaolin/water mixtures on weight percent solids is shown in Figure 2.5. Rheology data (yield stress and plastic viscosity) are shown for selected kaolin clay/water slurries in Figure 2.6.

The shear strength of sludge simulants is due to the combination of cohesive and frictional forces. Cohesive forces arise from colloidal attractive forces and bonding between adjacent particles. Frictional forces result when particles encounter each other when the simulant is deformed.

The shear strength of kaolin sludge simulants at relatively high solids fractions (i.e., above about 60 wt%) is principally due to frictional forces. Measurements indicate that roughly 7% of the shear strength of a 68 wt% kaolin/water mixture is due to cohesive forces, and 93% is due to friction (Gibson 1953). Decreasing the clay/water ratio is expected to alter this split such that cohesive forces become relatively more important because the increased space between adjacent particles will decrease friction. The cohesion of kaolin clay is primarily due to edge-to-face, electrostatic alignment of clay particles rather than to van der Waals attractive forces as is the case for bentonite. The total amount of cohesion obtained from these edge-to-face bonds is expected to be linearly related to the total number of such bonds per unit volume of clay. As the weight percent clay is decreased, fewer particles are available for bond formation, so the total cohesion decreases. The relationship between cohesion and weight percent solids is evident in a plot of tensile strength versus shear strength for kaolin clay. Tensile strength is directly proportional to cohesion (for an ideal solid). Figure 2.7 shows tensile strength versus shear strength for a variety of sludge simulants. Note how the kaolin clay tensile strength does not increase with increasing shear strength beyond a shear strength of about 2 kPa (20 kdyn/cm<sup>2</sup>).

The sensitivity of the waste to disruption is known to be significant. That is, mechanical disruption is known to decrease the shear strength of wet sludge. The amount of this decrease in strength varies depending on the waste type. The kaolin clay simulant has a relatively low sensitivity to disruption. This difference between waste and simulant may make the simulant more difficult to retrieve than the waste in some circumstances.

The rate at which waste imbibes fresh water is not known. Tests have shown that the kaolin clay simulant imbibes water very slowly (Powell et al. 1995). Thus, kaolin may be conservative with respect to water-absorption rate.

---

(a) Tingey, J. M., R. D. Scheele, M. E. Peterson, and M. R. Elmore. 1990. *Characterization of Waste from Double-Shell Tank 103-AW*. Letter report prepared for Westinghouse Hanford Company by Pacific Northwest Laboratory, Richland, Washington.

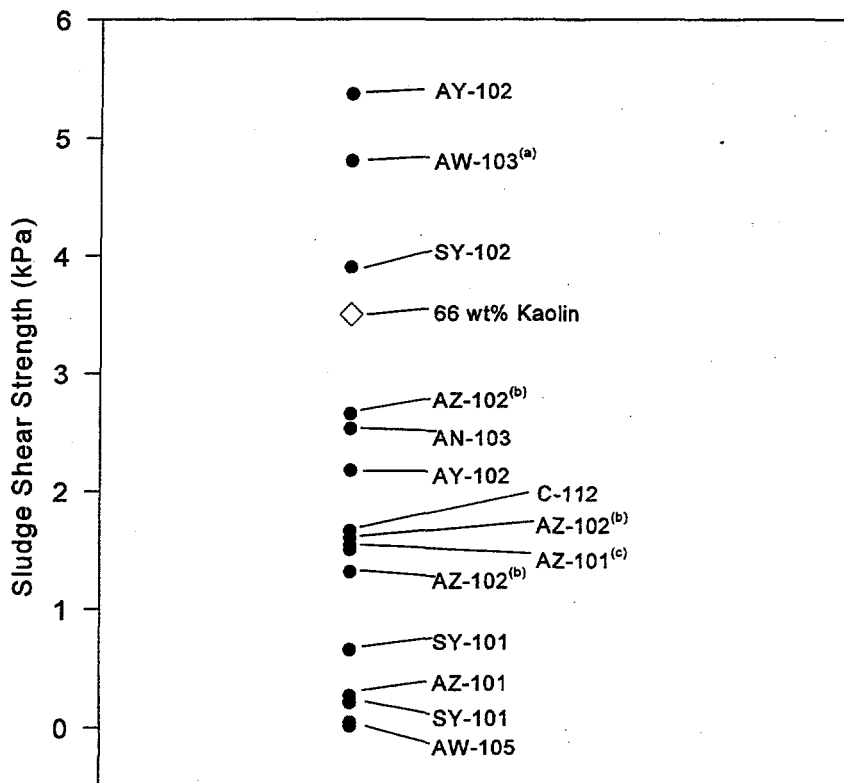


**Figure 2.4.** Plot Showing Range of Sludge Shear Strengths

**Note:** The data used to generate this plot were taken from Willingham (1994) except as noted by superscripts a, b, and c. The data for the superscripted tanks are from:

(a) Tingey, J. M., R. D. Scheele, M. E. Peterson, and M. R. Elmore. 1990. *Characterization of Waste from Double-Shell Tank 103-AW*. Letter report prepared for Westinghouse Hanford Company by Pacific Northwest Laboratory, Richland, Washington.

(b) Gray, W. J., M. E. Peterson, R. D. Scheele, and J. M. Tingey. 1991. *Characterization of the First Core Sample of NCAW from DST 102-AZ*. Letter report prepared for Westinghouse Hanford Company by Pacific Northwest Laboratory, Richland, Washington.

(c) Gray, W. J., M. E. Peterson, R. D. Scheele, and J. M. Tingey. 1990. *Characterization of the Second Core Sample of NCAW from DST 101-AZ*. Letter report prepared for Westinghouse Hanford Company by Pacific Northwest Laboratory, Richland, Washington.

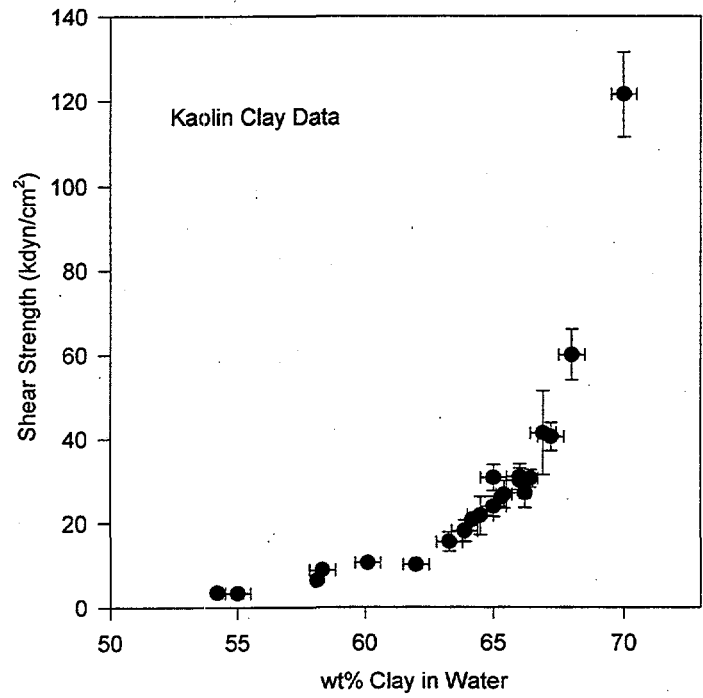


Figure 2.5. Kaolin Shear Strength vs. wt% Kaolin

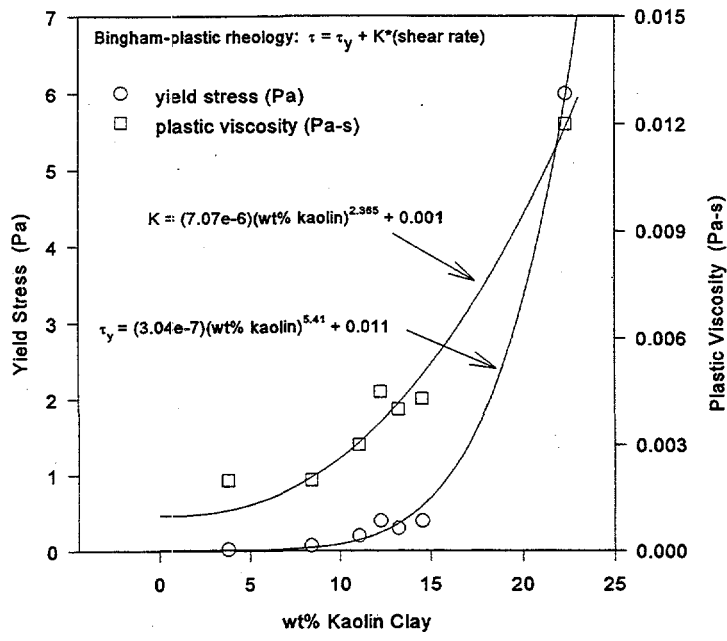


Figure 2.6. Kaolin Slurry Rheology Data

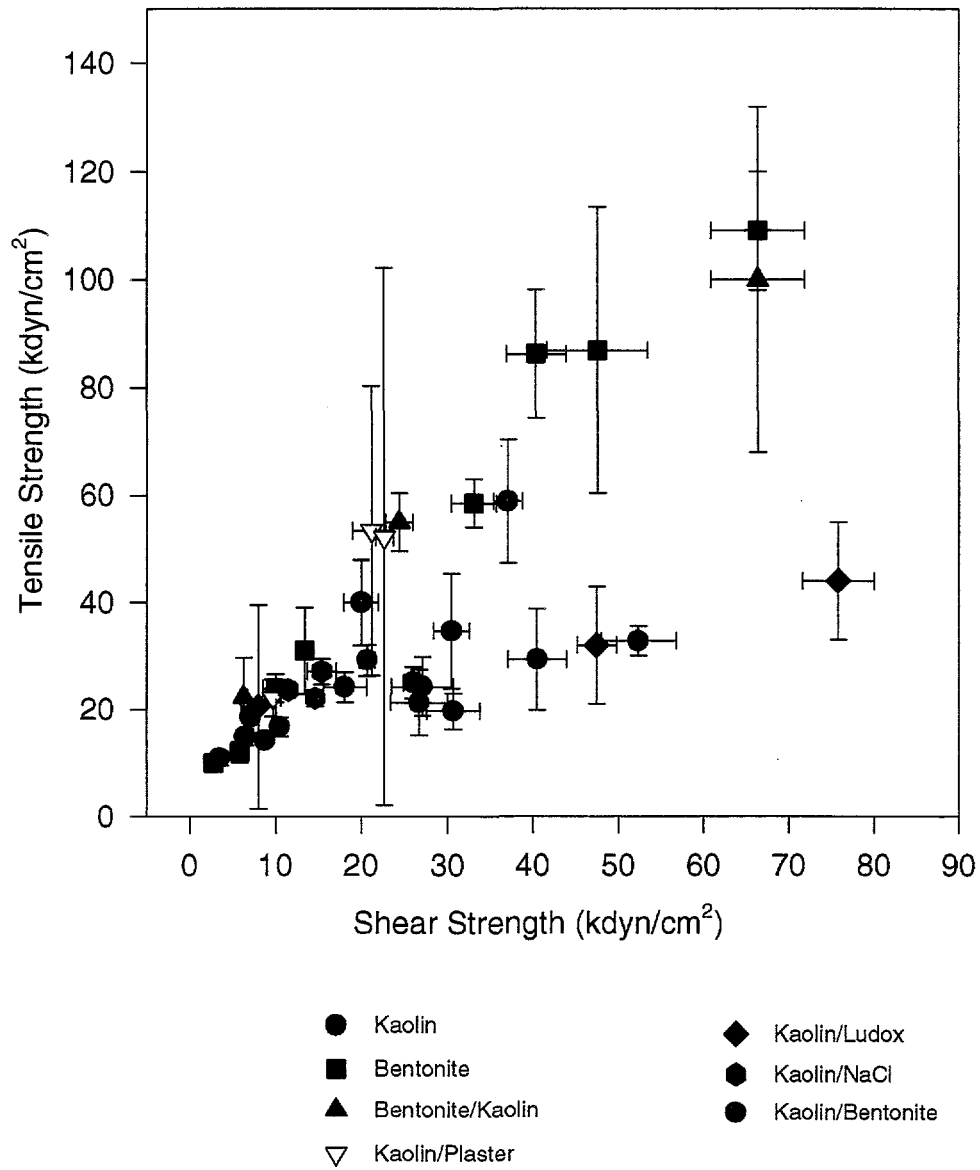


Figure 2.7. Split-Cell Tensile Strength vs. Shear Strength

The range of wet sludge densities reported by Willingham (1994) is compared with the density of 66 wt% kaolin clay in Figure 2.8. The kaolin mixture density is seen to fall within the range of measured sludge densities. Assuming negligible air entrainment, the density of a kaolin/water mixture can be estimated using the formula

$$\rho \text{ (g/cm}^3\text{)} = \frac{100}{\frac{x_k}{2.65} + \frac{100-x_k}{0.998}} \quad (2.1)$$

where  $x_k$  is the wt% kaolin clay in the mixture. The particle density of kaolin clay is about 2.65 g/cm<sup>3</sup> (Lambe and Whitman 1969).

There are many factors that complicate simple comparisons of waste property data to simulant property data. For example, the disruption effects of core sampling may decrease the shear strength measured in the hot cell considerably, depending on the properties of the waste. Similarly, the fact that the particle size distributions, as given by the Brinkmann Model 2010 Particle Size Analyzer, are similar does not necessarily mean that the distributions actually are similar. The Brinkmann is not sensitive to particles smaller than about 0.5 microns, so any differences in the concentrations of these small particles will not be detected by the Brinkmann. It should be clear that some refinement to the waste simulants may be required as more waste characterization data become available.

A kaolin clay simulant was used to simulate the Oak Ridge National Laboratory (ORNL) gunite tank sludge for the purpose of developing and testing the confined sluicing end-effector (Rinker et al. 1996). The composition used for the testing is provided in Table 2.1 below. Sand, rice, and crushed rock were added to the mix to model the effects of the sand, gunite chips, and salt crystals that have been found in sludge samples taken from the ORNL gunite tanks (Bechtel National 1995). Plugging of the inlet screen on the end-effector was a concern, so some testing also included miscellaneous items in the sludge such as plastic bags. The shear strength of this ORNL "representative" simulant was 0.5 ± 0.1 kPa. This shear strength target was established by observing the flow behavior of gunite tank sludge samples as they were extruded from the sampling tube. No shear strength measurements were made on the undisturbed samples.

**Table 2.1. Composition of ORNL Gunite Tank Sludge Simulant**

Material	Concentration (wt%)
water	40.0
kaolin clay	42.0
sand	8.0
rice	7.0
crushed rock (gravel)	3.0

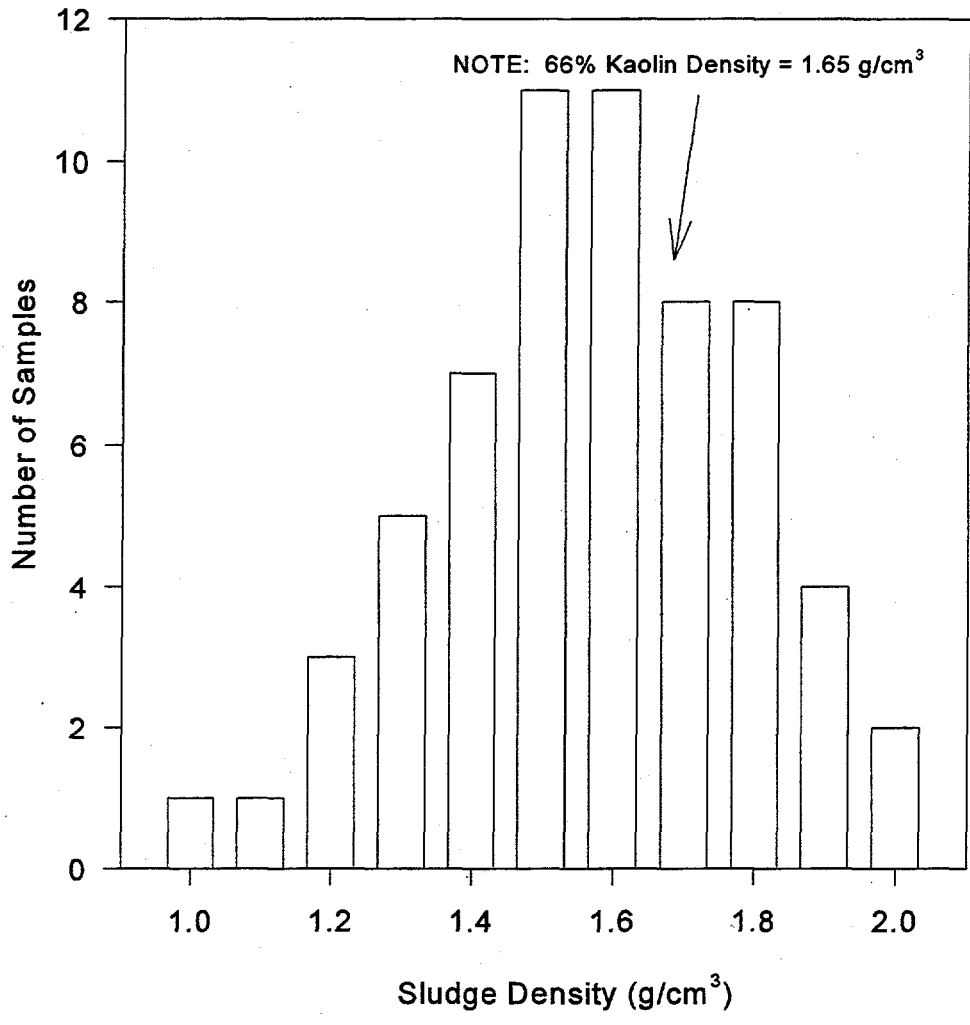


Figure 2.8. Histogram of Sludge Sample Densities (from Willingham 1994)

### 2.1.3 Bentonite Clay in Water

Bentonite clay is composed primarily of montmorillonite clay particles. The atomic mineralogical structure of montmorillonite allows the formation of very small, very thin, plate-shaped particles. Typical particles of bentonite clay range from 0.1 to 1 micron in diameter with thickness of about 0.001 to 0.01 microns, which is smaller and thinner than kaolin clay (see Section 2.1.2).

Various mixtures of bentonite clay and water have been used to produce sludge simulants. The smaller particles of the bentonite give the bentonite-based simulants somewhat different properties than the kaolin/water simulants. The shear strength, for example, is higher for a given weight percent solids. A plot of shear strength versus weight percent solids is shown in Figure 2.9. The density of bentonite sludge simulants can be estimated using Equation 2.1 and substituting the weight percent bentonite for  $x_w$ .

In many respects, bentonite-based sludge simulants behave similarly to the kaolin simulants provided that equal shear strengths are used for comparison. The bentonite simulants, however, have two properties that make them distinct from kaolin simulants. First, bentonite undergoes osmotic swelling when exposed to water. Second, the bentonite clay simulants are highly elastic and owe only a small portion of their shear strength to interparticle friction. Each of these properties is discussed below.

The osmotic swelling of bentonite clay is due to the double-layer repulsion between the surfaces of the bentonite particles. Due to impurities in the crystal lattice of clay minerals, the surface of clay particles are negatively charged under most conditions. This negative surface charge electrostatically attracts a cloud of cations that tend to diminish the electric field of the negative particles. When two bentonite particles are close enough, their respective cation clouds will overlap. This creates a repulsive force because the positively charged cations electrostatically repel each other. The swelling of the bentonite clay is termed osmotic swelling because the water outside the clay permeates into the region between particles in an effort to equalize the local high cation concentration with that of the water far away from the particles. This influx of water tends to push the particles apart until double-layer overlap is no longer significant (van Olphen 1977).

The degree to which a clay will imbibe water due to osmotic swelling depends on the average double-layer thickness compared to the distance between adjacent clay particles. Double-layer thickness is determined by the clay's surface charge density, which is a function of its mineralogical composition, and by the ionic strength of the fluid surrounding the clay. The distance between clay particles is a function of the weight fraction of clay in the clay/fluid mixture. White and Pichler (1959) studied the rate of water absorption of several different clay types. Beyond the liquid limit of each clay, osmotic swelling was small or nonexistent for illite clay, kaolin clay, and calcium-bentonite clay. Sodium-bentonite, however, showed continuing osmotic swelling even when the weight percent clay had fallen to about 12 wt%. The swelling of sodium-bentonite is expected to cease when the particles are so far apart that double-layer repulsions are balanced by the attractive van der Waals and edge-to-face cross-linking forces (van Olphen 1977). Calcium-bentonite does not show the same continuous swelling as the sodium-bentonite due to the ability of the calcium cations to compress the double layers. In calcium-bentonite, the weight percent at which the double layers cease to overlap is higher than for sodium-bentonite.

Osmotic swelling up to about the liquid limit is commonly observed in concentrated dispersions like clay pastes when the behavior of the particles is principally governed by colloidal effects. It has been

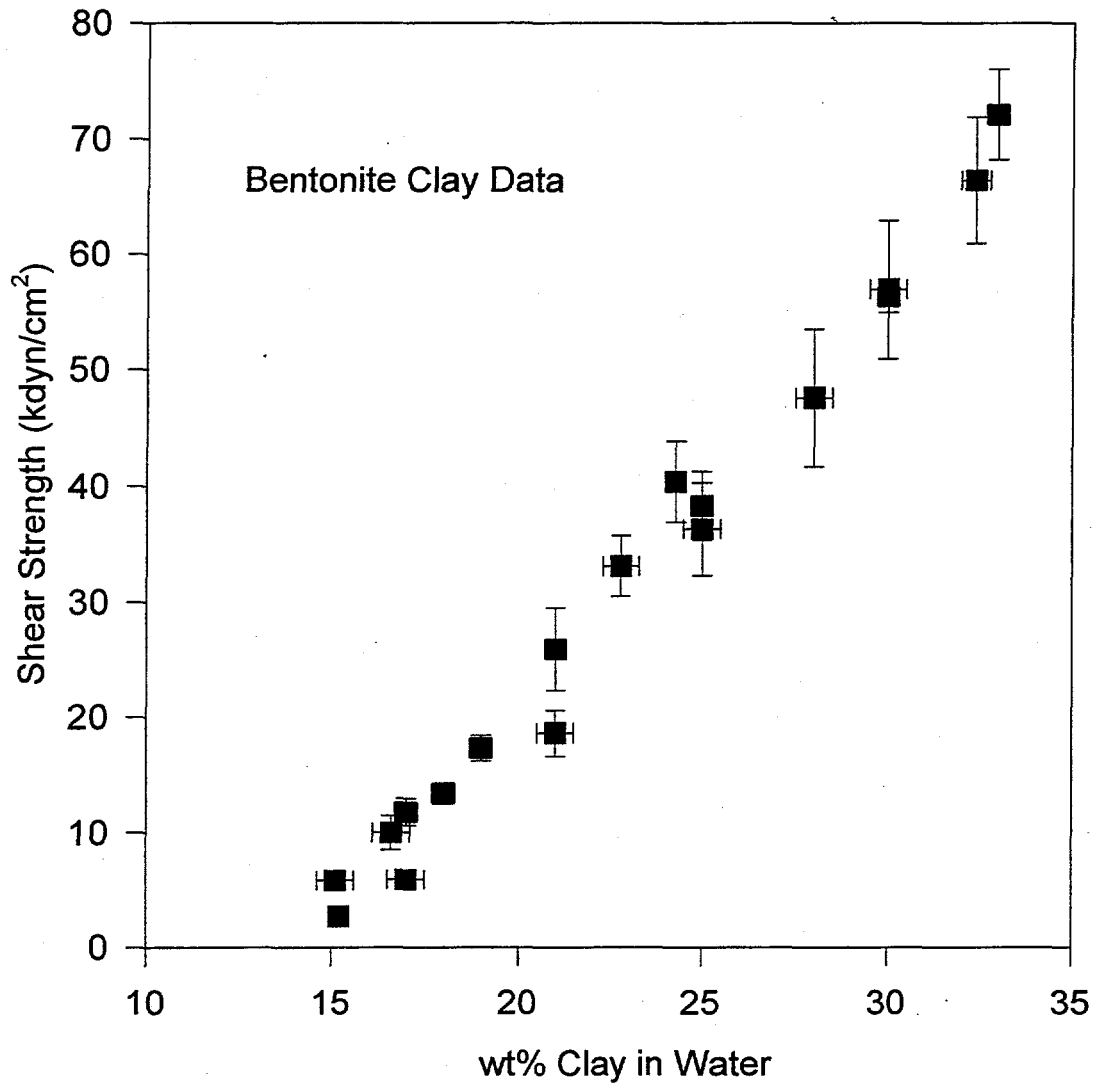


**Figure 2.9.** Bentonite Shear Strength vs. wt% Bentonite

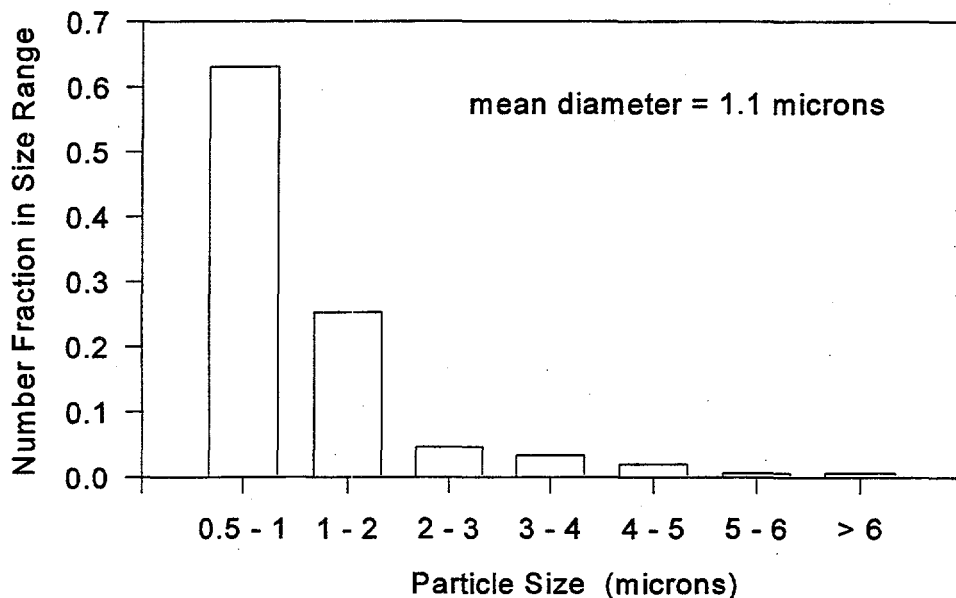


Figure 2.10. Particle Size Distribution for Bentonite Clay

suggested that colloidal effects dominate behavior when the total surface area per unit mass of particles exceeds about  $25 \text{ m}^2/\text{g}$  (Lambe and Whitman 1969). Osmotic swelling is not observed in dispersions of large particles like sand because colloidal effects do not significantly affect sand particles.

Whether osmotic swelling is a potentially significant mechanism for the retrieval of sludge is not known. The permeability of the sludge and the osmotic pressure driving force will determine the rate at which any osmotic swelling could occur. The osmotic pressure driving force will be a function of both the specific surface area of the sludge and the difference in ionic strength between the eroding and interstitial fluids. For osmotic swelling to be a significant effect, the swelling rate of the sludge must be high enough that appreciable waste retrieval rate is obtained.

Bentonite sludge simulants exhibit considerable elasticity. The elasticity results from the house-of-cards structure the bentonite particles form. This structure allows the bentonite suspensions to respond elastically to much greater strain than can kaolin suspensions. Viscoelastic characterization of bentonite simulants confirms the high bentonite elasticity and relatively low kaolin elasticity (Powell et al. 1995).

The particle size distribution of CS-50 Bentonite clay (from American Colloid Co.) was measured using the Brinkmann Model 5050 particle size analyzer. The data from this analysis are presented in Figure 2.10. The bentonite particles are thin sheets rather than spheres as is implicitly assumed by the particle size analyzer, so this particle size distribution is not necessarily representative of the actual particle sizes. The Brinkmann particle size analyzer utilizes a laser-chopping technique to determine the particle size distribution. The sample is slurried with water and subjected to a rapidly moving laser beam. A sensor detects when the laser is blocked by a particle. Using the rate of laser beam movement and an assumed particle geometry (e.g., spherical), the particle size distribution can be estimated based on the range of laser occlusion times.

### 2.1.4 Bentonite/BaSO<sub>4</sub> Sludge Simulants

As discussed in Section 2.1.3, bentonite-based sludge simulants are highly cohesive and achieve shear strengths similar to that of tank sludge at relatively low solids concentrations. As a result, the bulk density of the bentonite/water simulants is typically lower than that of tank sludge. A 25 wt% bentonite/water mixture, for example, has a shear strength of about 4000 Pa but a density of only 1.18 g/cm<sup>3</sup>.

To increase the density of bentonite-based sludge simulants, powdered barium sulfate can be added. Barium sulfate, also known as barite, is a naturally occurring high density salt which is used extensively in the oil-well drilling industry as a slurry densifier. The particle density of barite is typically between 4.25 and 4.5 g/cm<sup>3</sup> (Brady and Clauser 1991). The natural barite crystals are polymorphous, thus a range of densities is typically observed.

Bentonite/BaSO<sub>4</sub> sludge simulants were used as part of the waterjet-based end-effector development work at Hanford (Thompson et al. 1993).

The density of bentonite/BaSO<sub>4</sub> simulants can be easily calculated, assuming minimal air entrainment, using the equation:

$$\rho \text{ (g/cm}^3\text{)} = \frac{100}{\frac{x_b}{2.65} + \frac{x_{barite}}{4.38} + \frac{100 - x_b - x_{barite}}{0.998}} \quad (2.2)$$

where  $x_b$  is the weight percent bentonite and  $x_{barite}$  is the weight percent barite used in the simulant.

### 2.1.5 Kaolin/Bentonite Sludge Simulants

Mixtures of kaolin and bentonite clays with water have been used as sludge simulants for the scaled testing of jet mixer pumps (e.g., Powell et al. 1995). For some applications, these simulants are preferred to the kaolin/water and bentonite/water simulants.

Kaolin/bentonite sludge simulants have a higher density than the bentonite/water simulants for a given shear strength. By adjusting the ratio of kaolin to bentonite and the total solids fraction in the mix, the sludge density and shear strength can be varied independently over a range of values. The bulk density of a kaolin/bentonite simulant can be estimated using Equation 2.1 where  $x_t$  is taken to be the sum of the kaolin and bentonite weight percentages.

No easily used correlation of shear strength with kaolin/bentonite simulant composition has been developed. The shear strength data for several compositions are shown in the table below. Tensile strength data for these simulants are shown in Figure 2.7 where "bentonite/kaolin" refers to simulants 1 through 3, and "kaolin/bentonite" refers to simulants 4 through 6 in Table 2.2 (data taken from Powell et al. 1995).

**Table 2.2. Kaolin/Bentonite Sludge Simulant Properties**

Simulant No.	Composition (wt%)	Kaolin to Bentonite Ratio	Bulk Density (g/cm <sup>3</sup> )	Shear Strength (kdyn/cm <sup>2</sup> )
1	18% bentonite 36% kaolin --> 54% solids 46% water	2.00	1.50	66.4 ± 5.5
2	14.4% bentonite 28.9% kaolin --> 43.3% solids 56.7% water	2.01	1.37	24.4 ± 1.6
3	12.1% bentonite 24.8% kaolin --> 36.9% solids 63.1% water	2.05	1.30	6.3 ± 0.4
4	1.33% bentonite 65.0% kaolin --> 66.3% solids 33.7% water	48.9	1.70	37.1 ± 1.7
5	1.27% bentonite 62.08% kaolin --> 63.4% solids 34.0% water	48.9	1.65	20.1 ± 2.1
6	1.22% bentonite 59.87% kaolin --> 61.1% solids 38.91% water	49.1	1.61	7.1 ± 0.7

Another advantage of the kaolin/bentonite simulant is that it has a negligible water absorption rate. As can be seen in Figure 2.7, the tensile strength versus shear strength relationship shown by the kaolin/bentonite simulants is the same as that of the bentonite/water simulants. Thus, the kaolin/bentonite simulants apparently owe most of their shear strengths to cohesive rather than frictional forces. In this sense, the kaolin/bentonite simulants are like the bentonite/water simulants. However, as discussed in Section 2.1.3, the bentonite/water simulants absorb water. Water absorption can be undesirable for some applications. In these cases, the kaolin/bentonite simulants offer high cohesion along with minimal water absorption and independently adjustable density and shear strength. The improved flexibility of the kaolin/bentonite simulants allows the simulant density and strength to more closely match those of the waste.

### 2.1.6 Kaolin/Plaster Sludge Simulants

Mixtures of kaolin clay and plaster of Paris have been used to create sludge simulants that obtain their shear strengths via a different mechanism than either the kaolin/water or bentonite/water simulants. Most of the shear strength for these simulants results from the curing of the plaster of Paris; the kaolin clay helps to absorb the excess water and to increase the bulk density. This is advantageous for two

reasons. First, the preparation of high shear strength simulants is made easier when the simulant can be prepared as a pumpable slurry that subsequently cures. High shear strength kaolin and bentonite simulants require a special mixer to prepare, and transport of the simulant is usually accomplished by hand.

Second, it is important to test candidate retrieval processes against simulants that obtain their properties through a variety of different mechanisms. As was discussed in Section 1.2, these kinds of tests will often reveal whether the retrieval process performance is dependent on sludge properties in addition to (or instead of) those that have been selected as the "key properties."

The kaolin/plaster simulant has a shear strength on the order of 25% to 50% of its cured strength when it is first prepared (i.e., before significant curing takes place). This initial strength is due to the combination of the kaolin clay cohesion and friction as well as the frictional contribution of the plaster particles. As the plaster of Paris cures, the calcium sulfate hemihydrate ( $2\text{CaSO}_4 \cdot \text{H}_2\text{O}$ ) undergoes dissolution and reprecipitation with additional complexed water molecules to form interlocking crystals of gypsum ( $\text{CaSO}_4 \cdot 2\text{H}_2\text{O}$ ). These crystals precipitate between and around the kaolin particles as they grow together and interlock. The growth of interlocking crystals between insoluble sludge particles has been suggested as a possible mechanism for strength development in some tank sludges. This is based on the observation that the shear strength from Hanford double-shell Tank 101-SY decreased markedly as the temperature increased (Herting 1992). The increase in temperature, it is postulated, results in the dissolution of some of the salts, thereby decreasing the degree of interlocking.

The kaolin/plaster sludge simulants are not without drawbacks, however. The properties obtained once the simulant cures can be quite sensitive to small variations in the simulant preparation procedure. Under some conditions, for example, mixing for 15 minutes instead of 10 minutes can result in a much lower ultimate strength. The additional mixing breaks down the calcium sulfate dihydrate crystals that begin forming once the plaster of Paris contacts water. Thus, careful attention to the simulant preparation procedure is needed to ensure that multiple batches of kaolin/plaster simulant have similar properties.

Physical properties for several kaolin/plaster simulants are given in Table 2.3. Again, the shear strengths for the kaolin/plaster simulants will vary depending on mixing time and temperature, so the values given in Table 2.3 will not be obtained in some circumstances. Clearly, when using the kaolin/plaster simulants, it is necessary to characterize each batch of simulant once it cures.

The bulk density of kaolin/plaster sludge simulants can be predicted based on the known densities of kaolin clay particles ( $2.65 \text{ g/cm}^3$ ), water ( $0.998 \text{ g/cm}^3$ ), calcium carbonate ( $2.83 \text{ g/cm}^3$ ), and calcium sulfate dihydrate ( $2.32 \text{ g/cm}^3$ ). According to the manufacturer, the plaster of Paris contains 20%  $\pm$  5% by weight of calcium carbonate as a nonreactive filler. Assuming complete hydration of the plaster of Paris, the following equation can be derived for the bulk density of kaolin/plaster simulants:

$$\rho \text{ (g/cm}^3\text{)} = \frac{100}{\frac{x_k}{2.65} + \frac{0.2x_p}{2.83} + \frac{0.95x_p}{2.32} + \frac{x_w - 0.149x_p}{0.998}} \quad (2.3)$$

**Table 2.3. Properties of Kaolin/Plaster Sludge Simulants**

Composition (wt%)	Shear Strength (kPa)	Density (kg/m <sup>3</sup> )
50.0% kaolin 10.0% plaster of Paris 40.0% water	0.97 ± 0.09	1610
50.0% kaolin 12.0% plaster of Paris 38.0% water	2.12 ± 0.22	1640
50.0% kaolin 13.0% plaster of Paris 37.0% water	2.9 ± 0.4	1660
50.0% kaolin 14.0% plaster of Paris 36.0% water	4.0 ± 0.7	1680

where,  $x_k$  = weight percent kaolin clay  
 $x_p$  = weight percent plaster of Paris  
 $x_w$  = weight percent water

This equation was used to calculate the densities shown in Table 2.3. The calculated densities are similar to the experimentally measured densities.

Kaolin/plaster sludge simulants were used in the testing of the extendible nozzle at PNNL (Bamberger et al. 1997). A kaolin/plaster formulation was developed to mimic the estimated tensile strength and sensitivity to disruption of samples taken from the ORNL Old Hydrofracture (OHF) tanks. The properties of the OHF sludge were estimated based on observation of the flow behavior and response to mixing of samples extruded in a glove box at ORNL.

As the OHF samples were vertically extruded from the sampling tubes, pieces were observed to break away and fall into the beaker positioned below. The length of these pieces, along with the bulk sludge density, can be used to estimate the sludge tensile strength (Powell et al. 1995). According to the relationship shown in Figure 2.7, the tensile strength of a cohesive sludge can be used to estimate the shear strength. Based on the OHF sample observations, an estimated shear strength of between 1.0 and 2.0 kPa was established. To provide some conservatism in the extendible nozzle tests, a target shear strength of 2.5 kPa was used for the sludge simulant. The simulant composition used for the OHF extendible nozzle testing is given in Table 2.4. The simulant density was measured at 1.65 g/cm<sup>3</sup> and the shear strength was measured at 2.5 ± 0.5 kPa.

The glove-box extrusions also revealed that the OHF tank sludge loses nearly all of its strength when subjected to mixing. Pieces of extruded OHF sludge were mixed with a stirring rod inside a beaker for less than one minute and a slurry with an estimated yield stress of less than 0.1 kPa was formed. The

**Table 2.4.** Composition of ORNL OHF Tank Sludge Simulant

Material	Concentration (wt%)
water	37.0
kaolin clay	50.0
plaster of Paris	13.0

OHF simulant shown in Table 2.4 also mimics this aspect of the OHF sludge behavior, although conservatively. Mixing the fully cured OHF simulant reduces the shear strength from 2.5 kPa to about 0.5 kPa.

### 2.1.7 Kaolin/Ludox® Sludge Simulants

Mixtures of kaolin clay, water, salt, and Ludox have been used to simulate double-shell tank sludge for scaled mixer pump tests conducted in fiscal years 1988 and 1994 (see Powell et al. 1997). Following a series of fiscal year 1987 1/12-scale sludge mobilization tests using a silica/soda ash simulant (see Section 3.1.2.6), a series of additional 1/12-scale tests were performed using a kaolin/Ludox sludge simulant. It was desired that these mobilization tests be conducted using sludge simulants with higher shear strengths than those practically attainable using the silica/soda ash sludge simulant. To meet this need, a new simulant was developed. This simulant used the gelation of colloidal silica to create strength. The colloidal silica chosen is sold under the trade name Ludox HS-30. Kaolin clay was added to give the gel the target sludge density of 1.5 kg/L. This simulant was convenient to use for the 1/12-scale tests because it could be mixed as a slurry and pumped into the tank where it cured to form a sludge. The shear strength of the sludge and curing time are predictably controlled by the Ludox and salt concentrations used.

The mechanism for strength development in the kaolin/Ludox sludge simulant is similar in some respects to bentonite clay, but different in others. The Ludox HS-30 is purchased in the form of a 30 wt% mixture of very small amorphous silica particles (roughly 12 nm) in water. The particles are small enough to be maintained in suspension by Brownian motion and they do not flocculate because of their high surface charge. Adding salt (sodium chloride) suppresses the interparticle electrostatic repulsions which allows the particles to aggregate and form a three-dimensional gel structure that gives the simulant strength. Similarly, bentonite/water mixtures obtain strength from the gel structure formed by the colloiddally bonded bentonite particles.

Where the kaolin/Ludox simulant differs, however, is in the reversibility of the interparticle bonds. The Ludox particles undergo a condensation reaction at the interparticle contact points that results in a chemical bond between the particles. These bonds form relatively slowly and can be broken by an applied strain. Further, once broken, these bonds do not readily reform. Thus, kaolin/Ludox sludge simulants lose their shear strength when mixed after they have been allowed to cure. Bentonite sludge simulants in the concentration range typically used lose comparatively little of their strength even upon vigorous mixing.

The kaolin in the kaolin/Ludox simulant mixture does not contribute appreciably to the shear strength of the cured simulant. The kaolin is included in the mixture primarily to increase the simulant density and to absorb the free water inside the cured simulant.

Kaolin/Ludox simulants are highly elastic and have been described qualitatively as a cross between thick mud and Jell-O®. Viscoelastic rheometry has not been performed on samples of kaolin/Ludox, but it is expected that such samples would exhibit a very small loss tangent, which implies that very little of its strength is due to interparticle friction. Viscoelastic characterization of bentonite simulants, which are similar in this respect, is described in Golcar et al. (1997).

The relationship between tensile strength and shear strength for the kaolin/Ludox simulants is shown in Figure 2.7. According to these data, the tensile strength does not follow the behavior of the other cohesive sludge simulants (e.g., bentonite, bentonite/kaolin, and kaolin/bentonite). There are reasons to believe, however, that these data are in error, and kaolin/Ludox actually does follow the same relationship as the other cohesive simulants. The low tensile strengths for kaolin/Ludox may be an artifact of the tensile strength measurement technique used (see Powell et al. 1995).

Correlations between the cure time, the shear strength of kaolin/Ludox simulants, and their compositions were developed previously.<sup>(a)</sup> Using Figure 2.11, determine the weight percent Ludox ( $x_L$ ) that corresponds to both the target shear strength and the desired cure time. Use  $x_L$  in the following equation to determine the value of the parameter  $a$ :

$$a = 3.1234 \frac{x_L}{1 - 0.003x_L} \quad (2.4)$$

Next, calculate the weight percentages of kaolin ( $x_k$ ), water ( $x_w$ ), and salt ( $x_{NaCl}$ ) using the equations:

$$x_k = \frac{16000}{312.34 + 0.3a} \quad (2.5)$$

$$x_w = \frac{100(150 - 0.7a)}{312.34 + 0.3a} \quad (2.6)$$

$$x_{NaCl} = \frac{234}{312.34 + 0.3a} \quad (2.7)$$

---

(a) Whyatt, G. A. 1987. *Development of a Double-Shell Slurry Physical Simulant to be Used for Pilot-Scale Sludge Mobilization Testing*. GAW-02-88. Letter report for Westinghouse Hanford by Pacific Northwest Laboratory, Richland, Washington.

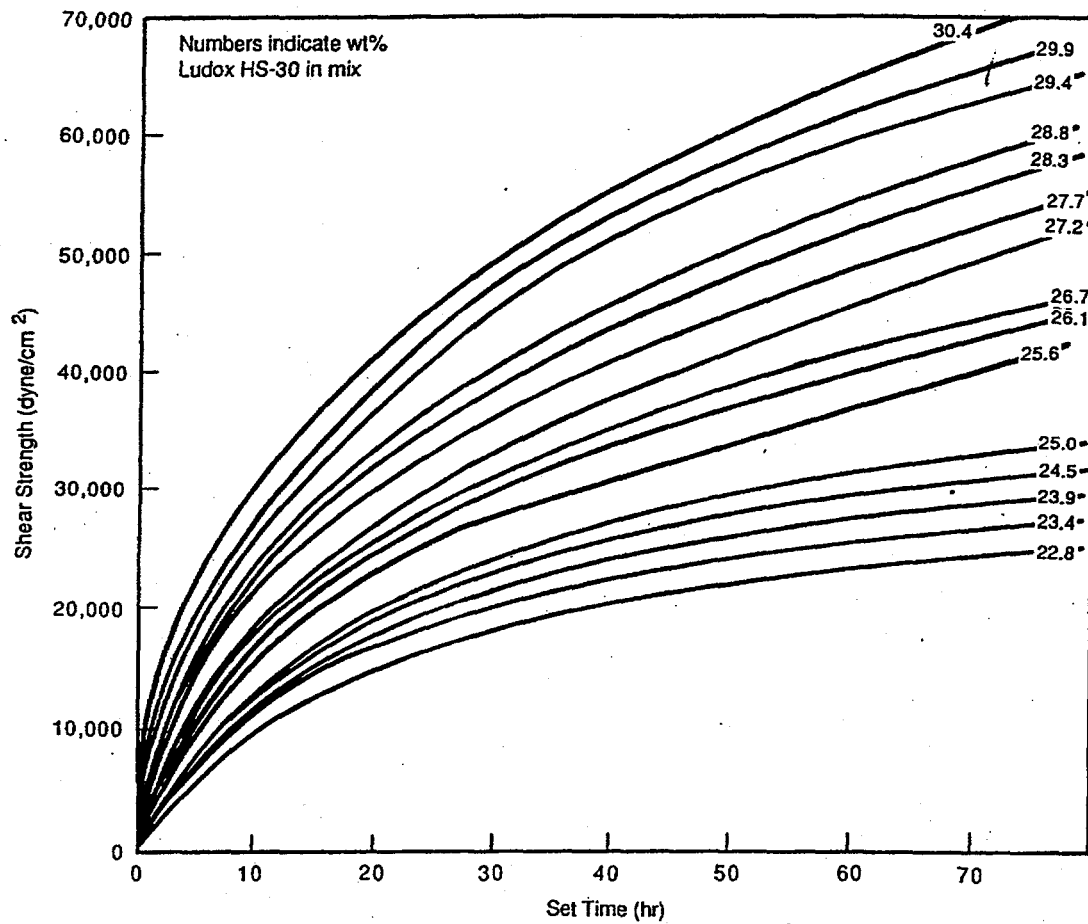


Figure 2.11. Strength Gain over Time as a Function of Ludox Content

**Table 2.5. Kaolin/Ludox Sludge Simulant Properties**

Composition	Target Shear Strength (kPa)	Measured Shear Strength (kPa)	Bulk Density (kg/L)
48.6% kaolin 17.0% Ludox 33.7% water 0.71% NaCl	≈ 10.0 ≈ 10.0	8.0 ± 2.0 (24 h) 8.3 ± 1.4 (48 h)	1.50
47.4% kaolin 25.0% Ludox 26.9% water 0.69% NaCl	≈ 23 ≈ 30	47.4 ± 2.3 (24 h) 64.2 ± 2.3 (48 h)	1.50
47.1% kaolin 27.0% Ludox 25.2% water 0.69% NaCl	≈ 30 ≈ 40	75.8 ± 4.2 (24 h) 95.2 ± 5.3 (48 h)	1.50

Using this algorithm, the composition for a kaolin/Ludox sludge simulant will be determined. The bulk density of the simulant will be 1.50 g/cm<sup>3</sup>. Shear strength data for several kaolin/Ludox compositions are shown in Table 2.5 below. For two of the compositions shown in the table, the target shear strength differs significantly from the measured shear strength. The reason for this difference is not known, but was likely due to a variation in the simulant preparation procedure and/or variations in the quality of the Ludox used.<sup>(a)</sup> When designing future kaolin/Ludox simulants, it is recommended that the above equations be used to establish a preliminary composition, the properties of which should then be verified.

### 2.1.8 Silica/Soda Ash Sludge Simulants

The first sludge simulant used for scaled mixer pump testing at Hanford was silica/soda ash. Mixtures of silica and soda ash solution were used in 1/12-scale sludge mobilization tests in fiscal year 1987 (see Powell et al. 1997).

This simulant is a mixture of Min-U-Sil<sup>®</sup> 30 (U.S. Silica, Pacific, Missouri) silica powder and a nearly saturated sodium carbonate (soda ash) solution. Min-U-Sil<sup>®</sup> 30 is composed of ground quartz silica particles with a number average particle size of 1.25 μm and a volume-average size of 13.5 μm. The number-average particle size distribution is shown in Figure 2.12. The "30" in the product name indicates that 95 wt% of this material is smaller than 30 microns.

(a) Ludox properties can be significantly altered by exposure to freezing weather. It is not known whether the Ludox used for the Table 2.5 samples had been affected in this way.

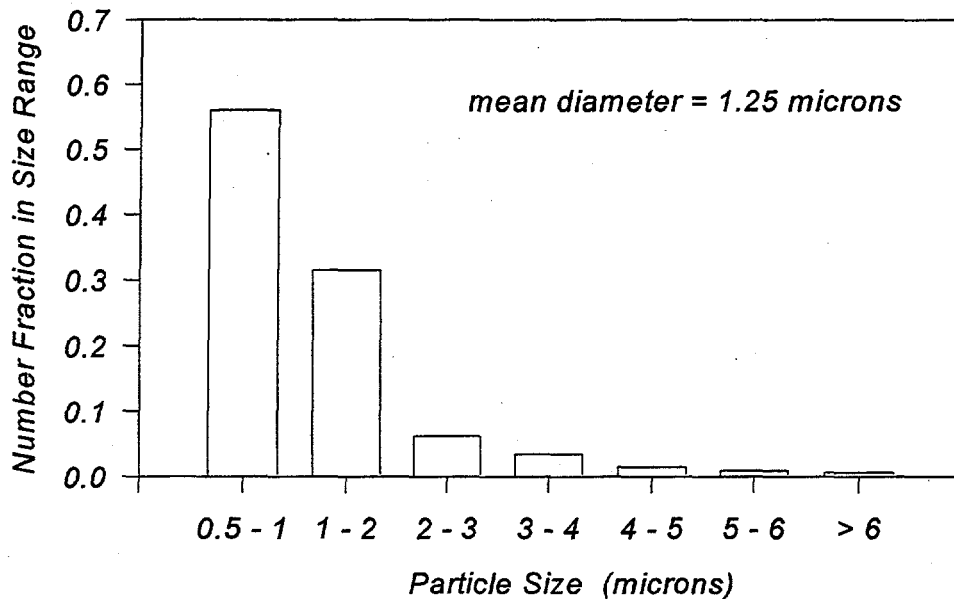


**Figure 2.12.** Brinkmann Particle Size Distribution for Min-U-Si® 30 Silica

The mechanism of shear strength development in the silica/soda ash simulant is not fully understood, but it clearly involves some sort of chemical reaction between the silica particles and the soda ash solution.<sup>(a)</sup> Mixtures of silica with sodium chloride and sodium hydroxide at the same pH and cation concentration as the soda ash solution do not exhibit the linear shear strength development with time as does the silica/soda ash simulant. It is speculated that the silica/soda ash strength-development reaction may involve the formation of low solubility salts (e.g., sodium silicate) that precipitate near the interparticle contact points because of surface curvature effects on solubility. This type of strength development reaction is one possible mechanism for strength development in tank wastes.

The shear strength for silica/soda ash can be decreased to near zero by vigorous mixing. Mixing destroys the bonds and/or salt crystals that have formed between particles. A similar sensitivity to disruption has been observed in the testing of tank waste samples. Further, the shear strength of silica/soda ash decreases with increasing temperature. While this can be problematic in some testing applications, there is evidence that some waste samples exhibit similar behavior (see Figure 2.13).

---

(a) Powell, M. R. 1993. *Fiscal Year 1992 Laboratory-Scale Sludge Mobilization Simulant Testing*. Letter report for Westinghouse Hanford Company, Pacific Northwest Laboratory, Richland, Washington.

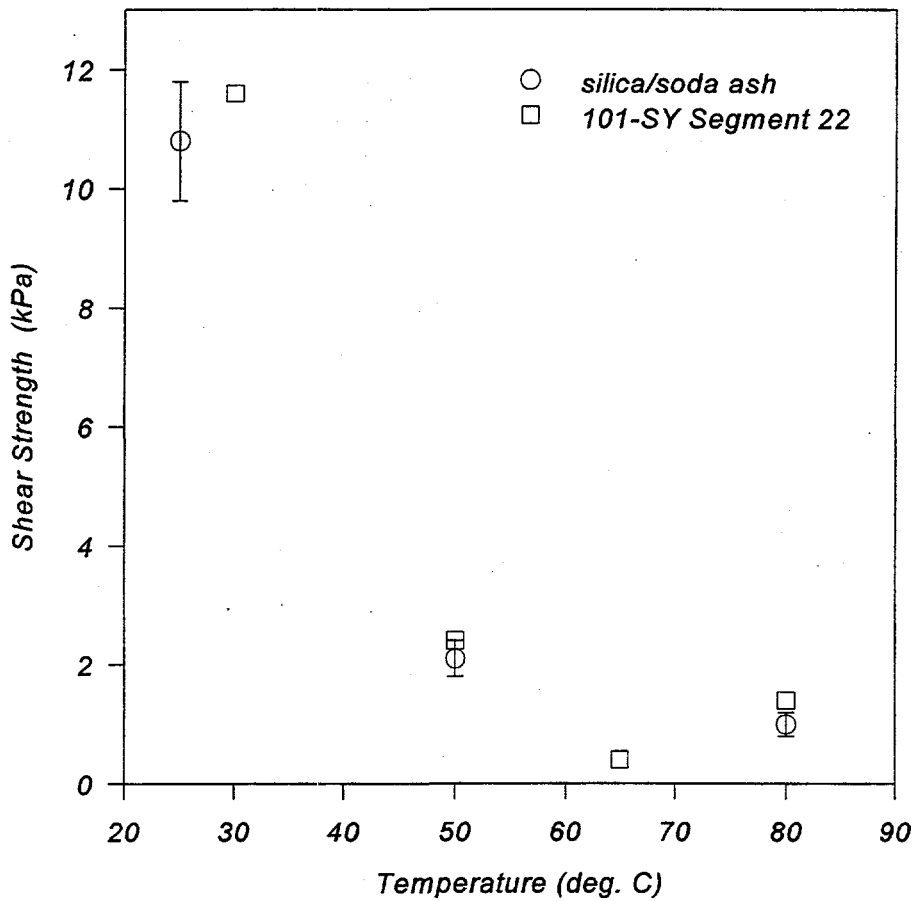


**Figure 2.13.** Shear Strength vs. Temperature for Silica/Soda Ash and 101-SY Sludge

**Notes:**

Silica/soda ash data taken from Powell, M. R. 1993. *Fiscal Year 1992 laboratory-Scale Sludge Mobilization Simulant Testing*. Letter report prepared for Westinghouse Hanford Company by the Pacific Northwest Laboratory, Richland, Washington.

101-SY Segment 22 data taken from Tingey, J. M. 1992. *Rheological Properties of Waste from Tank 101-SY*. Letter report for Westinghouse Hanford Company by Pacific Northwest Laboratory, Richland, Washington.

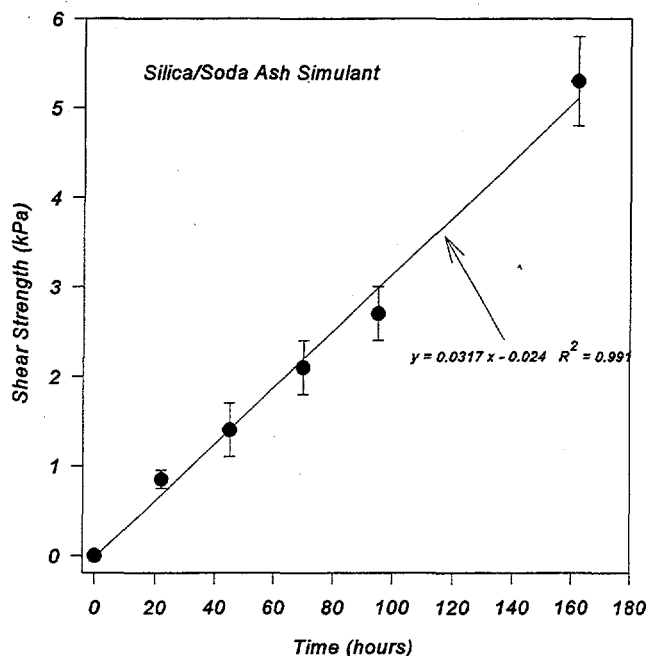


**Figure 2.14.** Silica/Soda Ash Shear Strength Development with Time

A plot of shear strength versus time for the silica/soda ash simulant is given in Figure 2.14. The relatively slow shear strength development makes this simulant an impractical choice when schedules demand a high shear strength simulant that can be tested within a day or two after it is prepared. It was for this very reason that a different sludge simulant was developed for the 1/12-scale sludge mobilization tests in fiscal year 1988 (see Section 3.1.2.5).

The composition of the silica/soda ash simulant is given in Table 2.6. This same composition was used for all the fiscal year 1987 1/12-scale sludge mobilization experiments. The sludge shear strength was varied simply by varying the amount of time between simulant preparation and testing. Density of the silica/soda ash simulant is constant at 1.82 g/cm<sup>3</sup>.

**Table 2.6.** Silica/Soda Ash Simulant Composition

Material	Concentration (wt%)
Min-U-Sil® 30 Silica	61.8
sand	3.2
soda ash (Na <sub>2</sub> CO <sub>3</sub> )	5.8
water	29.2

## 2.2 Hardpan Waste Simulants

Many Hanford tanks are known to contain a layer of sludge-like material that has solidified. Layers of hard sludge were encountered during past tank-slucing campaigns. The sluice jets were found to be largely ineffective at removing this layer of "hardpan" waste. In some cases, the hardpan layer could be sluiced if fresh water was used as the sluice stream. It was hypothesized that some of the hardpan layers were composed of insoluble sludge particles and crystals of sodium uranyl carbonate (Rodenhizer 1987). In other tanks, the sludge has been allowed to dry and, in some cases, reach temperatures in excess of 100°C. Bonding reactions between adjacent sludge particles are accelerated at higher temperatures and when the sludge is dried. It is postulated that these reactions have resulted in the formation of very hard sludge in some tanks. No samples of high-strength sludge have yet been obtained and characterized, so the extent to which these reactions may have affected the waste can only be speculated.

### 2.2.1 Relevant Properties for Hardpan/Dried Sludge

Retrieval technologies are needed to recover the hardpan sludge wastes. Simulants have been developed to allow the evaluation of candidate retrieval technologies against simulated hardpan wastes. The recipes for these test materials are given in Section 2.2.3. The hardpan/dried sludge properties that control the performance of retrieval processes are not yet known.

It is hypothesized that waterjet-based and mechanical-cutting-based retrieval approaches for hardpan and dried sludge are most strongly dependent on the mechanical strength of the undisturbed waste. The sensitivity to disruption and waste density are also judged to be important, as both affect settling and the rate of slurry formation. Salt dissolution may also be important, but this effect cannot yet be adequately predicted so it has not been included in the hardpan simulants. The extent to which the hardpan wastes are soluble is not known. Because it is possible that at least some of the hardpan wastes are wholly insoluble, it was judged prudent to formulate nondissolving hardpan simulants. Retrieval rates obtained from testing these simulants may be lower than those that would be obtained from a partially soluble hardpan simulant. Testing of these materials is needed to establish whether or not all the relevant properties are addressed by the simulants.

The waterjet pressure required to induce mobilization of hardpan simulants was shown along with the sludge simulant data in Figure 2.1, which demonstrates the importance of sludge shear strength in determining the resistance of a sludge to sluicing or other low-pressure waterjet-based waste retrieval methods.

### 2.2.2 Hardpan Simulant and Waste Property Comparison

The development of defensible hardpan/dried-sludge simulants is hindered by the complete lack of physical property data from hardpan waste samples. Some defensibility, however, can be obtained if the waste simulants are designed to develop strength through the same (or similar) mechanisms that operate in the tank waste. For the purpose of the present and past simulant-development efforts, the mechanisms operating in the hardpan and dried sludge waste types were assumed to be the binding together of insoluble sludge particles by interstitial salt crystals (hardpan) and chemical bonding of sludge particles at their contact points.

The kaolin/plaster hardpan simulants described in Section 2.2.3 obtain mechanical strength via the formation of interlocking hydrated calcium sulfate crystals in the voids between kaolin clay particles. The strength of the cured simulant is controlled by adjusting the plaster concentration in the initial mix. The kaolin particles do not add significantly to the simulant strength, but instead serve to dilute the plaster (thereby limiting its strength) and to absorb the water that remains following the completion of the hydration reaction.

Because the strengths of the kaolin/plaster simulants are determined by the interlocking salt crystals, mixing this simulant (after it is cured) will greatly reduce its apparent strength. Mixing breaks down the calcium sulfate dihydrate crystals into small, non-interlocking pieces. The simulant strength remaining after extended mixing will be determined largely by the amount of free water that remains in the simulant mixed with kaolin clay. The simulants specified here have a relatively high water content to facilitate simulant preparation.<sup>(a)</sup> As a result, the hardpan simulant residual strength after disruption is quite low. The residual strength can be increased by increasing the fraction of kaolin (or, equivalently, decreasing the fraction of water) in the simulant recipe.

The tendency of a fluid or paste to experience a decrease in its apparent viscosity with continued mixing is called thixotropy. This type of rheological behavior is common in slurries that obtain their shear resistance via the formation of gel structures or the interlocking of particles and crystals. Sludge-like materials that develop mechanical strength using these mechanisms are expected to be thixotropic. Materials that develop strength exclusively via interparticle attractive forces (e.g., van der Waals attraction) and interparticle friction are expected to not exhibit significant thixotropy.

The hardpan/dried sludge in the Hanford waste tanks is expected to develop its mechanical strength via a combination of interparticle attractions, friction, interlocking salt crystals, and chemical reactions at particle contact points. Mechanical disruption of this waste, then, should result in a decrease in its strength. The tank hardpan/dried sludge should exhibit some degree of thixotropy. The extent to which the strength is reduced by the disruption will depend on the fraction of the strength that is due to disruptable forces (e.g., interlocking salt crystals and interparticle reactions). Since these relative fractions are not yet known, the amount of thixotropy expected from tank waste is unknown. Adjustments to the relative fractions of kaolin and water, which control the residual strength, may be required as hardpan characterization data become available.

There are only two sources of semi-quantitative hardpan physical property data available. First, it has been noted that the Hanford past-practice sluicing jets were not capable of mobilizing the hardpan wastes at a significant rate. Second, samples of the hardpan layer have been described as having the "consistency of blackboard chalk" (Rodenhizer 1987).

Some Hanford past-practice sluicing campaigns were conducted using a flow rate of 300 to 350 gpm out of a 1-inch nozzle (Rodenhizer 1987). The nozzle pressure required to obtain this flow with

---

(a) The specified hardpan/dried sludge simulant recipes contain enough water to allow the preparation of these simulants with commonly available mixing equipment. Decreasing the fraction of water in the simulant increases both the cured shear strength and the uncured apparent viscosity. The water fraction can be reduced to increase the residual strength (reduce the extent of thixotropy), but a specialized paste mixer may then be required to prepare the simulants.

water is approximately 140 psig. It was found that the hardpan wastes in some tanks were capable of resisting the mobilizing force of these sluice jets. Accurate correlations between sludge strength and the jet pressure required to induce mobilization have not yet been developed. However, the tests described in Section 2.2 imply that the threshold impact pressure for mobilization is on the order of the sludge shear strength or perhaps a factor of 4 higher. The data in Figure 2.1 show that the kaolin/plaster hardpan simulants require a waterjet impact pressure of about 1.2 times the shear strength before significant mobilization occurs. It is not yet known why the bentonite and kaolin clay simulants follow a different relationship.

If the jet impact pressure exceeds the threshold pressure for mobilization, it is expected that mobilization will take place. Mobilization probably takes place at lower pressures as well, but it is not yet known how much lower these pressures may be. The sluice jets lose some of their impact force as the jet breaks up in the air before impacting the sludge. At a typical sluicing distance of 30 feet, for example, the remaining maximum jet impact pressure is approximately 22% of the nozzle pressure.<sup>(a)</sup> Since the 140 psig sluice jets were not capable of mobilizing the hardpan wastes, it seems reasonable that the minimum penetration resistance of the hardpan is probably around  $(0.22)(140 \text{ psi}) = 31 \text{ psi}$  (214 kPa). Assuming the relationship shown in Figure 2.1 between the threshold waterjet impact pressure and shear strength holds for the hardpan waste, the shear strength of the hardpan is estimated to be between  $(1/4)(31 \text{ psi}) = 7.8 \text{ psi} = 53 \text{ kPa}$  and  $(1/1.2)(31 \text{ psi}) = 25.8 \text{ psi} = 178 \text{ kPa}$ .

As mentioned above, the hardpan waste has been described as having the "consistency of blackboard chalk." The shear strengths of two different brands of blackboard chalk were measured, using a direct-shear testing device. This device is pictured in Figure 2.15. Each 3/8-inch diameter piece of chalk was positioned within the shear tester, then weight was added slowly to the lower half of the tester until the chalk sample failed in shear. The average chalk shear strength was found to be 1720 kPa (250 psi). This is considerably greater than the shear strengths of the hardpan simulants described in Section 2.2.3. Whether the actual hardpan wastes are as strong as (or stronger than) the chalk samples is not known.

A sample of the hardpan layer in Hanford single-shell tank 106-C was obtained via rotary mode core sampling in 1986 (Weiss 1988). The bottom-most section of the core sample was a hard white material that did not break up under the action of a plastic "masher" (i.e., a hand-held device used in the preparation of mashed potatoes). The mechanical strength of this material, which is presumed to be the hardpan, has been described as being similar to that of frozen margarine.<sup>(b)</sup>

Shear strength measurements were performed on several brands of margarine that had been inside a freezer for three days (temperature of  $-18^{\circ}\text{C}$ ). A hand-held shear vane from ELE International, Inc. (Lake Bluff, Illinois; model CL-612 Hand Vane Tester) was used to make the measurements. To avoid disruption of the frozen margarine during vane insertion, the shear vane was inserted into the margarine with the margarine at refrigerator temperature ( $4^{\circ}\text{C}$ ). After 3 days in the freezer, the shear

---

(a) This is estimated using the empirical relationship between jet impact pressure and standoff distance given by Summers (1995).

(b) Personal communication with R. L. Weiss (July 28, 1997).

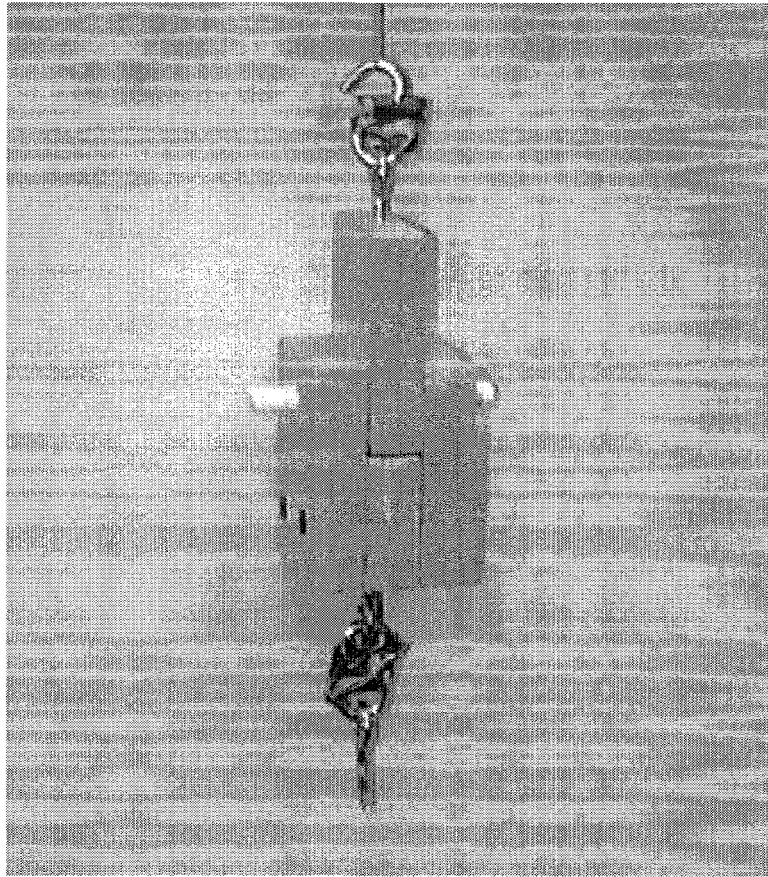


**Figure 2.15.** Photograph of Chalk Shear Strength Tester

strength was measured using the hand-held shear vane. Values ranging from 30 kPa to 70 kPa were obtained, depending on which brand of margarine was used. Based on these data, it is reasonable to expect that the C-106 hardpan has a shear strength of approximately 50 kPa.

It seems likely that the strength of the kaolin/plaster hardpan simulants described in Section 2.2.3 fall within the range of expected hardpan/dried sludge shear strengths, but it is possible that the hardpan simulants are weaker than the average hardpan waste. Whether this is the case cannot be determined until more hardpan characterization data are available.

### 2.2.3. Kaolin/Plaster Hardpan Simulants

Only a single type of simulant has been used to simulate the physical properties of hardpan wastes for the testing of retrieval systems. Mixtures of kaolin clay and plaster of Paris are used to simulate hardpan. The fraction of plaster of Paris used for the hardpan simulants is much higher than those of the sludge simulants described in Section 2.1.5.

Two hardpan simulant recipes, originally specified in Powell (1996), have been used for the testing of several different waste retrieval processes (Bamberger et al. 1997; Hatchell 1997). The compositions and properties of these simulants are given in Table 2.7 below.

**Table 2.7.** Kaolin/Plaster Hardpan Simulant Compositions and Properties

Material	Concentration (wt%)	Shear Strength (kPa)	Bulk Density (g/cm <sup>3</sup> )
kaolin clay	30.0	32 ± 6	1.56 ± 0.05
plaster of Paris	27.5		
water	42.5		
kaolin clay	40.0	150 ± 25	1.65 ± 0.05
plaster of Paris	22.5		
water	37.5		

The bulk densities given in the table are measured quantities, which agree reasonably well with the predicted densities from Equation 2.3.

The shear strengths given in Table 2.7 were measured after 24 hours of curing. As was noted in Section 2.1.5, the shear strength of kaolin/plaster simulants not only changes with time, but is sensitive to variations in the preparation procedure and conditions. Further, even though the cured hardpan simulants are relatively hard (the stronger hardpan can be walked upon), their strength will decrease when they are subjected to mixing or are otherwise disturbed. Consequently, insertion of a shear vane into the cured simulant can decrease the shear strength of the simulant surrounding the vane, which will result in the shear strength measurement being biased low. The preferred way to measure the shear strength of kaolin/plaster hardpan simulants is to insert the vane into the simulant before it cures. This method results in more reliable shear strength data.

The kaolin clay appears to have the unintended effect of causing the simulant strength to reach a peak and then decrease to a stable value. A plot of the 40% plaster hardpan simulant shear strength

versus time is shown in Figure 2.16. It is hypothesized that this behavior may be due to a cation exchange reaction between the plaster (calcium sulfate) and the naturally occurring sodium ions in the clay. Alternatively, the strength decrease may be due to disruption of the simulant structure by the small volume change that accompanies the hydration of plaster. While interesting, this tendency is not expected to be relevant to the simulant defensibility.

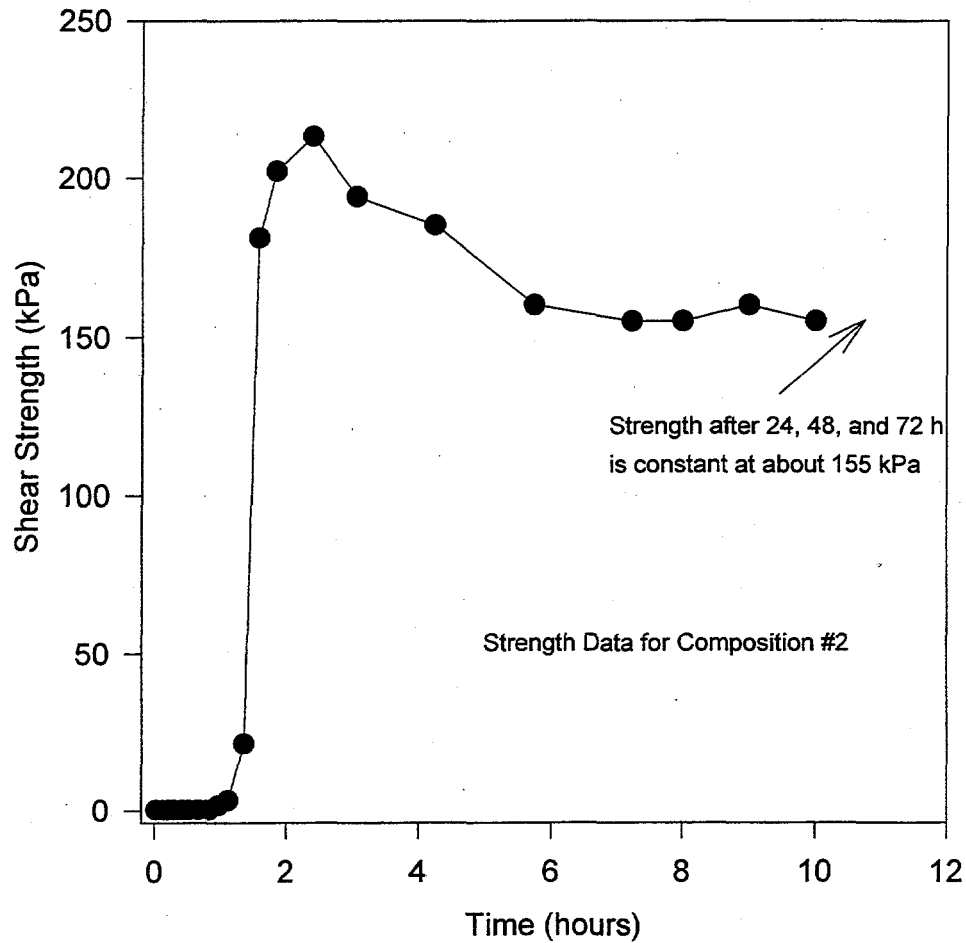


Figure 2.16. Shear Strength vs. Time for 40% Plaster Hardpan Simulant

## 2.3 Saltcake Waste Simulants

The saltcake present in the Hanford tanks consists largely of sodium salts of nitrate, aluminate, nitrite, carbonate, phosphate, hydroxide, and sulfate. The exact compositions vary according to which process generated the waste and according to the subsequent history of waste in each tank. These differences are expected to give rise to a wide variety of physical and chemical properties. The mechanical strength of the saltcake, for example, is expected to vary over a range of perhaps 2 or more orders of magnitude, depending on the saltcake composition and history.<sup>(a)</sup> Several different techniques have been proposed for saltcake retrieval at Hanford. These processes and the saltcake properties that determine the performance of these processes are described in this section. Composition and property data are also given for some of the saltcake simulants that have been used at Hanford.

### 2.3.1 Relevant Properties for Saltcake Retrieval

There are several saltcake properties known to influence the performance of saltcake retrieval systems. Which properties are most important, of course, depends on the type of retrieval process being considered. The performance of mechanical chopping techniques, for example, will be strongly dependent on the shear, compressive, and tensile strengths of the saltcake, but insensitive to the rate of saltcake dissolution. Waterjet-based techniques, however, are affected by saltcake dissolution rates as well as by selected mechanical strength and saltcake structure properties. The saltcake properties expected to have the greatest influence on several different saltcake retrieval techniques are discussed below.

A considerable effort has been made by EM-50 DOE to develop high-pressure, waterjet-based saltcake retrieval techniques (Rinker et al. 1996, 1997). Small diameter jets of high-pressure water (between 1,000 and 60,000 psi) are used to cut the hard saltcake materials into small chunks roughly 1 cm in size. The cuttings are gathered as they are produced by a vacuum-based air conveyance or jet-pump driven pumping system. The conveyance system gathers both the cuttings and the water from the waterjets so that significant amounts of water are not added to the waste. This is desired to minimize the chance that tank waste could leak from the tanks during retrieval.

The rate at which the high-pressure waterjets cut hard saltcake is thought to be a function primarily of the salt crystal grain size, bulk porosity, pore connectedness, and tensile strength. Other factors that may be important include salt solubility,<sup>(b)</sup> dissolution rate, and fracture toughness. This list

---

(a) Some chemically simulated saltcake has been found to have compressive strengths as high as 28 MPa (4000 psi) (Wanner 1993). Samples of hard saltcake have not been taken from the tanks and analyzed to verify this estimated strength. Samples of soft saltcake, however, have been described as having a "snow-cone" consistency, which would imply a very low compressive strength (i.e., < 10 psi).

(b) Recent testing at the University of Oklahoma implies that the dissolution of the K-Mag saltcake simulants may be significant during high-pressure (1 to 5 kpsi) waterjet cutting (*Performance Analysis of Water-Jet Cutting Technology on Saltcake Erosion as a Function of Temperature, Pressure, and Stand-off Distance*. Baeza, Scopel, and Gremillion of the University of Oklahoma. December 14, 1995). Increasing the temperature of the waterjet fluid was found to increase the rate of cutting. Whether this is due solely to enhanced K-Mag dissolution kinetics or to other, less obvious factors is not yet known. For

of physical and chemical properties was developed through consultation with waterjet cutting experts and a consideration of the physics of waterjet cutting. A detailed discussion of the reasons for selecting each of these properties is given in Golcar et al. (1997).

To better understand the relationship between saltcake properties and waterjet cutting, tests were conducted in which a variety of hard saltcake simulants were subjected to high-pressure waterjets. This work, which is described in Section 4.0, is being used to establish correlations between waterjet cutting and selected physical properties of saltcake simulants.

Lower-pressure, waterjet-based saltcake retrieval methods are also receiving attention. It is currently planned that the waste in many of the Hanford single-shell tanks will be retrieved by sluicing. The baseline sluicer design uses a 2.5-cm (1-inch) diameter nozzle discharging liquid (either a dilute slurry or inhibited water) at an exit velocity of about 46 m/s (150 ft/s). This high volumetric flow, low-pressure technique will rely primarily on dissolution to effect the retrieval of hard saltcake. Softer saltcake wastes may be dislodged by the impacting jet in addition to dissolving.

The saltcake sluicing retrieval rate is expected to be a function primarily of the dissolution rate of the saltcake. The dissolution rate will likely be increased if the sluice jet is powerful enough to overcome the mechanical strength of the soft saltcake, but this is unlikely to occur for the hard saltcake. The dissolution rate of saltcake-like materials is a function of the saltcake composition, porosity, grain size, and grain shape, as well as the properties of the sluicing fluid (e.g., fluid composition, flow rate, and temperature [Helgeson et al. 1984; Aagaard and Helgeson 1982]).

A series of tests were performed in which the dissolution rates of several salts were measured as a function of temperature, grain size, and solvent composition. These test results provide a basis for designing soluble saltcake simulants by allowing us to defensibly simulate the dissolution rate of saltcake waste, which contains hazardous constituents such as sodium nitrate and nitrite, with less hazardous, non-regulated salts such as sodium chloride. The salt crystal dissolution rate tests are described in Section 5.0.

### **2.3.2 Saltcake Simulant and Waste Property Comparison**

Very little characterization of Hanford saltcake physical properties has been completed. Some chemical composition data have been developed based on a combination of measurement and process flowsheet analyses (e.g., Kupfer 1981), but physical property data are qualitative at best. No measurements of saltcake tensile strength, compressive strength, porosity, or fracture toughness have been made. However, the need to support retrieval system testing with defensible saltcake simulants remains. At present, only qualitative comparisons between simulant and saltcake properties can be made for most of the key properties discussed in Section 2.3.1. The quantitative and qualitative comparisons that can be made are described below.

---

example, the higher temperature waterjet fluid may have a reduced interfacial tension (between the saltcake and the water) or decreased viscosity, which will tend to improve performance by allowing the waterjet to penetrate into the saltcake pores more readily. It is not known whether water temperature effects are significant for > 5 kpsi waterjets.

## Mechanical Strength Properties

The physical properties of tank saltcake have not been measured, but it is suspected that there is wide variation in those properties (Krieg 1992). In-tank photographs and operational experiences indicate that some tanks contain relatively soft saltcake while others contain very hard saltcake. It has been suggested that the soft saltcake waste was formed when solids-laden evaporator effluent slurry was pumped into the tanks. The interstitial liquor was subsequently removed by pumping and evaporation, leaving a loosely bound matrix of salt crystals. The hard saltcake supposedly formed via a slow, in-tank crystallization that resulted as water evaporated from the liquid tank waste.

Much of the previous saltcake simulant work has been focused on the development of simulants for the hard saltcake wastes (Golcar et al. 1997). The potassium-magnesium sulfate (K-Mag) simulants described in Section 2.3.3 were developed for testing high-pressure waterjet-based retrieval methods. The retrieval systems being designed had to be robust enough to retrieve all waste types at the target waste retrieval rate successfully. Because the hard saltcake was judged to represent the greatest challenge to these high-pressure waterjet systems, an effort was made to develop a simulant for the hard saltcake. If the waterjet systems could be designed to handle the hard saltcake simulant, then it was expected that they would also be able to handle the other waste types (e.g., sludge, hardpan, soft saltcake).

To support the high-pressure waterjet system development, saltcake simulants similar to the hard saltcake waste were needed. No samples of hard saltcake were available for characterization, so the physical properties of some chemically based simulants were measured (Wanner 1993). The compressive strengths of these chemical simulants were used to establish the target compressive strengths for the K-Mag saltcake simulants. The chemical simulants could not be used directly because of the hazards and associated disposal costs. The 84% K-Mag simulant was developed to produce the target hard saltcake compressive strength of about 21 MPa (3000 psi).<sup>(a)</sup>

The 10 MPa (1500 psi) K-Mag simulants (88% and 75% K-Mag in water) were developed to allow testing of high-pressure waterjet-based retrieval methods on simulants with different mechanical strengths and porosities. The porosity of the 88% K-Mag saltcake is much greater than that of the 75% saltcake (Golcar et al. 1997). Developing an understanding of the hard saltcake physical properties that control high-pressure waterjet effects is an ongoing effort in the Retrieval Process Development and Enhancements Project (see Section 4.0).

The simulants made from rock salt and plaster of Paris (Section 2.3.4) were developed to provide test materials expected to be similar to the soft saltcake. No quantitative sample characterization data are available on which to base the target mechanical strength of soft saltcake simulants. There are recent indications that some of the soft saltcake may be soft enough to allow the emplacement of in-tank probes with a minimal amount of force. What this means in terms of measurable strength properties (e.g.,

---

(a) Wanner (1993) measured the compressive strengths of both chemical saltcake simulants and several K-Mag simulant samples. The K-Mag strengths reported by Wanner are considerably lower than those found by more recent testing at PNNL. The discrepancy is due to differences in the K-Mag curing procedure. Wanner allowed the samples to dry while curing, which decreased the extent of langbeinite hydration. Much lower compressive strengths resulted.

compressive strength) must be evaluated. However, there are qualitative descriptions indicating the soft saltcake is a very weak material ("slushy snow cone" consistency; Wong 1990). This qualitative description was used as the basis for selecting mechanical strength target values for the weak salt/plaster simulants.

### **Saltcake Dissolution Rate**

It must be stressed that the K-Mag simulants were not originally developed to model the dissolution characteristics of hard saltcake. The dynamics of high-pressure waterjet cutting were thought to be fast enough that dissolution would be of secondary importance compared to properties like tensile strength, granularity, porosity, and fracture toughness.<sup>(a)</sup> K-Mag simulants, however, do dissolve slowly and, therefore, may have some usefulness as simulants for high-volumetric-flow sluicing-based retrieval methods that rely on waste dissolution. The dissolution rate of K-Mag, however, is considerably slower than that of the sodium nitrate and nitrite salts that compose the bulk of the actual saltcake wastes.

Whether or not K-Mag simulants can be used to model actual hard saltcake dissolution is not yet known and requires further study. However, for retrieval methods that do not rely heavily on salt-dissolution effects (e.g., high-pressure waterjets or mechanical choppers/cutters), the K-Mag simulants are reasonable. Efforts are being made to identify materials that can be used to formulate representatively soluble simulants for hard saltcake. This effort is made more difficult by the requirement that the simulants not be too expensive to prepare and/or dispose.

It was desired that the soft saltcake simulant be highly soluble and porous (like soft saltcake waste) so that dissolution-based retrieval methods (e.g., sluicing) could be evaluated using this test material. For this reason, rock salt (sodium chloride) was used rather than the more slowly soluble sulfur K-Mag. The rock salt dissolution rate is apparently not affected appreciably by the presence of the plaster. As more plaster is added to the mix, a greater fraction of the salt-crystal surface area becomes coated with plaster, which would be expected to result in a decreased dissolution rate. Comparisons of the dissolution rates for the plaster/rock salt simulants and the untreated (no plaster) rock salt reveal that this effect is minor. The plaster coating is observed to flake away rapidly from the surface of the dissolving salt particles.

To demonstrate the differences in dissolution rates between saltcake constituents (e.g., sodium nitrate and nitrite) and the specified simulant materials, a series of dissolution tests were conducted by Powell (1996). These tests demonstrated that sodium nitrate and nitrite salts tend to dissolve somewhat faster than comparably sized grains of sodium chloride, but K-Mag simulants dissolve much more slowly than any of the sodium salts. More than 15 minutes was required to dissolve a sample of K-Mag saltcake simulant, while the sodium salt crystals dissolved in about a minute or less. Some of these differences can be attributed to differences in initial particle size, but it is clear that the dissolution rate of the K-Mag simulants is much slower than that expected for tank waste.

The testing by Powell (1996) also demonstrated that the plaster coating on the soft saltcake simulants (see Section 2.3.4) does not appreciably affect the dissolution rate. A sodium chloride rock salt

---

(a) The University of Oklahoma study mentioned earlier provides evidence that K-Mag dissolution may be significant for high-pressure waterjet-based retrieval techniques.

sample (no plaster) was found to dissolve completely in 297 seconds. The rock salt/plaster simulants dissolved in about the same length of time (290 seconds and 314 seconds for the 86% salt and 95% salt compositions, respectively).

The dissolution rate data imply that the rock salt/plaster saltcake simulant will dissolve more slowly than the sodium nitrate and nitrite salts that make up most of the saltcake waste. There are a couple of factors, however, that complicate a direct comparison of the rock salt and sodium nitrate/nitrite dissolution data. First, the saltcake waste particle sizes/shapes are not accurately known and, in some cases, the relevant saltcake-particle characteristics will be dependent on the type of retrieval system employed. Second, the dissolution rate of sodium nitrate and nitrite salts in water does not necessarily reflect the dissolution rate of these salts into the retrieval fluid. During sluicing operations, for example, the retrieval fluid will likely be at a high pH and contain other dissolved salts. The common-ion effect on solubility is expected to decrease the dissolution rate of saltcake, compared to what would be measured if clean water was used as the retrieval fluid.

There are indications<sup>(a)</sup> that the size of some saltcake crystal particles range from about 0.2 mm to 0.6 mm. If this characterization is accurate, the saltcake dissolution rate into water is expected to be faster than that of the rock salt/plaster simulants. When salt-laden or high pH fluids are used to dissolve the waste, the saltcake dissolution rate is expected to be reduced by the common-ion effect on solubility. Whether the dissolution rate is significantly affected will depend on the dissolving fluid composition. The effects of salt crystal size and dissolving fluid composition are discussed further in Section 5.0.

Based on the data by Powell (1996), it is likely that the soft saltcake dissolution rate in high pH fluids will be greater than that exhibited by the rock salt/plaster saltcake simulants in water. The larger particle size and lower solubilization rate of the rock salt simulants (compared to sodium nitrate) result in a dissolution time in water roughly 3 times that of the sodium nitrate in 4 molar NaOH. Thus, it is expected that dissolution-based retrieval of the rock salt/plaster simulants will yield somewhat slower retrieval rates than the actual soft saltcake. The magnitude of the difference will depend largely on the actual particle size and porosity of the soft saltcake and on the composition of the dissolving fluid. It seems likely, though, that the rock salt/plaster simulants can provide an order-of-magnitude (or better) estimate of the soft saltcake retrieval rate.

### Porosity

The porosity of Hanford saltcake has not been measured, but estimates range between 10% and 50% (Krieg 1992). Porosity measurements of the K-Mag saltcake simulants have been made using a mercury porosimeter. The K-Mag porosity is found to vary between about 10% and 20%, depending on the water content in the initial mix. The porosity of the rock salt/plaster saltcake simulants (compositions 4 and 5) is estimated to be approximately 40% based on the known plaster, salt, and simulant densities. The K-Mag saltcake simulants are near the lower end of estimated saltcake porosities, and the rock salt/plaster simulants are near the upper end.

---

(a) Janicek, G. P. 1981. *Equipment Development Study for Hydraulic Recovery of Single-Shell Tank Sludges*. RHO-CD-1533. Letter report prepared for the U.S. Department of Energy by Rockwell Hanford Operations Energy Systems Group, Richland, Washington.

### 2.3.3 Hard Saltcake Simulants (K-Mag)

The hydration chemistry of potassium-magnesium sulfate (K-Mag) and its relationship to the physical properties of the saltcake simulants has been extensively studied as part of the EM-50 simulant development efforts. For a detailed discussion of the chemical and physical properties of K-Mag saltcake simulants see Golcar et al. (1997).

Table 2.8 gives the physical properties of eight different K-Mag simulant compositions. The compressive strength data are plotted versus water content in Figure 2.17, which shows that the peak compressive strength occurs at around 86 wt% K-Mag. Porosity and average pore size data obtained by a mercury intrusion method are plotted in Figures 2.18 and 2.19. The variations in compressive strength and porosity with water content are discussed in Golcar et al. (1997).

**Table 2.8. Hard Saltcake Simulant (K-Mag) Compositions and Properties (from Golcar et al. 1997)**

Composition	Bulk Density g/cm <sup>3</sup>	Porosity %	Compressive Strength MPa (psi)
10 wt% water 90 wt% K-Mag	2.08	17.2	9.8 (1420)
12 wt% water 88 wt% K-Mag	1.94	18.9	18.1 (2620)
14 wt% water 86 wt% K-Mag	2.22	10.5	29 (4140)
16 wt% water 84 wt% K-Mag	2.25	13.7	19 (2750)
18 wt% water 82 wt% K-Mag	2.19	14.8	15 (2190)
20 wt% water 80 wt% K-Mag	2.27	6.8	15 (2220)
25 wt% water 75 wt% K-Mag	2.56	12.5	13 (1840)
30 wt% water 70 wt% K-Mag	2.33	4.0	12 (1720)

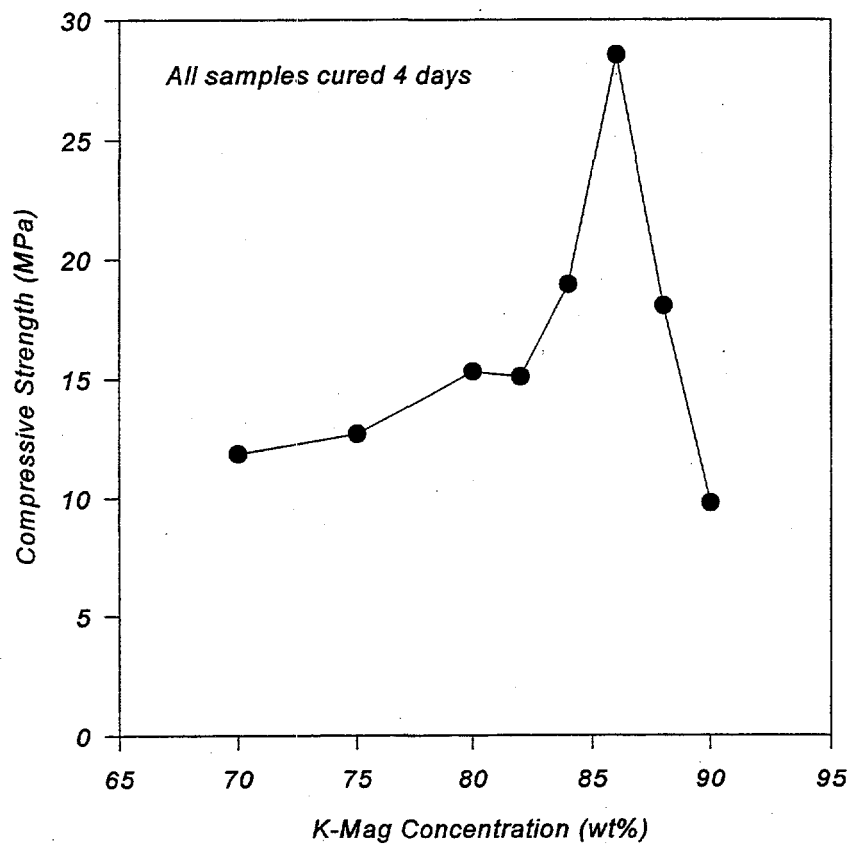


Figure 2.17. Hard Saltcake Simulant (K-Mag) Compressive Strengths

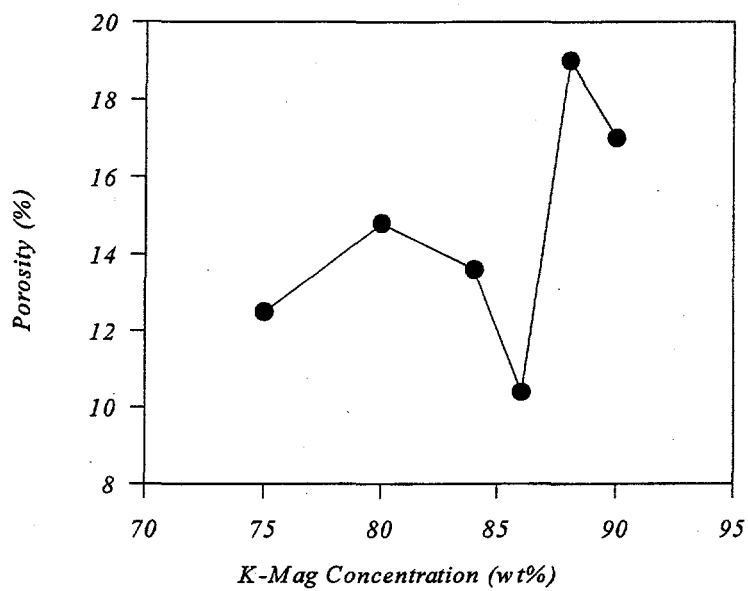


Figure 2.18. K-Mag Porosity vs. Concentration

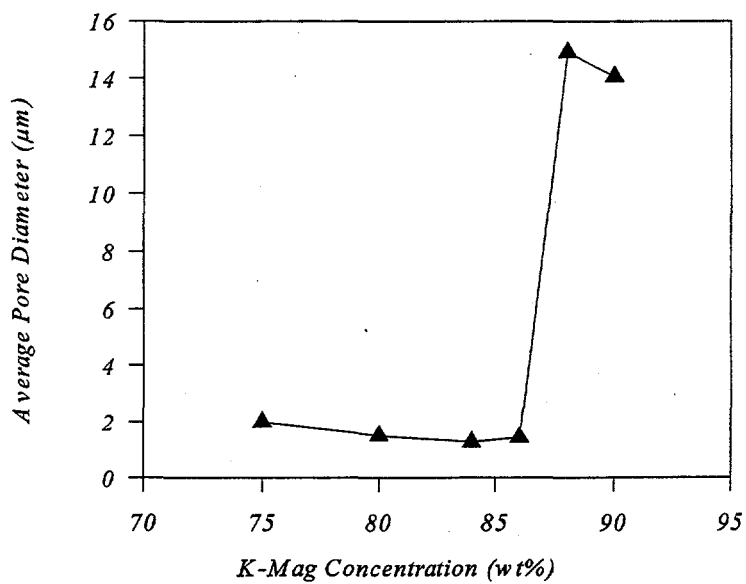


Figure 2.19. K-Mag Average Pore Diameter vs. Concentration

### 2.3.4 Soft Saltcake Simulants

The soft, soluble saltcake simulant compositions and properties are given in Table 2.9 below. The mechanical strength is increased by increasing the ratio of mixed plaster of Paris slurry to rock salt. A constant 2:1 ratio of plaster of Paris mass to water mass is maintained in the preparation of the plaster slurry.

**Table 2.9.** Soft Saltcake Simulant Compositions and Properties (from Powell 1996)

Composition wt%	Density g/cm <sup>3</sup>	Porosity %	Compressive Strength kPa (psi)
86.0% NaCl rock salt 9.33% plaster of Paris 4.67% water	1.20 ± 0.05	45%	48 (7)
90.0% NaCl rock salt 6.67% plaster of Paris 3.33% water	1.20 ± 0.05	46%	31 (4.5)
95.0% NaCl rock salt 3.33% plaster of Paris 1.67% water	1.20 ± 0.05	47%	10 (1.5)

The specified simulants have very low compressive strengths, as shown in Table 2.9 and in Figure 2.20.<sup>(a)</sup> These strengths are low enough that it is likely a directly impinging sluice jet will effect mechanical disruption of the simulants. As is the case with all the plaster of Paris-based simulants, some variability in the simulant properties is expected with changes in the simulant preparation method and conditions. The properties of these simulants should always be measured before testing commences.

### 2.4 Supernatant Liquid and Slurry Simulants

Efforts have been made to develop simulants specifically for the purpose of studying the transport of waste slurries in pipelines. Long-distance waste transport is of concern at all the DOE waste sites, but particularly so at Hanford where some wastes must be transported through a six-mile-long pipeline for processing. Both chemical simulants (e.g., Fow et al. 1986a, 1986b; Carleson et al. 1987) and physical simulants (Reynolds et al. 1996) have been formulated for rheological and pipe-loop testing.

For the development and testing of most waste retrieval methods, however, the properties of the waste slurries and supernatant liquids are of secondary importance. The greater challenge is usually the initial mobilization and breakup of the waste solids. Waste slurry properties can be important for evaluating how readily the mobilized waste is transported to the inlet of a waste transfer pump, but this

---

(a) The 5% plaster/95% rock salt simulant is weak enough that samples of this simulant must be handled carefully. Even light pressure can cause the sample to crumble.

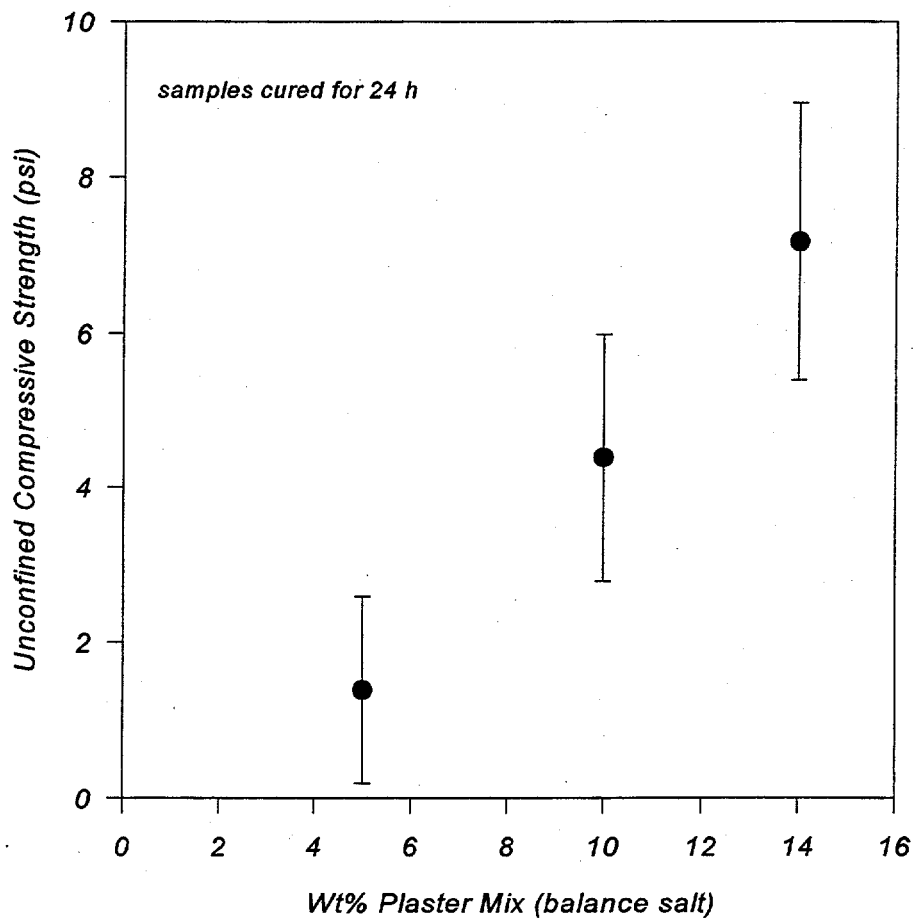


**Figure 2.20.** Compressive Strength of Salt/Plaster Simulants

problem is usually considered when designing the sludge and saltcake simulants (see Section 2.1.1). Because waste slurry properties are of reduced importance for retrieval system development and testing, slurry and supernate simulants will not be discussed further in this document. Refer to Reynolds et al. (1996) and Hudson (1996) for descriptions of slurry simulants and their relationship to tank waste.

## 2.5 Miscellaneous Waste Simulants

Not all of the waste simulants needed to support retrieval system development and testing fit within one of the categories of sludge, hardpan, saltcake, or slurry/supernate. Three such cases are briefly described in this section.

### 2.5.1 ORNL Tank Gunitite Simulant

As part of the waste retrieval and tank closure operations at ORNL, it is planned that a high-pressure scarifier will be used to remove roughly 1 cm of gunitite from the inside walls and floor of the Gunitite Tanks. To support the design of this high-pressure gunitite scarifier, tests were performed in which simulated ORNL tank gunitite was subjected to impinging high-pressure waterjets at various pressures and traverse rates (Mullen 1997).

Development of the simulated gunitite required that all available information on the original ORNL gunitite formulation be gathered. Unfortunately, very little information was available. It was known that a 3:1 ratio of aggregate to Portland cement was used, but no data describing the aggregate size distribution or the cement composition were found. Core samples were removed from a section of the dome of gunitite Tank W-10 and tested for compressive strength. The strengths ranged from about 10 to 16 kpsi, which are relatively high but not surprisingly so given the age of the gunitite.<sup>(a)</sup>

Unfortunately, no samples of gunitite taken from the tank wall or floor were available. There was some concern that the strength of the tank walls and floor in contact with the waste may have been significantly degraded by sulfate attack (see Lea 1971 for a description of sulfate attack on concrete). The extent of the degradation is unknown.

Based on the mechanisms by which high-pressure waterjets cut porous materials it was decided that the gunitite simulant should match the strength, aggregate size, and porosity of the original ORNL gunitite. No data were available to allow estimates to be made of the ORNL gunitite porosity (or pore sizes), and the gunitite aggregate size distribution was only specified as "fine sand." In addition to these physical properties, it was necessary that the simulant composition result in rapid strength development so that waterjet testing could proceed within 4 days of simulant preparation.

The aggregate to cement ratio was maintained at 3 to 1, a target compressive strength of 5000 psi was selected for the testing, and the aggregate size distribution was taken to be consistent with the ASTM C33 specification for "fine aggregate." The resulting simulant composition was

---

(a) Intra-Laboratory Correspondence Letter from D. J. Naus to J. D. Huggins dated August 27, 1981. Union Carbide Corp. Nuclear Division, Oak Ridge, Tennessee.

22.16 wt%	type III Portland cement
66.47 wt%	fine aggregate (ASTM C33)
11.08 wt%	water
0.29 wt%	Pozzutec™ 20 admixture accelerant

Type III Portland cement is formulated to cure such that it reaches a useable strength quickly. The Pozzutec™ 20 admixture accelerates the curing of the cement even further.

This gunite simulant was used for some of the gunite waterjet cutting tests, but some problems with consistent strength development necessitated an increase in the quantity of Pozzutec added to each batch (Mullen 1997).

Because the aggregate size distribution is known to significantly influence the ability of a high-pressure waterjet to cut concrete and gunite, efforts were made to develop a technique for estimating the aggregate size distribution from a sample of cured gunite. Several small chips from a block of gunite simulant were cut, polished, and subjected to an microscopic image analysis technique to determine the aggregate size distribution visible on the cut surface. A photograph of one of the surfaces is shown in Figure 2.21. The aggregate size distribution, however, is not identical to the visible size distribution because smaller particles are less likely to be present in any given cross section. Using a technique described in Powell and Mahalingam (1992), the size distribution given by the cross section was corrected to give an estimate for the true aggregate size distribution. A comparison of this estimated size distribution with the measured (by sieve analysis) size distribution is shown in Figure 2.22.

This technique was judged to be likely to yield a sufficiently accurate aggregate size distribution from the analysis of a small piece of cured gunite. Unfortunately, the available ORNL gunite tank samples were radioactively contaminated and could not be released to an area where this analysis could be done. If the need to determine the gunite aggregate size distribution arises again in the future, this technique should be revisited.

Compressive strength development as a function of time for the composition given above is shown in Figure 2.23. The target compressive strength was reached after about 3 days, which allowed waterjet testing to proceed according to the required schedule.

### **2.5.2 Savannah River Site Tank 19 Zeolite Heel Simulant**

A 1980 waste retrieval campaign in Tank 19 at the Savannah River Site left a significant quantity of waste remaining in the tank. This waste heel consists primarily of zeolite particles, sludge, and saltcake. A simulant for this waste heel was requested so that various waste sampling methods could be evaluated. A physical property simulant was developed for the Tank 19 zeolite heel based on the chemical analysis of a sample from Tank 19 and on hypothesized strength development mechanisms. To better illustrate the simulant development process, this effort is described in detail in the Appendix.

The recommended waste simulant was prepared from plaster of Paris, sand, kaolin clay, and water. This simulant was used to test the sludge sampling device before waste samples were taken from Tank 19.

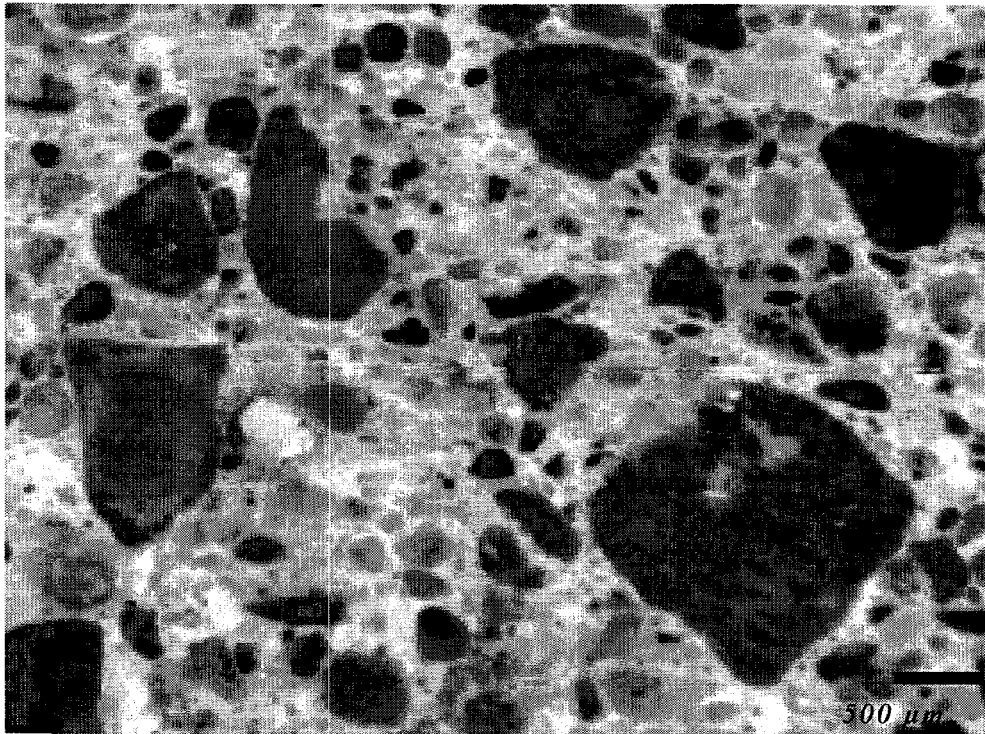


**Figure 2.21.** Microscope Photograph of Aggregate

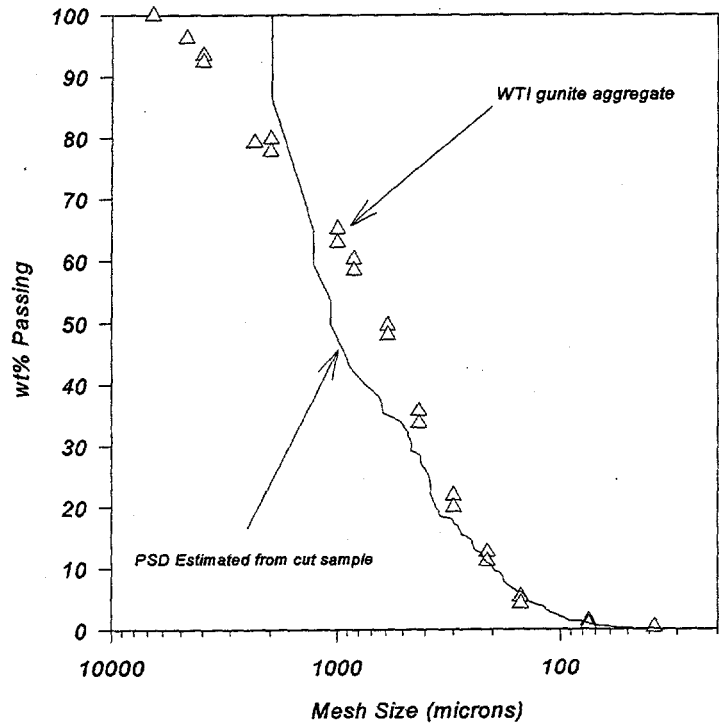


Figure 2.22. Aggregate Size Distribution for ORNL Gunite Simulant

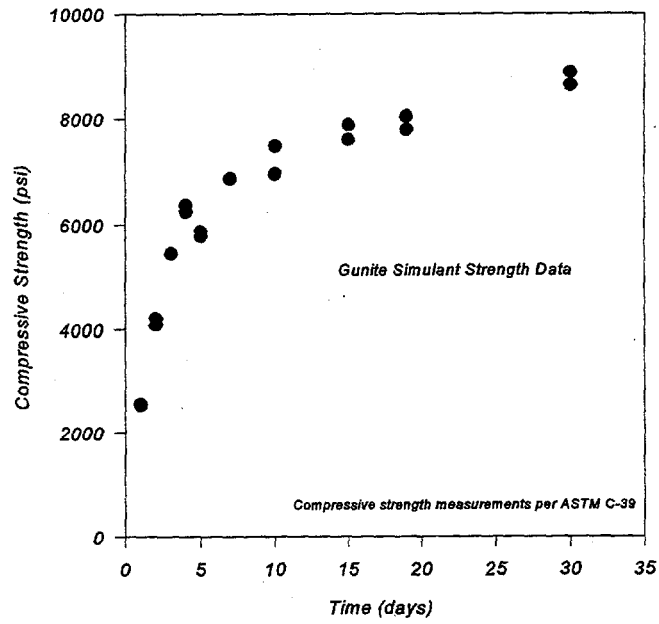


Figure 2.23. Compressive Strength of ORNL Gunite Simulant vs. Time

### 2.5.3 Tar-Like Substance Simulant Development for INEEL End-Effector Testing

Johnson et al. (1997) developed and tested a medium-pressure waterjet-based waste retrieval device designed to remove waste from the high-level waste tanks at the Idaho National Engineering and Environmental Laboratory (INEEL). This device was called the confined sluicing end effector (CSEE). The waste simulants used in the CSEE testing were developed as described in this section.

During the inspection of a radio frequency (RF) probe in one of the INEEL radioactive waste storage tanks, a quantity of black, tar-like material was observed clinging to the probe surface (Barnes 1994). Because this material did not readily wash away, there is some concern that removal of this material may be difficult. To evaluate the ability of the INEEL CSEE to retrieve this tar-like substance, a series of tests were run using a prototype CSEE and a material designed to simulate the relevant properties of the tar-like material.

Unfortunately, there is very little information regarding the nature of the tar-like material. In fact, aside from its being black, it is not clear whether the material actually possesses any of the physical properties typically associated with tar (e.g., sticky and highly viscous). It is unknown how much of this material might be in the waste tanks and its chemical composition is not known. The only evidence for its existence comes from the observations made during the RF probe inspection. The tank farm workers performing the inspection did not attempt to touch the material, so very little can be inferred about its mechanical properties. It was noted that the substance *looked* like tar and that it did not wash off the RF probe under the action of the 550 kPa (80 psi) spray-ring waterjets (Barnes 1994). This implies that the material can adhere to surfaces - at least to an extent sufficient to resist the waterjets used during the RF probe inspection.

The lack of any quantitative physical or chemical characterization data for this tar-like substance makes the development of a defensible waste simulant extremely difficult. With no target values for the relevant properties, it cannot be established whether a candidate waste simulant has properties in the range expected for the actual waste.

For the purpose of CSEE testing, it was desired that a simulant for the tar-like material be identified. It was desired that this simulant cover the range of relevant physical and chemical properties expected in the actual waste. Because so little is known about the tar-like material properties, however, a "bounding" set of simulants would need to be very challenging to the CSEE performance. In this case, no clear upper bound on the strength of the tar-like substance can be inferred based on the available data. As a result, a "bounding" simulant would be extremely strong and resistant to the CSEE waterjets.<sup>(a)</sup>

An alternative approach is to make assumptions about the nature of the tar-like substance and then proceed to develop a simulant that may be representative of the tar-like waste material. This is a more risky strategy because, if the assumptions are incorrect, the CSEE may perform adequately on the

---

(a) It is the upper bound on the tar-like material's strength that is important for simulant development. The magnitude of the lower bound on its strength may be inferred from the fact that the waterjets used during the RF probe inspection did not wash away the material. However, the lower-bound strength is of limited interest for CSEE testing because the CSEE must be designed and operated such that it can retrieve material that is stronger than the lower-bound strength (which, by definition, the actual waste is).

"representative" simulant but not adequately on the actual waste. To be successful, this approach requires that the assumptions made about the waste be carefully reviewed as more waste characterization data become available. Should future waste characterization data invalidate any of the assumptions, the results of any CSEE testing using simulants must be reviewed to assess their validity. This alternative approach is the one used here.

Based on the qualitative description of the tar-like substance, it is assumed that asphalt (i.e., road tar) has analogous physical properties. Asphalt is a mixture of hydrocarbons that is solid or semi-solid with a very high viscosity at room temperature. Asphalt is not water soluble and it adheres well to a variety of materials including steel. However, safety and regulatory concerns did not permit asphalt to be used as a simulant for the tar-like material during CSEE testing.

Instead, it was decided that the tar-like substance would be simulated using a water-based roofing and flashing sealant that is sold under the trade name Patchworks™ (Masters Choice, Jamestown, New York). When cured, Patchworks™ forms a thin rubber coating that will resist impinging 550 kPa waterjets (Johnson et al. 1997).

The INEEL tanks contain a series of horizontal cooling pipes, which were assumed to be coated with some amount of the tar-like material. To simulate this, pipes of the same size and approximate surface roughness were coated with the Patchworks™ sealant. The sealant was then allowed to partially dry before the CSEE was used to clean the pipes. The CSEE tests revealed that even the partially dried Patchworks™ effectively resisted the scouring action of the waterjets under the simulated cooling coils.

An effort was made to develop a simulant for the tar-like substance that was weak enough for *some* of the simulant to be scoured from the underside of the simulated cooling coils. This was needed to allow the comparison of CSEE performance under a variety of different operating conditions (e.g., waterjet pressures, traverse rates, and standoff distances). After some trial and error, it was decided that the simulated cooling coils would be coated with a low-melting-temperature wax and then given a thin coat of spray paint. The paint could be easily removed by touching the coated surface or by an impinging 550 kPa (80 psi) waterjet, so this simulant represented a very weakly bonded coating. Testing of the CSEE with this simulant revealed that no significant cleaning of the underside of the cooling coils could be expected using the CSEE (Johnson et al. 1997).

It had been postulated that an important mechanism for the removal of tar-like substances from the underside of the cooling coils is the abrasion of the pipe surface caused the waterjet-induced agitation of the surrounding slurry, which contains potentially abrasive particles. The particles in the INEEL waste storage tanks came from a waste calcining process. The calcine particles are reported to be 75% by weight larger than 45 microns (Barnes 1994). An upper-bound for the particle size is not known, but was assumed to be approximately 200 microns.

The abrasiveness of the calcine particles is not known, but efforts were made to bound the particle abrasiveness by creating simulants for the calcine material that bounded the particle size, particle density, and particle hardness of a sample of non-radioactive calcine. This is described further in Johnson et al. (1997).

## 3.0 Simulant Preparation and Characterization

The simulant recipes given in Section 2.0 will not always yield simulants with the expected properties. The properties of some simulants are sensitive to variations in the preparation procedure, while others are relatively insensitive. This variability can be reduced by strict adherence to the recommended simulant preparation procedures given in Section 3.1. Section 3.1.1 describes the preparation of simulants that are relatively insensitive to variations in preparation conditions and Section 3.1.2 addresses the simulants that are sensitive to preparation conditions.

The methods and standards used to characterize the waste simulants are described in Section 3.2. Brand names and manufacturers for the simulant materials are given in Section 3.3.

### 3.1 Simulant Preparation Procedures

The procedures used to prepare the waste simulants described in Section 2.0 are given in this section.

#### 3.1.1 Insensitive Simulants

Many of the waste simulants show relatively little sensitivity to changes in preparation procedure. These "insensitive" simulants are

kaolin/water  
bentonite/water  
bentonite/BaSO<sub>4</sub>/water  
bentonite/kaolin/water.

These simulants are prepared simply by mixing together the desired quantities of materials until a uniform mixture is obtained. No cure time is associated with these simulants and they may be used immediately after preparation or weeks afterward without significant changes in their properties provided that no water evaporates from the mixture.<sup>(a)</sup>

Any type of mixer that will result in a uniform product is acceptable for use with these simulants. Simulants with relatively high shear strengths ( $> 1$  kPa) may require the use of special mixing equipment designed for mixing pastes. PNNL uses a Littleford (Florence, Kentucky) paste mixer to prepare 20-gallon batches of high shear strength simulants. The Littleford mixer is pictured in Figure 3.1.

---

(a) These simulants should not be allowed to freeze as this will dramatically alter their properties. The simulants will also be affected by prolonged contact with water or salt solutions.

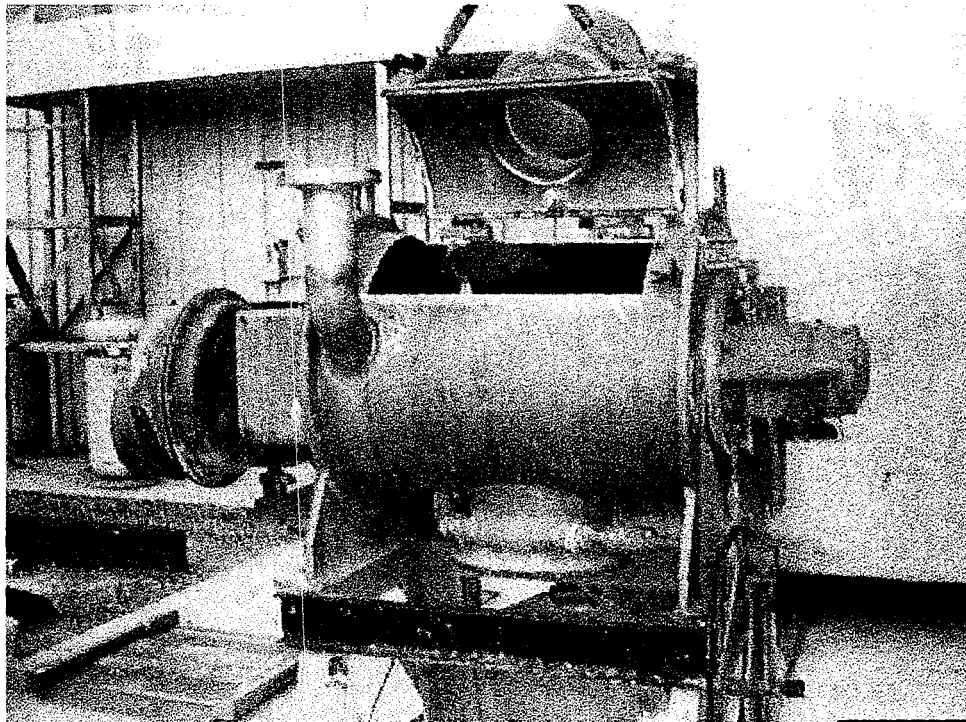


Figure 3.1. Littleford Paste Mixer at PNNL

### 3.1.2 Sensitive Simulants

The properties of the simulants listed in this section are sensitive to changes in the simulant preparation procedures.

The kaolin/plaster (both sludge and hardpan) and rock salt/plaster simulants must not be mixed any longer than necessary after addition of the plaster of Paris. Once the plaster of Paris comes in contact with the water, the hydration reaction begins. Prolonged mixing can hinder the growth of the gypsum crystals and this will decrease the cured strength of the simulant. High-shear mixers should not be used for preparing these simulants. Rolling-drum concrete mixers (see Figure 3.2) have provided suitable mixing for the kaolin/plaster, rock salt/plaster, and K-Mag simulants.

Kaolin/plaster sludge and hardpan simulant should be prepared as follows. The required quantities of kaolin and water are first mixed to form a uniform slurry. If large quantities are being prepared or if the ambient temperature exceeds about 20 °C, it is advisable to substitute ice for a portion of the water in the mix. This will ensure that the kaolin/water slurry is cold before the plaster of Paris is added. The plaster of Paris hydration reaction is greatly accelerated by elevated temperature, so premature curing of the simulant can occur if the slurry temperature is too high. This is especially problematic when large quantities of hardpan are being prepared. Once the kaolin/water slurry is uniform, the plaster of Paris should be added as rapidly as possible while continuing to mix. Batches should be sized so that the plaster of Paris is uniformly mixed into the slurry and the slurry is placed into its curing mold no more than about 10 minutes after the plaster of Paris is added. Mixing for longer periods can result in markedly lower strengths for the cured simulant.

Rock salt/plaster saltcake simulant is prepared by first mixing the plaster of Paris and water to form a uniform slurry and then adding the rock salt. Mixing should be continued only as long is necessary to ensure that the rock salt particles are uniformly coated with plaster of Paris. This simulant should not be prepared when the ambient temperature is high (i.e., greater than 25 °C).

The remaining waste simulants can be prepared without undue regard for the ambient temperature and they have less sensitivity to mixing time. Silica/soda ash, kaolin/Ludox, and the K-Mag saltcake simulants are prepared by mixing the components together until uniform and then the resulting slurry is placed in a mold to cure.

All the waste simulants must be covered to prevent water loss during curing.

## 3.2 Characterization Procedures

The simulant characterization procedures are described in the sections below.

### 3.2.1 Shear Strength

The shear strength of sludge and hardpan simulants is measured using a shear vane. This technique is a standard shear strength measurement method most often used in the characterization of soils. ASTM standard D4648-94 describes the proper use of shear vanes for shear strength measurement.



**Figure 3.2.** Rolling Drum Concrete Mixer

A vane (typically with 4 blades) is inserted into the sample to be tested. The maximum torque ( $T_{peak}$ ) required to slowly rotate a fully submerged vane is related to the sample shear strength ( $\tau_s$ ) according to the equation (Das 1983):

$$\tau_s = \frac{T_{peak}}{\pi \left( \frac{D_v^2 H_v}{2} + \frac{D_v^3}{6} \right)} \quad (3.1)$$

where  $D_v$  is the vane diameter and  $H_v$  is the vane blade height.

A photograph of the Haake M5 rheometer with a shear vane attached is shown in Figure 3.3. The Haake rheometer allows the accurate measurement of vane torque as the vane is rotated at a constant, slow rate equal to or less than 0.3 rpm. For field measurements, a hand-held shear vane (Model CL-612 from ELE International, Inc.) is used. The hand-held vane spring is calibrated to accurately read the vane torque, but it is difficult to maintain a steadily increasing torque and maintain the vane perfectly vertical. For this reason, the Haake system is preferred when accurate shear strength measurements are required.

### 3.2.2 Compressive Strength

Compressive strength of the saltcake simulants is measured using the ASTM C39 specifications for the compressive strength testing of concrete cylinders. It is preferred that samples for compressive and tensile strength testing be removed from the simulant bed using a core drill, but when this is not practical cylindrical test molds are filled at the time of simulant preparation. A photograph of a K-Mag simulant undergoing compressive strength testing is shown in Figure 3.4.

### 3.2.3 Tensile Strength

Tensile strength measurement for sludge simulants is difficult. No standard techniques have yet been developed, although several methods have been described in the soil mechanics literature (e.g., Nearing et al. 1991). PNNL has evaluated several tensile strength measurement techniques for sludge simulants.<sup>(a)</sup> The most practical method is vertical extrusion in which the simulant is extruded vertically downward out the end of a tube until a cylindrical piece breaks free and falls. The weight of the piece divided by the cross-sectional area of the tube equals the tensile strength. See Gauglitz et al. (1995) for a detailed description of this tensile strength measurement technique. Figure 3.5 is a photograph of the vertical extrusion tensometer and Figure 3.6 shows a sludge simulant being tested.

The tensile strengths of the hard saltcake simulants (K-Mag) are measured using the Brazilian Tensile Strength test, which is described by ASTM standard C496-96. Figure 3.7 is a photograph of a K-Mag sample undergoing the Brazilian Tensile Strength test.

---

(a) Powell, M. R. April 1994. *Devices for the Measurement of the Tensile Strength of Sludge Simulants*. Letter report prepared for Westinghouse Hanford Company by Pacific Northwest Laboratory, Richland, Washington.

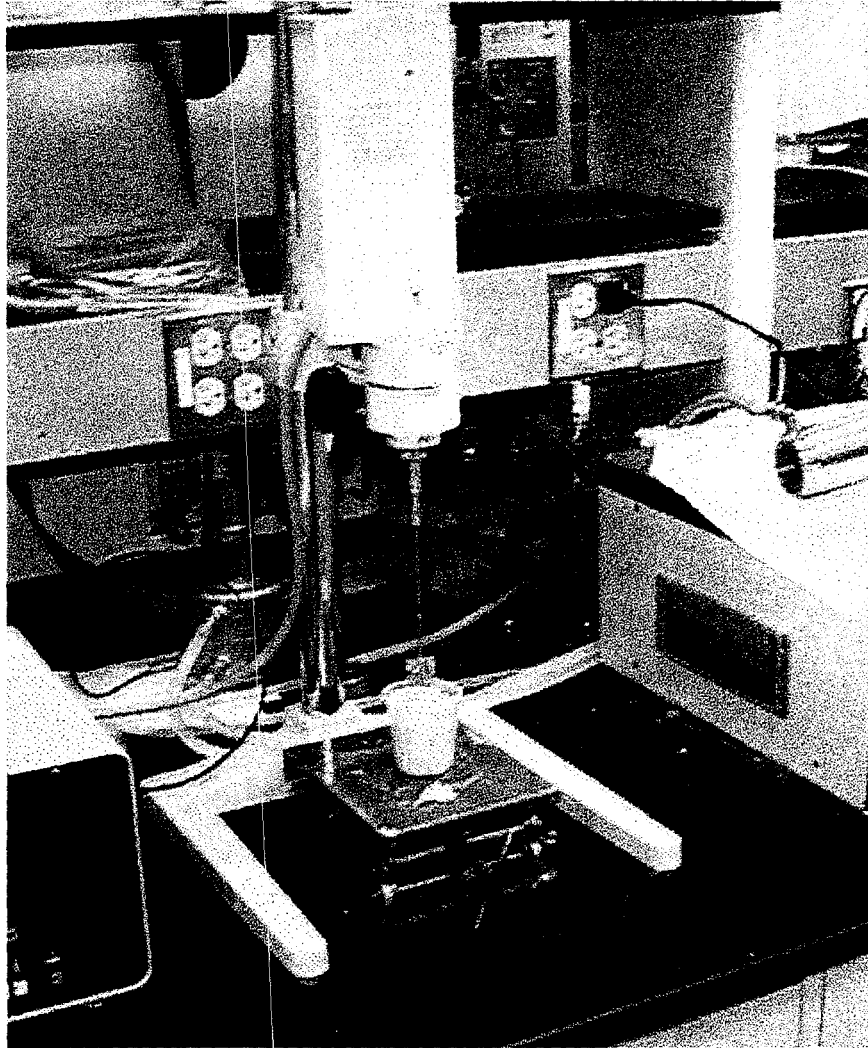
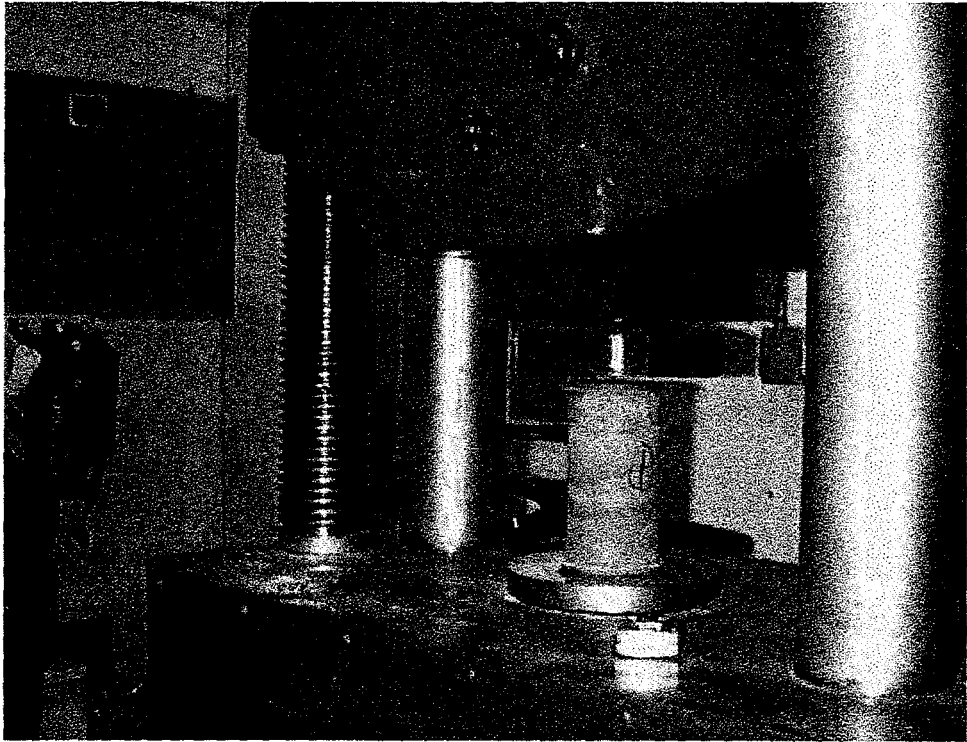


Figure 3.3. Haake M5 with Shear Vane



**Figure 3.4.** Compressive Strength Testing of a K-Mag Simulant



**Figure 3.5.** Sludge Tensometer

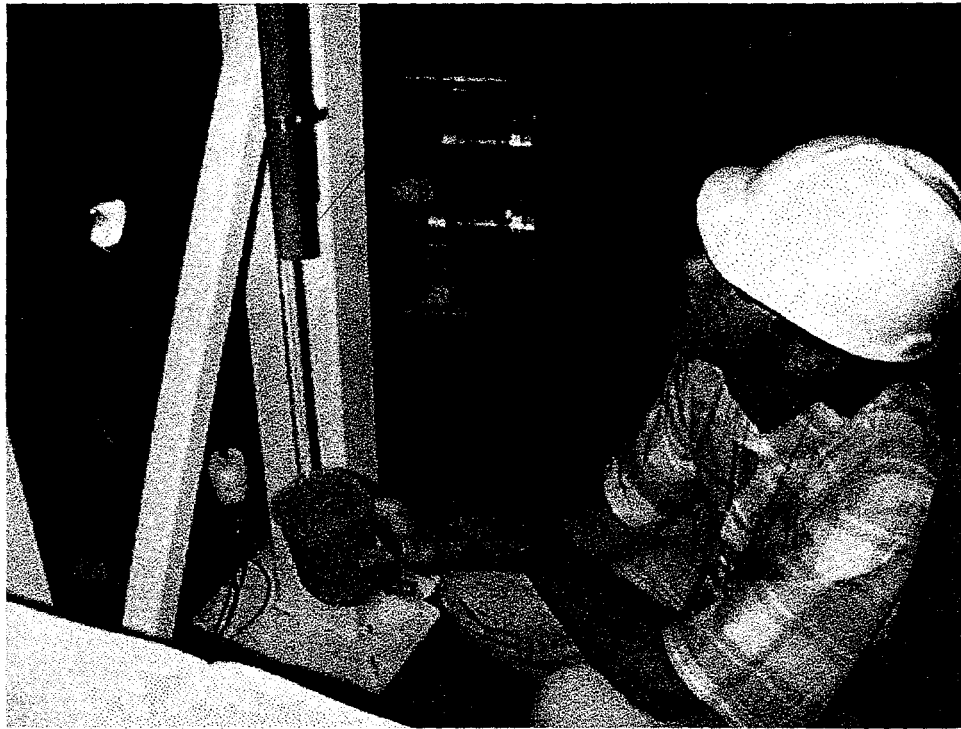


**Figure 3.6.** Sludge Sample Undergoing Vertical Extrusion Tensile Strength Test

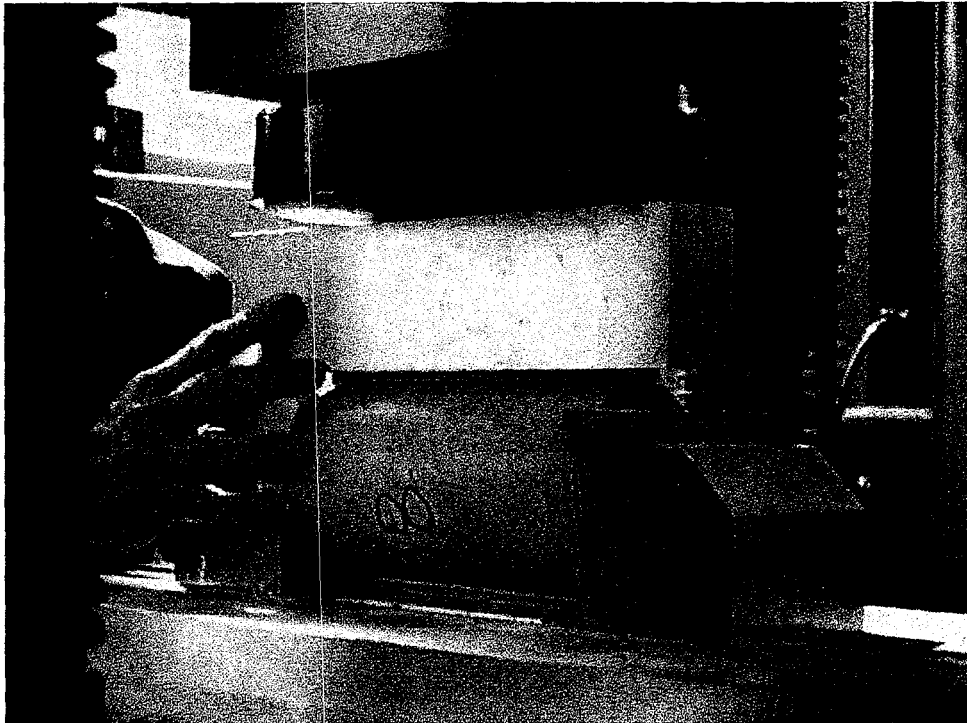


**Figure 3.7.** Brazillian Tensile Test on a K-Mag Simulant Sample

### 3.2.4 Simulant Material Suppliers

Simulant properties will vary from those listed in this report if alternative sources for simulant components are used. The properties of kaolin clay, for example, vary considerably depending on where the clay was mined. The brand names of each of the simulant components used for the waste simulants described in Section 2.0 are given in Table 3.1 below.

**Table 3.1. Simulant Material Specifications**

Simulant Material	Manufacturer	Product Name
kaolin clay	Feldspar Corporation Edgar, Florida	EPK Pulverized Kaolin Clay
bentonite clay	American Colloid, Inc. Upton, Wyoming	CS-50 bentonite clay
plaster of Paris	DAP, Inc. Dayton, Ohio	Plaster Wall Patch - Long Working Time Plaster of Paris
K-Mag	Western Ag-Minerals Co. Houston, Texas	Feed Grade Dynamate potassium-magnesium sulfate
rock salt (NaCl)	Morton International, Inc. Chicago, Illinois	Extra Coarse White Crystal Solar Salt
Ludox® colloidal silica	DuPont Specialty Chemicals Wilmington, Delaware	Ludox® HS-30
silica powder	U.S. Silica Pacific, Missouri	Min-U-Sil® 30

## 4.0 Hard Saltcake Waterjet Cutting Tests

In an effort to determine which physical properties of saltcake simulants control waterjet cutting performance, a series of tests was performed in which saltcake simulants were subjected to high-pressure waterjets. In parallel with the waterjet testing, physical property measurements were made on the saltcake simulants. The data from these tests are currently being analyzed to determine which properties can be used to predict waterjet cutting performance. Identification of key physical properties and determination of process sensitivity to those properties is a key element in the simulant development strategy outlined in Section 1.2. The saltcake cutting sensitivity testing and correlation development completed thus far are described in this section. A future report will provide the completed test results and correlations.

### 4.1 Introduction

Over the past several years the RPD&E project has designed, developed, and identified commercially available waterjet-based retrieval end effectors (Rinker et al. 1996, 1997). These technologies can potentially be deployed in underground storage tank wastes across the DOE complex. The ability of various waterjet cutting processes to cut and remove a volume of consolidated waste such as saltcake depends on both waste material properties and on the waterjet pressure, diameter, standoff distance, and traverse rate.

To better understand the dependence of waterjet cutting performance on saltcake and waterjet properties, the performance of medium to ultrahigh pressure waterjets (10 to 50 kpsi) is being correlated with the physical properties of various saltcake simulants. In this study, fundamental material properties such as mechanical strength (tensile, compressive, and fracture toughness), grain size, and porosity of the simulants were measured. The results of waterjet cutting tests are now being correlated with the physical property data. The data obtained from this testing provides a database for assessment of high-pressure-waterjet-based retrieval methods for saltcake and other hard wastes.

### 4.2 Background

The fracture of nonhomogeneous materials from waterjet impact has been extensively studied by the experts in the waterjet cutting industry (Summers 1995). A list of material properties that are expected to influence waterjet cutting was developed based on collaborations with waterjet cutting experts at Waterjet Technology Inc. (WTI), Kent, Washington, and the University of Missouri-Rolla Rock Mechanics and Explosives Research Center, Rolla, Missouri.

After the waterjet leaves the nozzle, friction between the waterjet surface and the air results in a substantial radial stagnation pressure gradient that ranges from near zero pressure at the water-air interface to a maximum at the centerline of the waterjet. This pressure gradient is significant during the impact of the jet at the surface of the material. The axial rate of change in this distribution varies with the jet pressure and the jet diameter. Once a full, parabolic radial pressure distribution develops, the jet breaks up into segments and small droplets very quickly. Droplets rapidly break into smaller droplets and lose both velocity and cutting power with additional distance from the nozzle.

The mechanism of waterjet-induced failure in a brittle, multiphase, granular material such as saltcake waste can be described in several steps. As water penetrates into cracks or other perturbations on the surface of the material, the waterjet flow acts to pressurize the fluid in the crack, which tends to cause the crack to grow. Eventually, the cracks produced by the waterjet grow large and numerous enough that small chunks are dislodged and swept away. As the material is dislodged, the cracks grow around the underlying particles or crystals thus propagating an incipient state of material failure.

The first step in assessing the response of the target material to jet attack requires a knowledge of exactly what form the jet is taking as it arrives at the surface. It is known that material failure is likely caused by crack extension from existing surface flaws based on Griffith's fracture criteria. The applicability of such criteria to material erosion under waterjet impact is discussed by Summers (1995).

When the jet arrives at the surface, if the pressure profile is relatively flat at the time of impact, very little material across the diameter of the jet-impact region will be removed because the pressure is relatively constant in this region. In the surrounding region, however, the large radial pressure gradient results in effective material removal. Alternatively, when the radial pressure gradient in the impacting jet is increased, material is removed across the diameter of the jet-impact region. Material is removed in regions where large radial pressure gradients are present because these gradients form and open up cracks within the impact zone (Summers 1995).

Considering the postulated mechanisms of waterjet cutting in materials similar to saltcake and the experiences of the waterjet cutting industry, the controlling material parameters for waterjet cutting are thought to be

- grain size and structure
- porosity and permeability
- fracture toughness
- tensile strength
- compressive strength
- solubility
- density of the saltcake, which is related to its pore characteristics.

### 4.3 Experimental Design

Ten 91-kg (200-lb) blocks of saltcake were prepared by mixing the dry constituents with water in a rotating drum mixer (refer to Figure 3.2). After the blocks had cured for one week, they were cut into three large pieces using a circular saw with a carbide-tipped blade. Figure 4.1 shows several of the blocks after they were cut. One piece from each saltcake block was delivered to WTI for waterjet testing, and the remaining two pieces were delivered to the Washington State University (WSU) Department of Mechanical and Materials Engineering for physical property characterization. The pieces delivered to WTI were roughly 50 cm (20 in.) long, 20 cm (8 in.) wide, and 13 cm (5 in.) thick.

When selecting the saltcake simulant compositions, efforts were made to design the simulants such that a range of porosities and strengths resulted. The simulant compositions used in this testing are provided in Table 4.1.



**Figure 4.1.** Saltcake Simulant Blocks used for Waterjet Sensitivity Tests

**Table 4.1. Saltcake Sensitivity Testing Simulant Compositions**

Simulant No.	Composition (wt%)	Cure Time Before Testing (days)
1	16% water 84% K-Mag (Dynamate)	25
2	16% water 84% K-Mag	25
3	20% water 80% K-Mag	25
4	16% water 14% kaolin clay 70% K-Mag	25
5	16% water 14% Min-U-Sil® 10 70% K-Mag	25
6	16% water 14% Min-U-Sil® 10 70% granular K-Mag	26
7	18% water 82% K-Mag	17
8	18% water 82% granular K-mag	17
9	20% water 5% plaster of Paris 75% K-Mag	26
10	16% water 84% K-Mag	26

At WTI, the samples were positioned as shown in Figure 4.2 and then subjected to waterjets of five different diameters at five pressures and two standoff distances. Many of the possible permutations of these settings were tested (partial-factorial experimental design), and the depth of waterjet cut was measured twice for each set of experimental conditions. A total of 360 cut depth measurements were made. The experimental conditions used to test each of the 10 saltcake simulants are provided in Table 4.2.

Five saltcake simulant blocks were loaded into the high-pressure waterjet test facility at WTI and positioned side-by-side. After selecting the desired nozzle diameter, the standoff distance and water pressure were adjusted to the target values and the jet passed over all five samples at 25 cm/s (10 in./s). The remaining five simulant blocks were subjected to the same tests after testing of the first set of five was completed. Waterjet movement was from right to left as viewed in Figure 4.2. Before making the next cut, the waterjet positioning mechanism was moved sideways (toward the back of the test facility shown in Figure 4.2) by approximately 1.2 cm (0.5 in.). Using this technique, 36 cuts were made on each

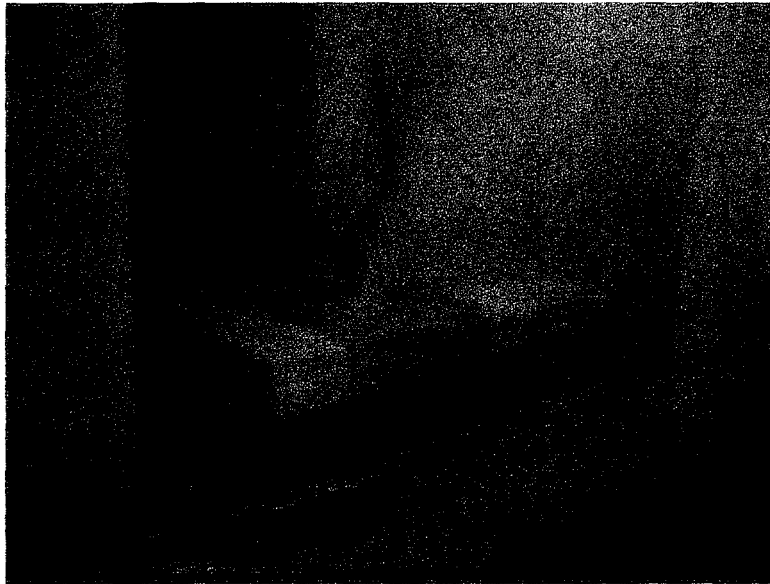


**Figure 4.2.** Waterjet Testing of Saltcake Simulants

**Table 4.2. Saltcake Sensitivity Testing Parameters**

Test Number	Nozzle Diam. (mm)	Standoff Distance (cm)	Waterjet Pressure (kpsi)	Waterjet Traverse Rate (cm/s)	Number of Cuts w/these Conditions
1	0.635	5.1	50	25.4	2
2	0.635	5.1	30	25.4	2
3	0.635	5.1	10	25.4	2
4	0.559	5.1	50	25.4	2
5	0.559	5.1	30	25.4	2
6	0.559	12.7	50	25.4	2
7	0.559	12.7	30	25.4	2
8	0.635	12.7	50	25.4	2
9	0.635	12.7	30	25.4	2
10	0.635	12.7	10	25.4	2
11	0.457	12.7	50	25.4	2
12	0.457	12.7	30	25.4	2
13	0.457	5.1	50	25.4	2
14	0.457	5.1	30	25.4	2
15	0.889	5.1	14	25.4	2
16	0.813	5.1	12	25.4	2
17	0.813	12.7	12	25.4	2
18	.889	12.7	14	25.4	2

sample as shown in Figure 4.3. Figure 4.4 shows a side view of one of the simulant blocks. Variation in the cut depths are evident in this picture.

In parallel with the waterjet cutting tests at WTI, selected physical property measurements were made on each simulant at WSU and PNNL. Porosity and pore size distribution measurements were made at PNNL using a Micromeritics Poresizer® model 9320 mercury porosimeter. Compressive strength, tensile strength, and fracture toughness measurements were performed at WSU. Refer to Section 3.0 of this report for descriptions of the compressive and tensile strength measurement techniques. Refer to ASTM standard E1820-96 for a description of fracture toughness measurement.

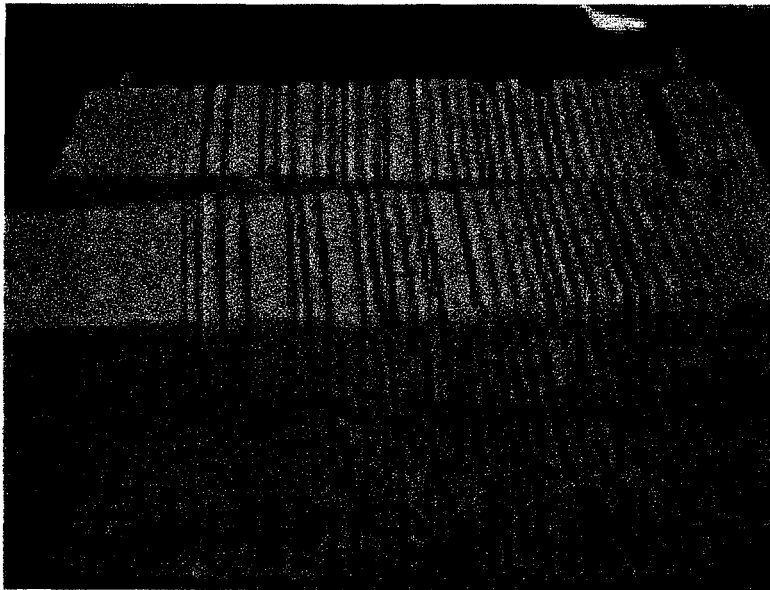


**Figure 4.3.** Saltcake Simulant Blocks Following Waterjet Testing



**Figure 4.4.** Side View of Waterjet Cuts in a Block of Saltcake Simulant

## 4.4 Saltcake Sensitivity Testing Results and Analysis

As mentioned earlier, the development of correlations between the test parameters and simulant properties has not yet been completed. All the needed physical property measurements have not yet been made, so publication of the correlations and identification of the key saltcake simulant properties for waterjet cutting must be done later. However, some preliminary conclusions regarding the effects of changes in jet diameter, pressure, and standoff distance can be made. These data are discussed in this section. Once all the simulant physical property data are obtained, correlations between waterjet properties and saltcake simulant properties will be determined.

Each of the 18 test conditions listed in Table 4.2 was applied to the 10 saltcake simulants. Two cuts were made under each set of conditions and the resulting cut depths measured. The cut depth data are provided in Table 4.3. Each cell in the body of the table contains two numbers. These are the cut depth data. Variations in the cut depth numbers across any given row are indicative of the dependence of waterjet cut depth on saltcake simulant properties. Variations in any given column show the effects of changes in waterjet pressure, diameter, and standoff distance.

Figure 4.5 shows the effect of jet pressure on the depth of cut for each of the simulant compositions. Simulants #1 and #2 had the same initial composition, but simulant #1 inadvertently dried to some extent while it was curing. Thus, a difference in waterjet cutting is not unexpected. Figure 4.5 shows that the cut depth is apparently directly proportional to jet pressure over the range studied. This is consistent with data presented by Summers (1995).

Because only two standoff distances were tested, it is not possible to determine whether the relationship between cut depth and standoff distance is nonlinear. However, Summers (1995) presents data that show depth of cut to be linearly related to standoff distance in some instances. For the purpose of evaluating the present data it has been assumed that cut depth decays linearly with increasing standoff distance.

Figure 4.6 shows the effect of nozzle diameter on cut depth. Because Figure 4.5 implies that cut depth is directly proportional to waterjet pressure, the cut depth data can be normalized by dividing by the waterjet pressure. This was done in Figure 4.6 to allow data from all waterjet pressures to be included. Generally, the normalized cut depths for the 12.7-cm standoff distance are seen to be smaller than those for the 5.1-cm standoff distance. There is significant scatter in the Figure 4.6 data, but there appears to be a general trend of increasing normalized cut depth with increasing nozzle diameter. Summers (1995) suggests that cut depth should be proportional to nozzle diameter to a power of 1.5. However, a power of 1.0 is used in the analysis below because it was found to provide a better fit of the saltcake cutting data.

Assuming that for all the simulants tested the cut depth ( $C_d$ ) is directly proportional to both nozzle diameter ( $D_n$ ) and waterjet pressure ( $P_j$ ) and that it decreases linearly with increasing standoff distance ( $\sigma$ ), then the relationship between these parameters can be described by:

$$C_d = f(x) D_n P_j (1 - k\sigma) \quad (4.1)$$

where  $k$  is an empirical constant and  $f(x)$  is a function whose value is determined by the saltcake simulant physical properties (e.g., tensile strength, porosity, and fracture toughness), which are symbolized by  $x$ .

Table 4.3. Waterjet Cut Depth Data (cm)

Test No.	Sim. 1	Sim. 2	Sim. 3	Sim. 4	Sim. 5	Sim. 6	Sim. 7	Sim. 8	Sim. 9	Sim. 10
1	4.2 4.7	2.2 2.2	1.7 1.9	5.1 4.8	4.5 5.0	3.1 3.2	1.5 1.5	1.5 1.5	3.6 3.7	2.7 2.7
2	4.2 4.2	1.4 1.4	1.1 1.0	3.7 3.3	2.8 2.9	1.5 1.7	0.8 0.8	1.0 1.0	2.4 2.5	2.8 2.8
3	1.6 1.5	0-0.5 0-0.5	0.4 0.4	1.0 0.8	0.9 0.8	0-0.6 0-0.6	0.3 0.3	0-0.5 0-0.5	0.8 0.8	0.6 0.6
4	4.6 3.7	1.8 1.5	1.5 1.3	4.3 3.9	4.2 3.8	3.2 3.2	1.7 1.7	1.8 1.8	3.3 3.4	2.4 2.4
5	2.3 2.5	1.1 1.0	0.9 0.8	2.5 2.4	2.4 2.3	1.8 1.8	0.9 0.9	1.1 1.1	2.4 2.5	1.4 1.4
6	3.8 3.2	1.4 1.4	1.0 0.8	3.3 3.1	3.7 3.3	2.3 2.3	1.1 1.1	1.1 1.3	2.7 2.7	2.7 2.7
7	2.2 3.2	0.8 1.0	0.8 0.6	2.0 2.0	1.9 1.8	1.3 1.3	0.6 0.6	0.6 0.6	1.5 1.7	2.0 2.2
8	2.8 3.7	1.5 1.8	1.0 1.1	2.8 3.6	3.1 3.4	2.3 2.4	0.9 0.9	1.0 1.0	1.9 1.9	2.5 2.5
9	1.8 2.5	0.9 1.0	0.5 0.6	1.7 2.3	1.7 1.9	1.0 1.0	0.5 0.5	0.5 0.5	1.3 1.4	1.0 1.1
10	1.1 1.3	0-0.5 0-0.5	0.4 0.4	0.8 0.9	0.6 0.8	0-0.5 0-0.5	0.3 0.4	0-0.5 0-0.5	0.8 0.8	0.5 0.5
11	3.1 2.9	1.1 1.3	0.8 1.0	2.8 2.8	2.8 2.8	1.7 1.7	1.0 1.0	1.0 1.0	2.9 2.7	2.0 2.0
12	1.7 1.7	0.9 1.0	0.5 0.6	1.8 1.8	1.7 1.8	1.0 1.0	0.5 0.5	0.6 0.6	1.7 1.7	1.5 1.5
13	3.3 3.2	1.8 1.5	1.3 1.3	3.6 3.3	3.2 3.2	2.8 3.3	1.4 1.3	1.3 1.3	2.8 2.5	2.7 2.4
14	2.2 2.4	0.8 0.8	0.6 0.6	2.0 2.4	1.9 2.2	0.5-1.3 0.5-1.3	0.9 0.8	0.8 0.8	1.5 1.5	1.9 1.9
15	2.0 1.8	0.5 0.8	0.4 0.5	1.5 1.4	1.1 1.0	1.1 1.1	0.4 0.4	0.5 0.5	0.8 0.9	0.8 0.8
16	1.8 1.5	0.5 0.4	0.3 0.3	1.1 1.0	1.0 1.0	0.3-0.8 0.3-0.8	0.3 0.3	0.3-0.5 0.3-0.5	0.8 0.8	0.8 0.8
17	1.7 1.3	0.4 0.4	0.3 0.25	0.8 0.8	0.8 0.9	0.3-0.8 0.3-0.8	0.4 0.4	0.3-0.5 0.3-0.5	0.8 0.8	0.9 0.9
18	1.5 1.7	0.5 0.5	0.4 0.4	1.1 1.1	1.1 1.3	1.1 1.1	0.4 0.4	0.5 0.5	0.8 0.8	0.8 0.8

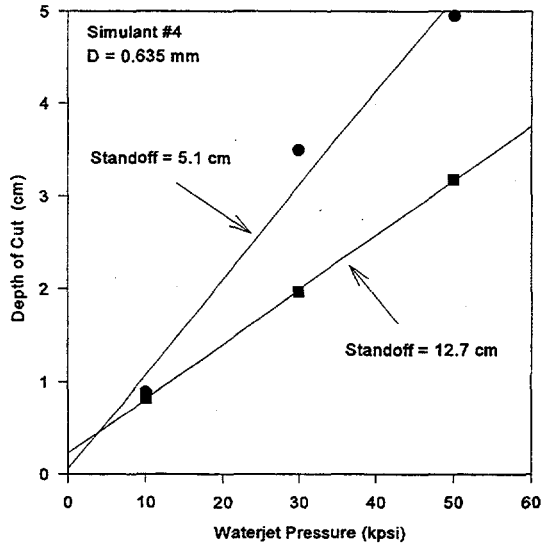
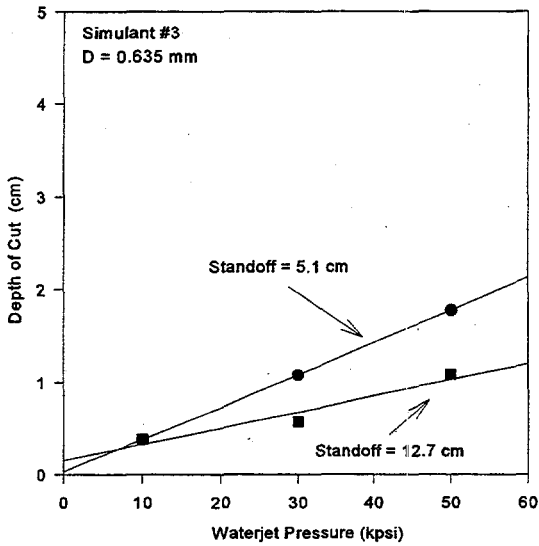
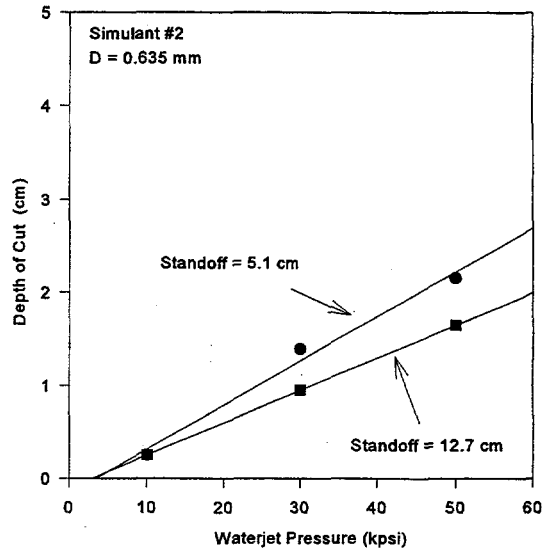
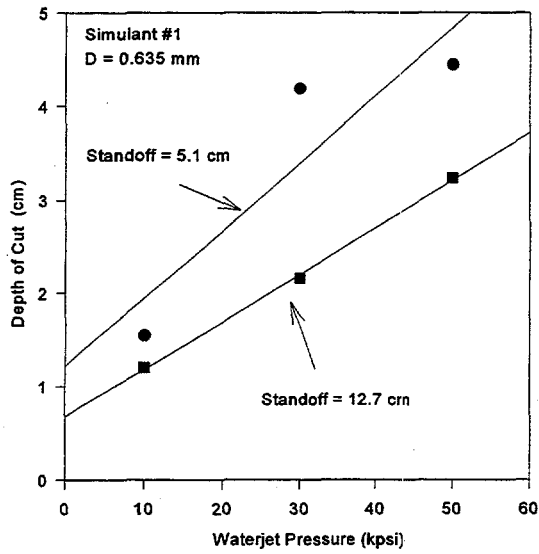


Figure 4.5. Effect of Waterjet Pressure on Depth of Cut

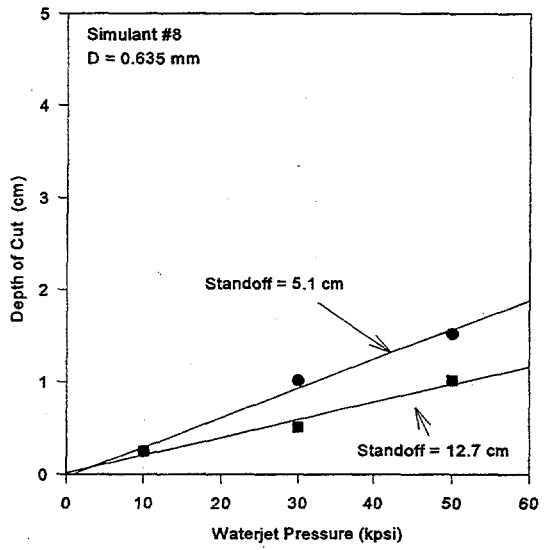
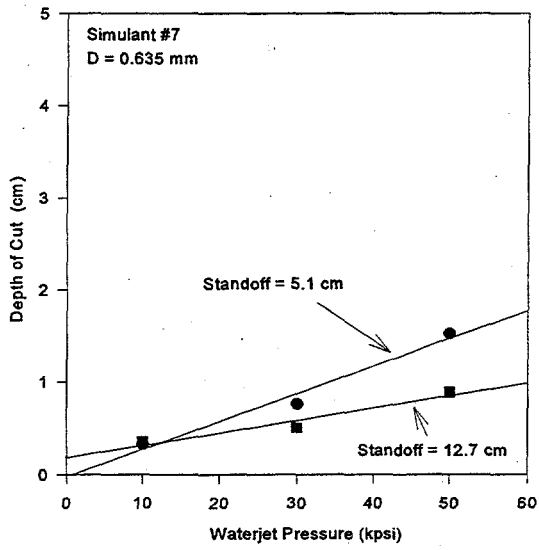
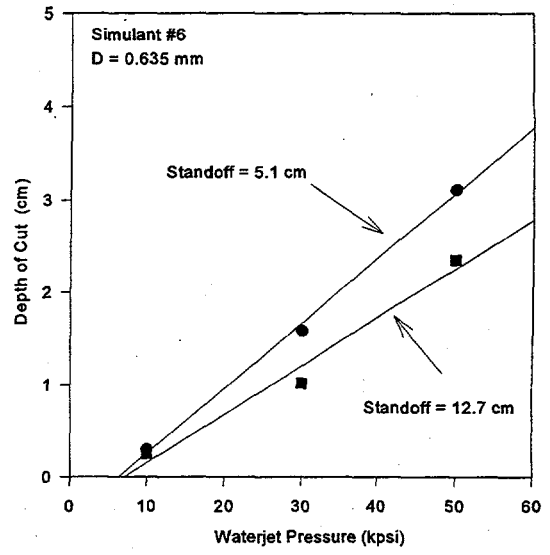
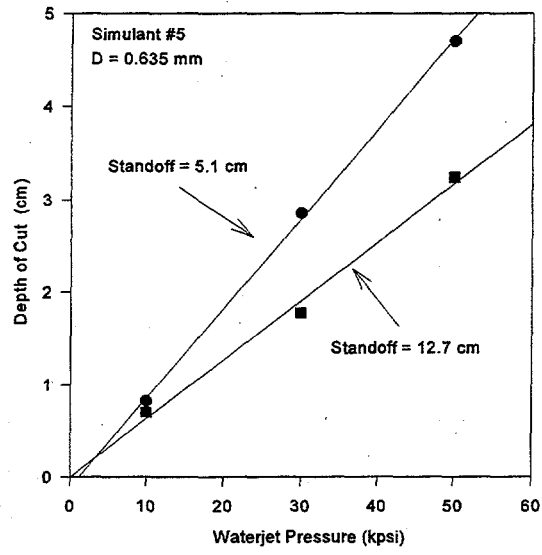


Figure 4.5. (cont.) Effect of Waterjet Pressure on Depth of Cut

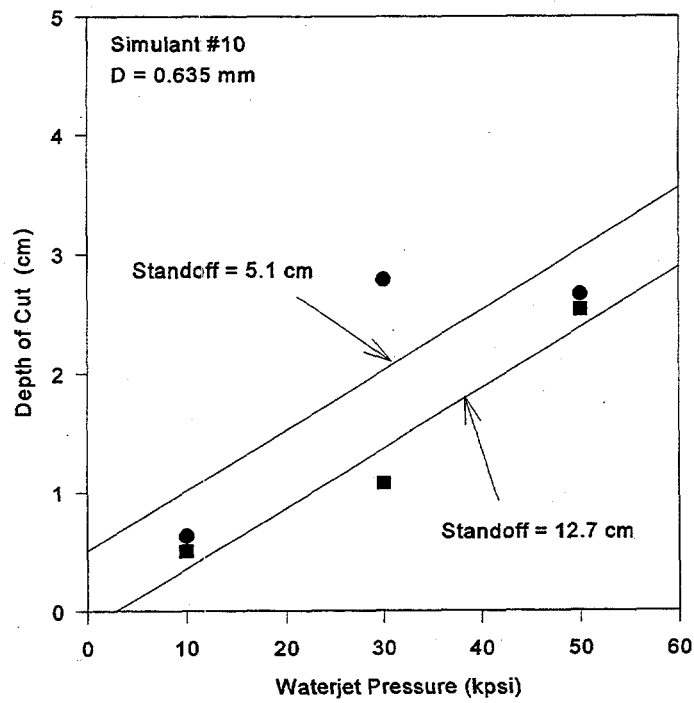
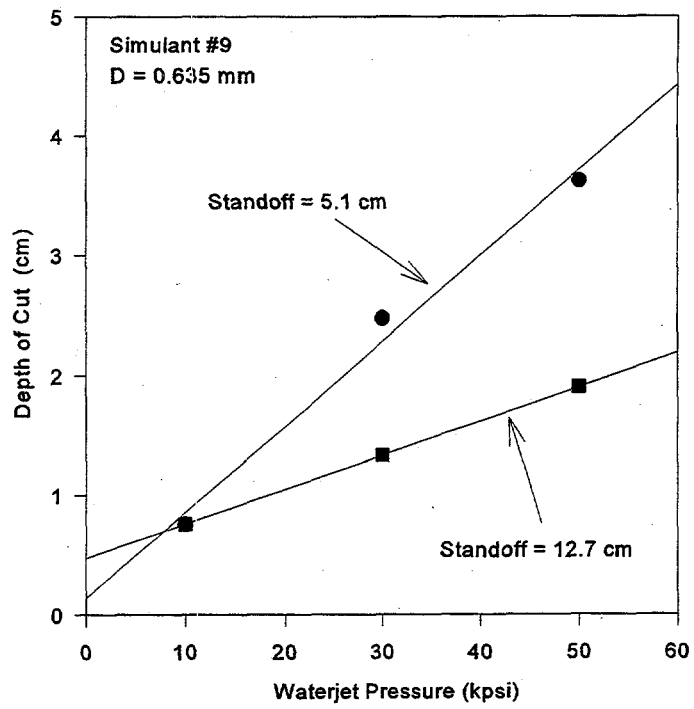


Figure 4.5. (cont.) Effect of Waterjet Pressure on Depth of Cut

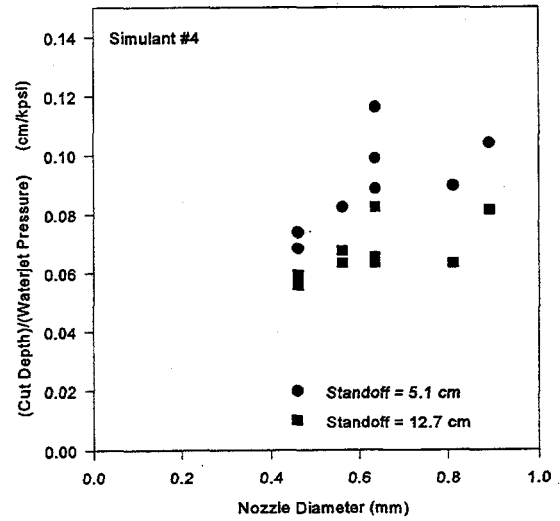
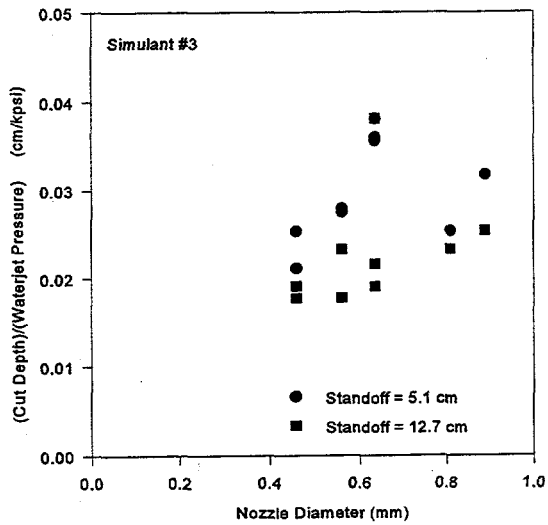
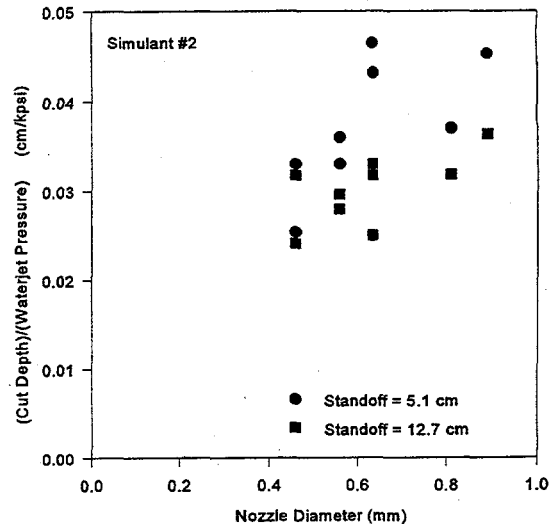
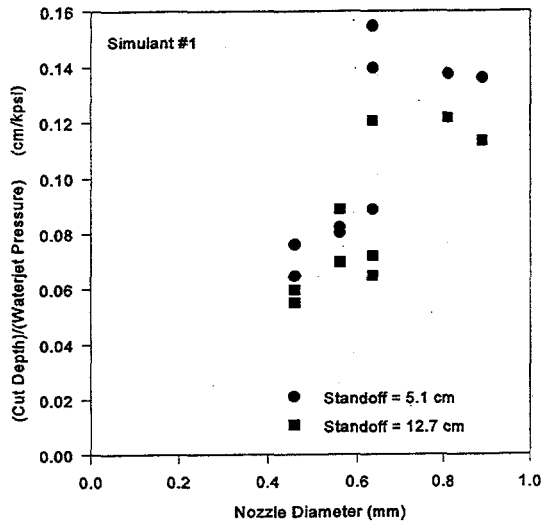


Figure 4.6. Effect of Nozzle Diameter on Depth of Cut

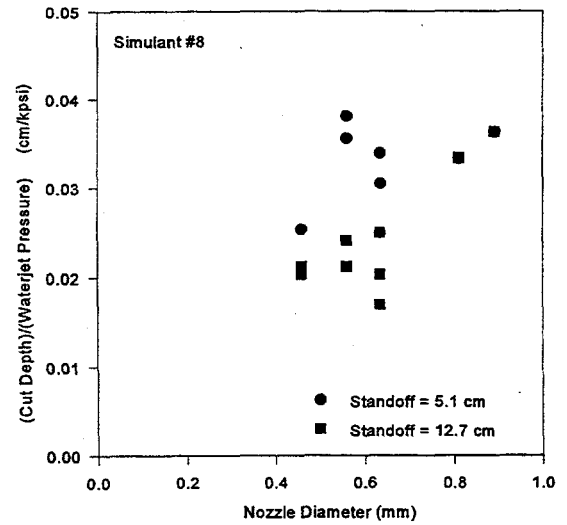
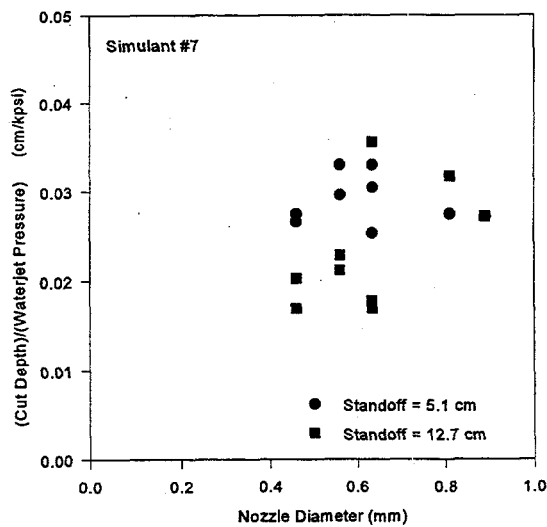
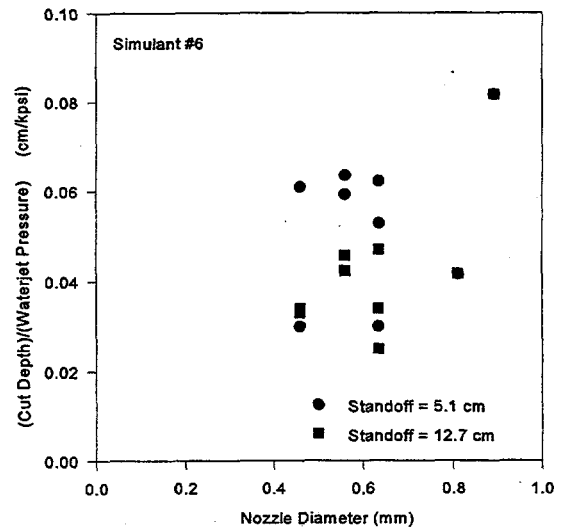
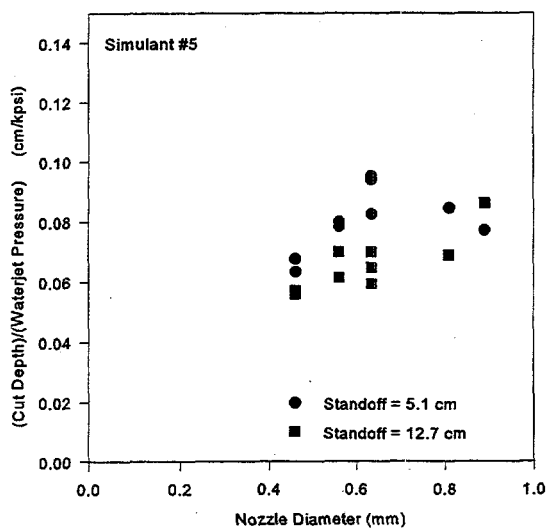


Figure 4.6. (cont.) Effect of Nozzle Diameter on Depth of Cut

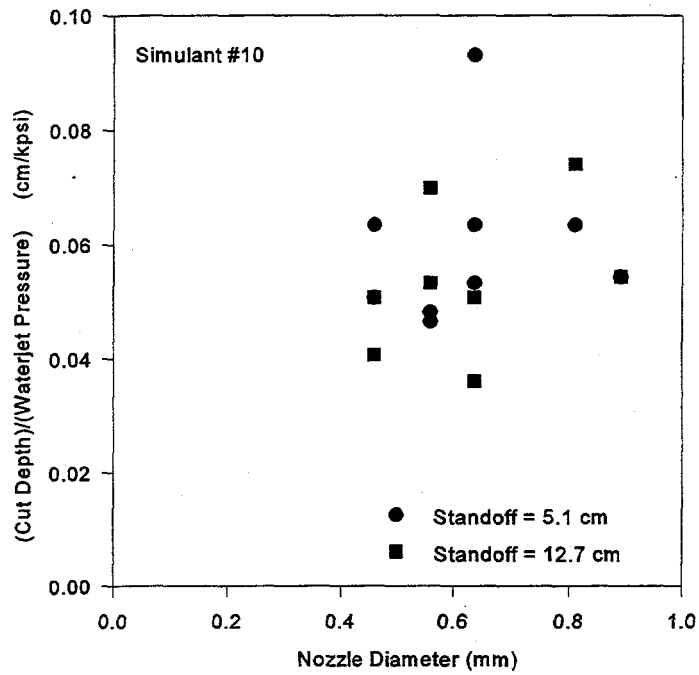
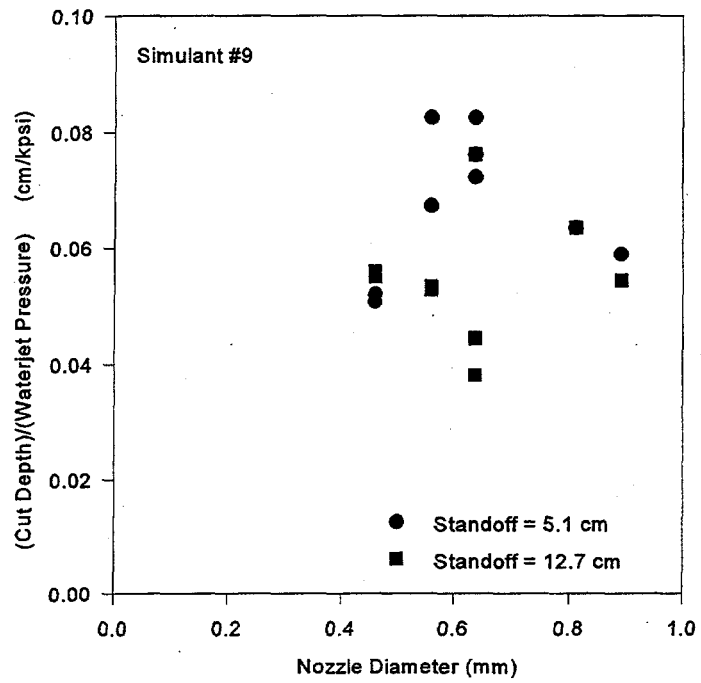


Figure 4.6. (cont.) Effect of Nozzle Diameter on Depth of Cut

Using Equation 4.1, the value of  $f(x)$  can be determined for each simulant composition. The value of  $k$  is first determined for each simulant using the pairs of  $C_d$  values that differ only in standoff distance (i.e., same pressure and nozzle diameter). There are nine such pairs for each simulant. A value for  $k$  is calculated from each pair and the resulting nine  $k$  values are averaged to give one value of  $k$  for each simulant. The calculated  $k$  values from each pair of cut depths for each simulant are shown in Figure 4.7. Considerable scatter is once again observed. This is attributed to a combination of cut depth uncertainty, simulant inhomogeneity, and the fact that Equation 4.1 probably represents an oversimplification of the true waterjet cutting relationship. The average of all the  $k$ 's on the plot was determined to be 0.018. Thus, Equation 4.1 becomes:

$$C_d = f(x) D_n P_j (1 - 0.018\sigma) \quad (4.2)$$

which can be solved for  $f(x)$  to give:

$$f(x) = \frac{C_d}{D_n P_j (1 - 0.018\sigma)} \quad (4.3)$$

Equation 4.3 was used to determine the average  $f(x)$  values for each simulant composition. Assuming the functional form of Equation 4.1 is a reasonable approximation of the true relationship between the test parameters, the  $f(x)$  values should quantify the cutting susceptibilities of the saltcake simulants.

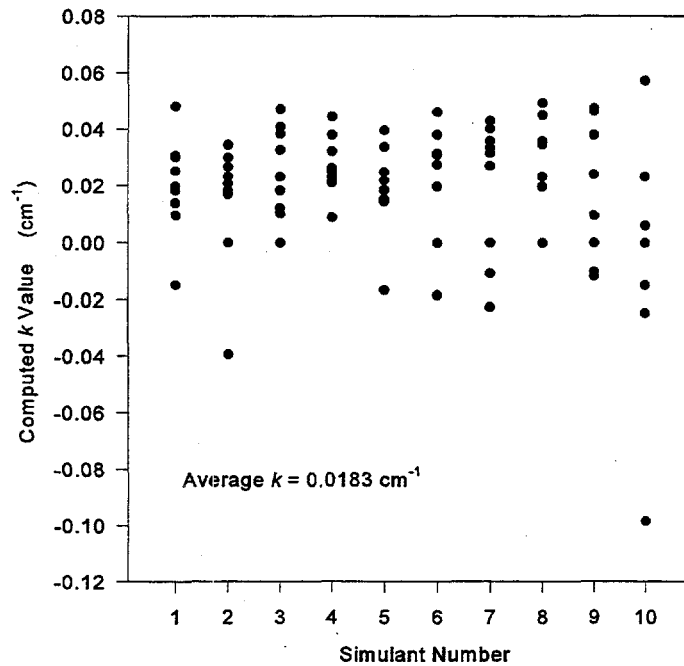


Figure 4.7. Computed  $k$  Values for Simulants

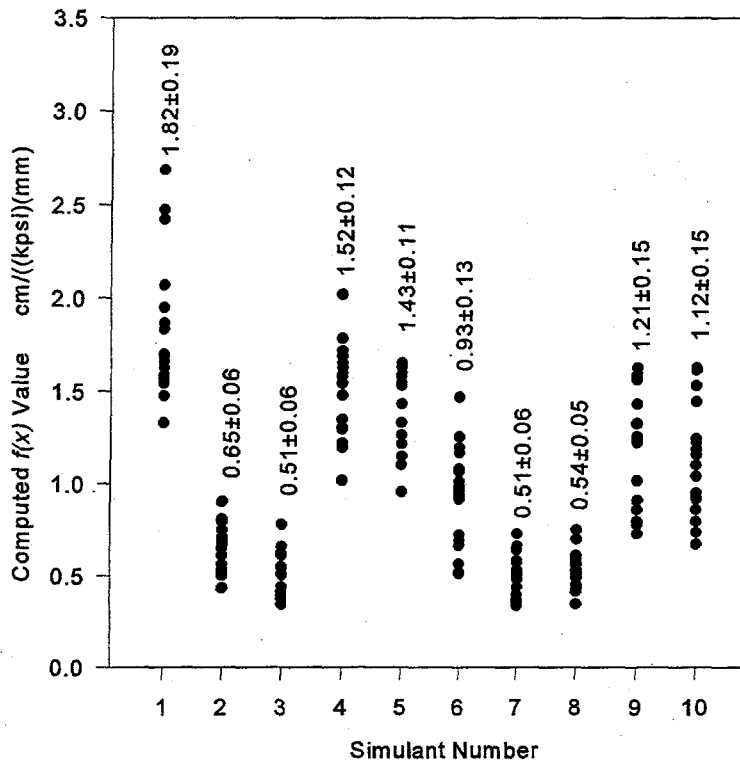


Figure 4.8. Computed  $f(x)$  Values for Each Simulant

Equation 4.3 was applied to all of the waterjet cut depth data in Table 4.3. Eighteen  $f(x)$  values were computed for each simulant composition. These values are shown by the data points in Figure 4.8. The average  $f(x)$  for each simulant is also given along with its respective 95% confidence interval, which was estimated based on the standard deviation of the computed  $f(x)$  values. Once the saltcake physical property data become available, efforts will be made to correlate the physical property data with these  $f(x)$  values. If these efforts are successful, the sensitivity of waterjet cutting to both saltcake and waterjet properties will be predicted with much greater confidence. The correlation of waterjet cutting with saltcake simulant properties will be published in a future report.

Using the computed  $f(x)$  values shown in Figure 4.8, Equation 4.3 was used to generate "predicted"  $C_d$  values for each simulant under each set of experimental conditions given in Table 4.2. Thus, a total of 360 predicted  $C_d$  values were generated. The measured  $C_d$  values from Table 4.3 are plotted versus these predicted values in Figure 4.9. A linear fit of the data in Figure 4.9 shows that there is no significant systematic bias in the predicted values. That is, errors in the predicted values appear to be random. The lack of systematic bias implies that Equation 4.3 appropriately models the relationships between  $C_d$ ,  $P_j$ ,  $D_n$ , and  $\sigma$ .

The data in Figure 4.10 were produced by modifying the data analysis technique described above such that  $C_d$  was assumed to be proportional to  $D_n^{1.5}$  instead of  $D_n^{1.0}$ . As is indicated by the decreased correlation coefficient ( $R^2$ ) in Figure 4.10 compared to that given in Figure 4.9, the experimental data are better fit when  $D_n^{1.0}$  is used.

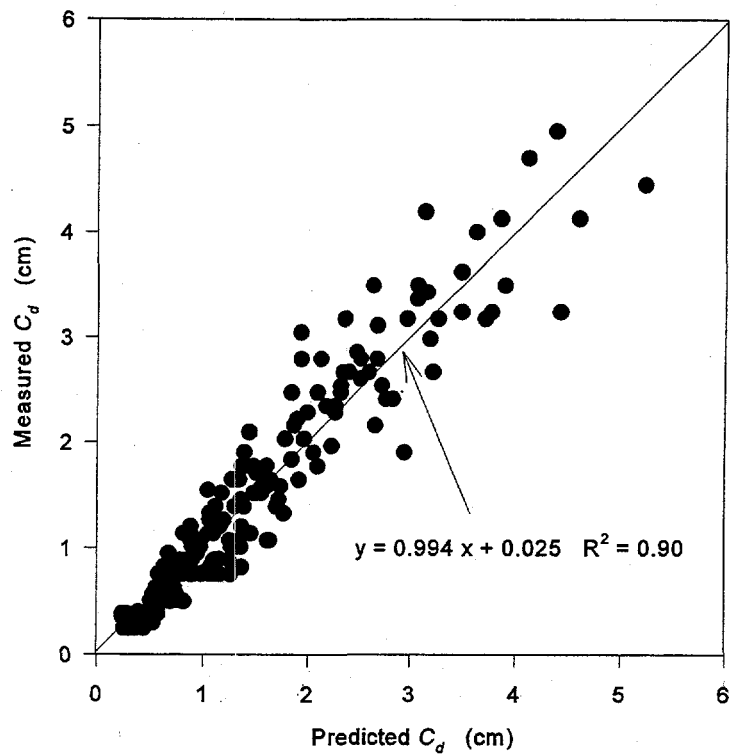


Figure 4.9. Comparison of Predicted and Measured  $C_d$  Values (all simulants)

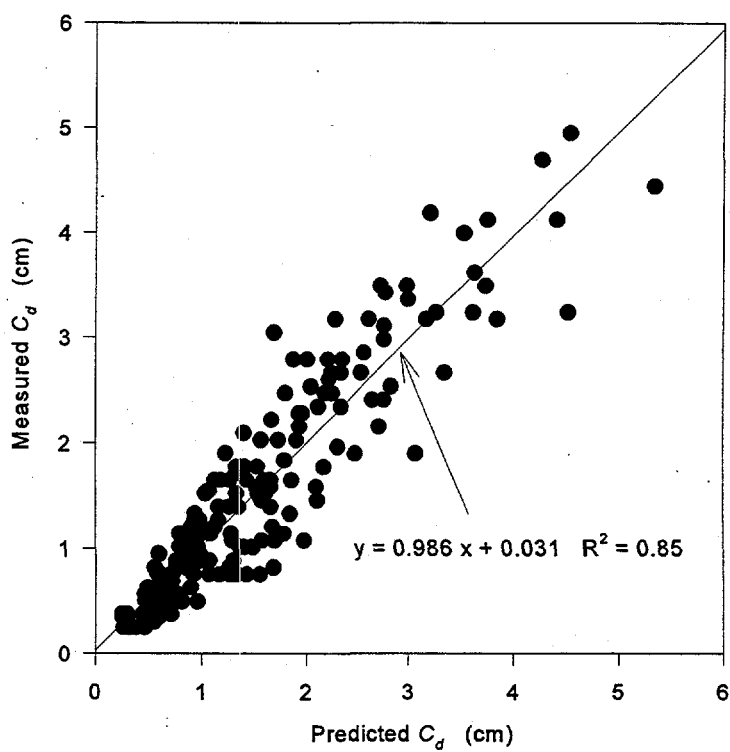


Figure 4.10. Comparison of Predicted and Measured  $C_d$  Values for  $D_n^{1.5}$

## 4.5 Conclusions

The waterjet cutting data provided in Section 4.4 demonstrate the feasibility of a correlation between waterjet properties ( $D_n$ ,  $P_j$ , and  $\sigma$ ) and depth of cut for the saltcake simulants. Whether the simulant-dependent portion of Equation 4.2 (i.e.,  $f(x)$ ) can be adequately correlated with the saltcake properties measured in this study is not yet known. Correlations of cut depth with saltcake properties will be developed once all the saltcake physical property data have been gathered. Figure 4.8 demonstrates that the range of saltcake simulant properties tested was large enough that statistically significant differences exist in the waterjet resistances of the simulants, so useful correlations are expected to result provided that the right saltcake properties were measured.

## 5.0 Salt Crystal Dissolution Studies

High-pressure waterjet scarifiers have been developed that can effectively retrieve sludge, hardpan, and saltcake waste (Hatchell 1997). The waste simulants used to support the scarifier development efforts did not account for the solubility and dissolution rate of the tank saltcake. Neglecting saltcake dissolution helped to ensure that the simulant testing results would conservatively predict scarifier performance.

Alternative saltcake retrieval methods have been suggested that rely directly on saltcake dissolution rather than on high-pressure waterjets. Sluicing a saltcake tank with relatively clean water, for example, would be expected to dissolve the saltcake. Whether saltcake sluicing will be effective and efficient is not yet known because the saltcake dissolution rate is not known with sufficient accuracy.

To support future testing of dissolution-based saltcake retrieval processes, a study was conducted of some of the factors that control salt dissolution rates. This study is described in this section.

### 5.1 Background

Dissolution of salt from the surface of a solid particle is a heterogeneous chemical process. The shrinking particle model is used to model the particle dissolution. The model assumes the reacting particle is a sphere with the dissolution occurring on the surface whose area is decreasing with time as the particle reacts to form fluid products.

We assume the surface reaction

(liquid solvent) + (solid salt species) = (various non-solid products)

and that we have the solid salt species and liquid solvent in excess, i.e., there is always sufficient salt and solvent at the surface for chemical reaction, and the concentration of neither may be increased. Such a reaction is inherently a zero-order reaction. The two rate equations expressed as moles of salt disappearing per unit time per particle, are

$$-\frac{dN}{dt} = 4\pi r^2 k \quad \text{chemical reaction at } r \quad (5.1)$$

$$-\frac{dN}{dt} = 4\pi r^2 k_m [C_s - C_b] \quad \text{diffusion from the reaction surface} \quad (5.2)$$

where  $r$  is the particle radius,  $k$  is the reaction rate (mole/cm<sup>2</sup>·s),  $k_m$  is the mass-transfer coefficient (cm/s) and  $C_s$  and  $C_b$  are the product concentrations (mole/cm<sup>3</sup>) at the particle surface and in the bulk solvent, respectively. It is useful to define an apparent reaction rate,

$$-\frac{dN}{dt} = 4\pi r^2 k_0 \quad (5.3)$$

with  $k_0$  related to  $k$  and  $k_m$  as follows:

$$\frac{1}{k_0} = \frac{1}{k} + \frac{1}{k_m [C_s - C_b]} \quad (5.4)$$

When collecting laboratory kinetic data,  $k_0$  would be measured.

Assuming a spherical geometry for the dissolving particles, the rate of reaction (moles per unit time per particle) may be written as

$$\frac{dN}{dt} = \frac{\rho_{salt}}{M_{salt}} \frac{d}{dt} \left( \frac{4}{3} \pi r^3 \right) = \frac{4\pi r^2 \rho_{salt}}{M_{salt}} \frac{dr}{dt} \quad (5.5)$$

where  $\rho_{salt}$  is the density of the salt, and  $M_{salt}$  the molecular weight. Combining this result with Equation 5.1 gives (assuming the dissolution is reaction rate limited rather than mass transfer limited):

$$\frac{dr}{dt} = -k \frac{M_{salt}}{\rho_{salt}} \quad (5.6)$$

Integrating Equation 5.6 from  $r = 0.5d$  to  $r = 0$  and  $t = 0$  to  $t_d$ , respectively, gives:

$$t_d = \frac{0.5d \rho_{salt}}{k M_{salt}} \quad (5.7)$$

Thus, we see that when the rate is controlled by the chemical reaction, the required dissolution time ( $t_d$ ) is proportional to the particle diameter ( $d$ ).

When diffusion and convection outside of a shrinking particle is rate controlling, the key variable becomes the mass transfer coefficient. The mass transfer coefficient is a function of the particle size and velocity relative to the solvent, and for a single particle it is often assumed to be (Cussler 1984):

$$\frac{k_m d}{D} = 2.0 + 0.6 \left( \frac{dv}{v} \right)^{1/2} \left( \frac{v}{D} \right)^{1/3} \quad (5.8)$$

where  $D$  is the diffusion coefficient,  $v$  is the fluid velocity relative to the particle, and  $\nu$  is the kinematic viscosity. For very small particles, this implies that

$$k_m = \frac{D}{r} \quad (5.9)$$

The mass balance for a single particle is now

$$\frac{dN}{dt} = \frac{\rho_{salt}}{M_{salt}} \frac{d}{dt} \left( \frac{4}{3} \pi r^3 \right) = -4\pi r D [C_s - C_b] \quad (5.10)$$

This equation can be integrated to give

$$t = \frac{\rho_{salt} r^2}{2dM_{salt}[C_s - C_b]} \quad (5.11)$$

For larger particles, the mass transfer coefficient is

$$k_m = \frac{0.42(v)^{\frac{1}{2}}(D)^{\frac{2}{3}}}{(v)^{\frac{1}{6}}(r)^{\frac{1}{2}}} \quad (5.12)$$

and the resulting variation of  $t$  is

$$t = \left( \frac{r^{\frac{3}{2}} \rho_{salt}}{M_{salt}[C_s - C_b]} \right) \left( \frac{v^{\frac{1}{6}}}{0.63 v^{\frac{1}{2}} D^{\frac{2}{3}}} \right) \quad (5.13)$$

Evaluation for NaCl in water (with  $D = 1.48E-5$  cm<sup>2</sup>/sec,  $v = 0.01$  cm<sup>2</sup>/sec, and the velocity calculated using the Stokes terminal velocity equation) provides an indication as to the definition of the subjective terms "large" and "smaller particle" diameter. Table 5.1 provides the mass transfer coefficient as a function of particle size as determined from Equations 5.8 and 5.9.

Based on this example, we see that when the particle diameter is 5 microns or less, the error in Equation 5.9 is <5%. As the particle diameter is increased to 50 microns, the error increases to 55%, and at 500 microns the error has swollen 98%. Figure 5.1 shows the general mass transfer coefficient dependence with particle size.

**Table 5.1.** Comparison of Mass Transfer Coefficients as Determined by Equations 5.8 and 5.9

Particle Diameter (microns)	$k_m = D/r$ (for "small particles") (cm/s)	$k_m = D/d(2.0 + 0.6(dv/v)^{1/2}(v/D)^{1/3})$ (cm/s)
5	0.059	0.062
50	0.0059	0.013
500	0.00059	0.024

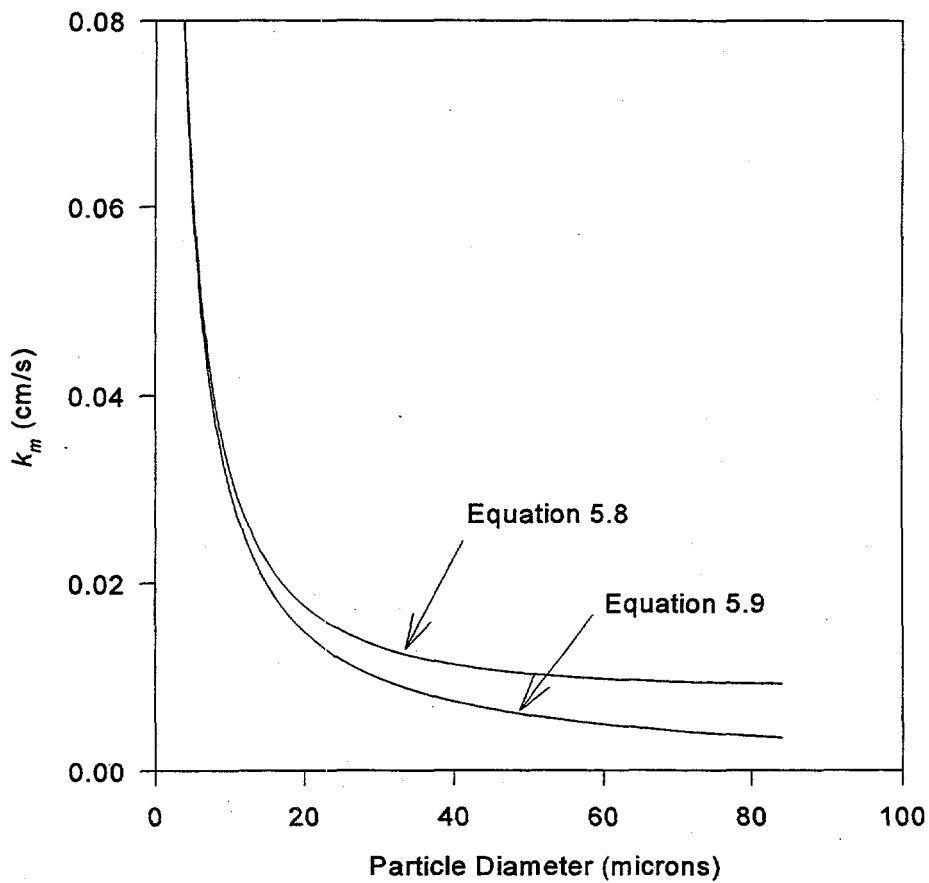


**Figure 5.1.** Mass Transfer Coefficient for a Free-Falling Particle as a Function of Particle Diameter

In summary, the proportionality relationships between the required dissolution times and the particle sizes are:

<u>Proportionality</u>	<u>Rate-Controlling Step</u>	<u>Comments</u>
$t \propto r$	reaction	
$t \propto r^2$	diffusion	small particles
$t \propto r^{3/2}$	diffusion	larger particles

These relationships will be used as a guide in assessing if the dissolution of salts tested are reaction or diffusion controlled.

## 5.2 Experimental Apparatus

Kinetic data were gathered by dropping single salt particles into a 15-cm diameter by 1.2-m high Pyrex glass column and measuring the time required for dissolution. The column was filled with water as a solvent.  $\text{Na}^+$  concentration and pH in the solvent were varied from 0 to 3.75 molar  $\text{Na}^+$  and 7 to 14 pH in accordance with a central composite experimental design. Salt particles were individually measured with a micrometer prior to dissolution. At each condition at least 5 particles were tested with sizes ranging approximately between 200 and 500 microns. An attempt was made to get an even distribution of particles within the range. Reagent grade  $\text{NaCl}$ ,  $\text{NaNO}_2$ , and  $\text{NaNO}_3$  were used in testing. Technical grade anhydrous  $\text{Na}_2\text{CO}_3$  (also known as soda ash, about 99% pure) was also used in testing. The reagent had previously been stored in an open container. Anhydrous sodium carbonate is hygroscopic and on exposure to air will absorb water and increase in molecular weight by ~15%. Density measurement confirmed that the kinetic data were measured on monohydrate sodium carbonate.

## 5.3 Assumptions and Approximations

The shrinking particle model assumes the reacting particle was spherical. While it is unlikely that any particle tested was spherical, the data were treated as such.

The mass transfer coefficient is a function of the particle diameter as shown by the Equation 5.8 curve in Figure 5.1, so as an individual particle dissolves, the mass transfer coefficient changes. For simplicity, an average value was used to interpret the falling-particle dissolution rate data.

## 5.4 Results

The results of the salt crystal dissolution studies are described below.

### 5.4.1 Evaluation of Rate Controlling Step

Evaluating the relationship between the dissolution time and the particle radius provides an indication of whether the reaction is diffusion or reaction controlled. Dissolution time proportional to the particle radius is an indicator that the rate is reaction controlled, while proportionality with  $r^2$  or  $r^{1.5}$  indicates diffusion control. Because of the limited number of particles tested at each condition, this method is susceptible to error. The method employed for determining reaction or diffusion controlled was based on the line fit for  $t$  versus  $r$ , and  $r^{1.5}$  and by comparing the apparent reaction rates. If the squared correlation coefficient,  $R^2$ , for each plot differed by more than 0.1, the best fit line indicated the

rate controlling step. If the goodness of fit from each plot were closer than 0.1, the apparent reaction rates was used to decide. Plots 5.2 through 5.5 provide the results.

Based on the method employed, dissolution of NaCl is generally diffusion controlled, except at low Na concentration. Dissolution of  $\text{Na}_2\text{CO}_3 \cdot 1\text{H}_2\text{O}$  was diffusion controlled at every point tested in the matrix. In contrast, the dissolution of  $\text{NaNO}_3$  and  $\text{NaNO}_2$  are diffusion controlled only at the higher sodium molarities.

#### 5.4.2 Evaluation of Rate Constant and Mass Transfer Coefficient

Figures 5.6 and 5.7 provide a plot of the inverse of the apparent rate constant,  $1/k_0$  as a function of the inverse of the mass transfer driving force,  $1/(C_s - C_b)$ , for NaCl and  $\text{Na}_2\text{CO}_3 \cdot 1\text{H}_2\text{O}$ , respectively. Based on Equation 5.4, the slope of the line is the inverse of the average mass transfer coefficient,  $1/k_m$ , and the intercept is the inverse of the reaction rate constant,  $1/k$ . The concentration of Na in the bulk fluid,  $C_b$ , is known,  $k_0$  is measured, and sodium concentration at the particle surface,  $C_s$ , is assumed to be concentration of the salt at saturation. Because these two salts were generally diffusion limited, this seems to be a reasonable assumption.

This method for determining  $k$  and  $k_m$  does not work for the  $\text{NaNO}_3$  and  $\text{NaNO}_2$  because these salts were generally not diffusion controlled and thus the sodium concentration at the particle surface,  $C_s$ , is unknown when the chemical reaction is rate controlling. Instead, in determining the values of Table 5.2, the apparent rate constant was assumed to be equal to the actual rate constant at low Na concentration ( $k_0 \approx k$ ). This was then used to evaluate the mass transfer coefficient at the highest Na concentrations, where both salts were diffusion controlled, and  $C_s$  is assumed to be equal to  $C_{\text{sat}}$ . It is recognized that if diffusional resistance is significant at the points where  $k$  is evaluated, this method will underpredict the rate constant,  $k$ , and consequently, overpredict  $k_m$ .

Table 5.2 also provides a comparison of the measured and calculated mass transfer coefficient. The calculated mass transfer coefficient is based on Equation 5.8 and the diffusivities provided in Table 5.3. Sodium chloride, sodium nitrate, and sodium nitrate all have similar densities and diffusivities which result in similar calculated mass transfer coefficients. The measured mass transfer coefficients matched well with each other, and were approximately 25% lower than the calculated value. The calculated mass transfer coefficient for  $\text{Na}_2\text{CO}_3 \cdot 1\text{H}_2\text{O}$  was lower than the other salts because of the lower diffusivity and the lower measured terminal velocity in water. The measured and calculated mass transfer coefficients agree within 18%.

**Table 5.2.** Summary of Reaction Rate Constants and Average Mass Transfer Coefficient

Salt	$k$ (mole/cm <sup>2</sup> *s) Measured	$k_m$ (cm/s) Measured	$k_m$ (cm/s) Calculated
NaCl	$7.3 \cdot 10^{-4}$	0.010	0.013
$\text{Na}_2\text{CO}_3 \cdot 1\text{H}_2\text{O}$	$2.1 \cdot 10^{-5}$	0.007	0.008
$\text{NaNO}_2$	$7.3 \cdot 10^{-5}$	0.010	0.013
$\text{NaNO}_3$	$7.5 \cdot 10^{-5}$	0.010	0.013

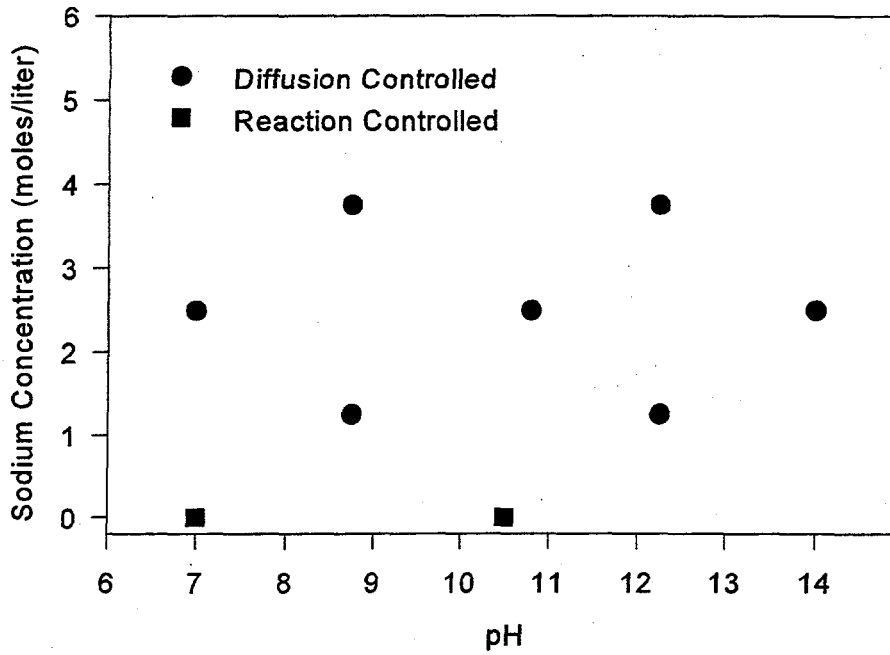


Figure 5.2. Rate Limiting Step Dependence for Dissolution of NaCl

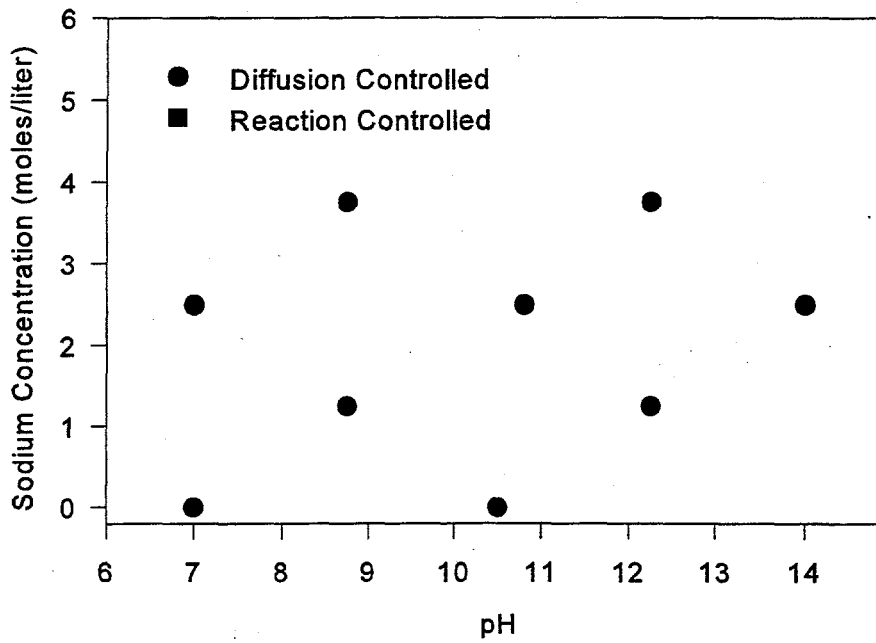


Figure 5.3. Rate Limiting Step Dependence for Dissolution of Na<sub>2</sub>CO<sub>3</sub>·1H<sub>2</sub>O

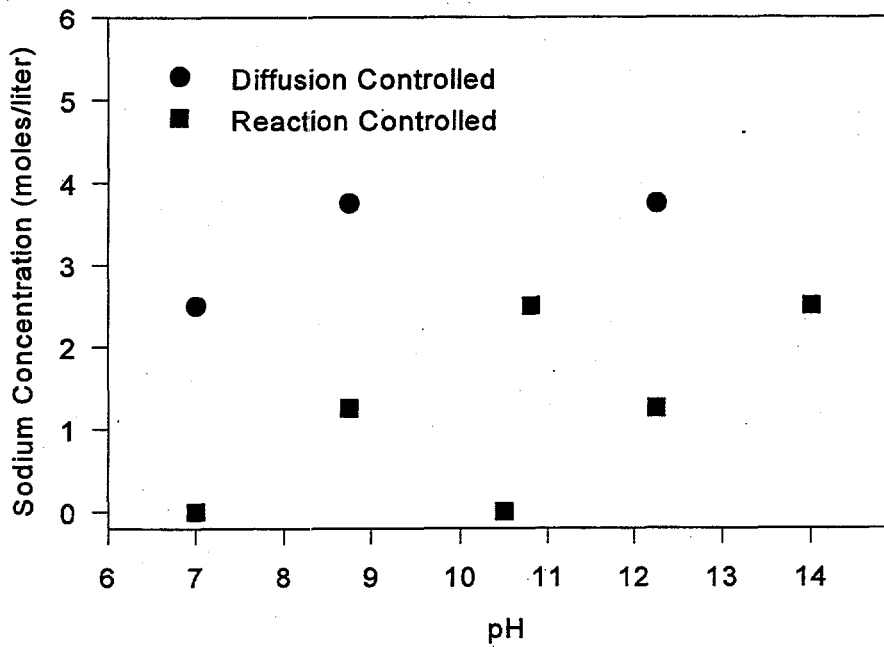


Figure 5.4. Rate Limiting Step Dependence for Dissolution of  $\text{NaNO}_2$

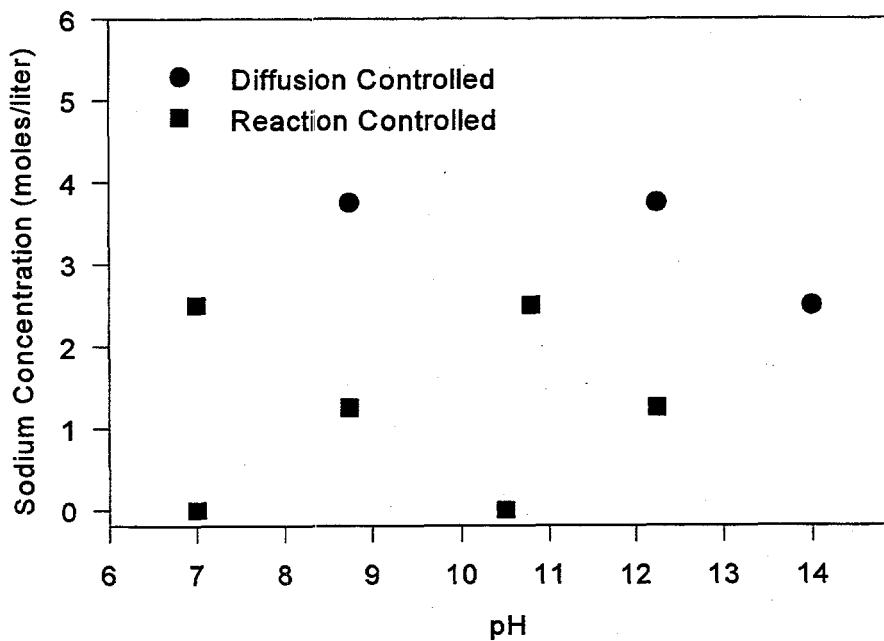
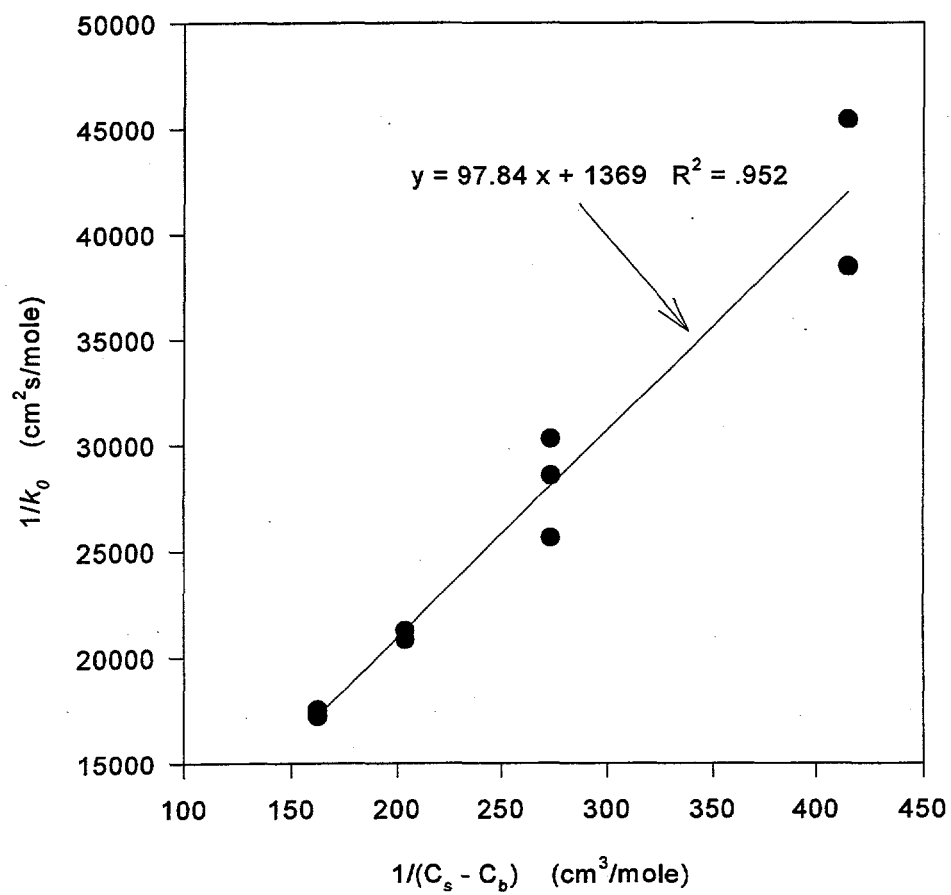


Figure 5.5. Rate Limiting Step Dependence for Dissolution of  $\text{NaNO}_3$



**Figure 5.6.** NaCl Dissolution Rate Data

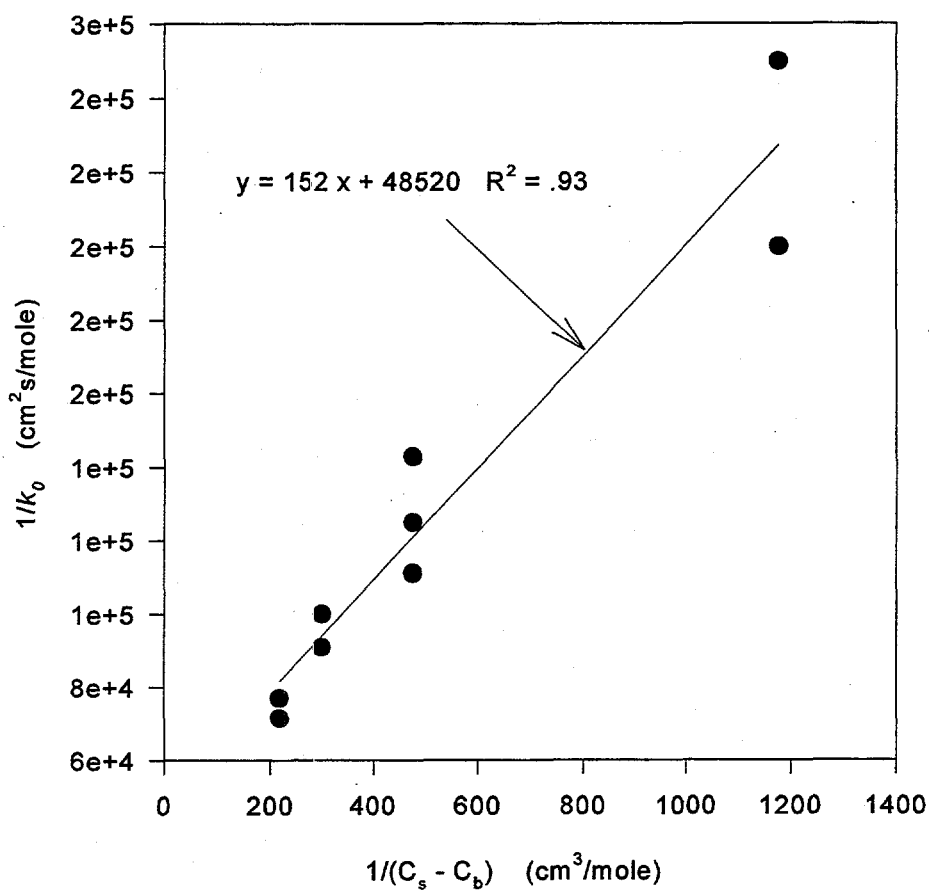


Figure 5.7. Na<sub>2</sub>CO<sub>3</sub>·1H<sub>2</sub>O Dissolution Rate Data

**Table 5.3. Selected Physical Constants**

Salt	Density	Molecular wt.	Solubility (g/100 cm <sup>3</sup> water) @ 20°C	Diffusivity (cm <sup>2</sup> /s) @ 25°C
NaCl	2.165	58.44	36.0	15 e-6
Na <sub>2</sub> CO <sub>3</sub> ·1H <sub>2</sub> O	2.25	124.00	28.8 @ 23°C	7.1 e-6 @ 20.5°C
NaNO <sub>2</sub>	2.168	69.00	84.5	15 e-6**
NaNO <sub>3</sub>	2.261	84.99	88	15 e-6

\*\*The diffusivity of NaNO<sub>2</sub> was not located in the literature, but was assumed to be equivalent to NaNO<sub>3</sub> based on physical and chemical similarities.

### 5.4.3 Least Squares Regression of Data from Central Composite Design

The apparent rate constant  $k_0$  was determined as a function of Na concentration and pH using a surface response model. The model fits the form  $k_0(\text{mole/cm}^2\cdot\text{s}) = \text{intercept} + a[\text{Na}] + b(\text{pH})$ , where  $[\text{Na}]$  is expressed in moles/cm<sup>3</sup>.

The parameters are only good under the falling sphere conditions tested, and between 0 and 3.75 molar Na<sup>+</sup> and pH 7 to 14. Perhaps the most useful information from the regression is that the effect of pH is small and not statistically significant. The goodness of fit is best for those salts which were primarily diffusion controlled in the test matrix (NaCl and Na<sub>2</sub>CO<sub>3</sub>·1H<sub>2</sub>O), as would be expected. Results are provided in Table 5.4.

**Table 5.4. Parameter Estimates for Determining the Apparent Rate Constant**

Salt	Intercept	a	b	Correlation Coefficient, R <sup>2</sup>
NaCl	6.2*10 <sup>-5</sup>	-9*10 <sup>-3</sup>	-4*10 <sup>-7</sup>	0.98
Na <sub>2</sub> CO <sub>3</sub> ·1H <sub>2</sub> O	1.3*10 <sup>-5</sup>	-2*10 <sup>-3</sup>	1*10 <sup>-7</sup>	0.96
NaNO <sub>2</sub>	7.1*10 <sup>-5</sup>	-8*10 <sup>-3</sup>	-4*10 <sup>-8</sup>	0.93
NaNO <sub>3</sub>	6.0*10 <sup>-5</sup>	-8*10 <sup>-3</sup>	8*10 <sup>-7</sup>	0.87

### 5.4.4 Temperature Effects

The effect of temperature on the apparent rate constant was evaluated independently of the effects of Na and pH. When diffusion is important, as has been demonstrated, such effects can lead to a false activation energy, as illustrated in Figure 5.8.

With this caveat in mind, we proceed to evaluate the apparent activation energy and frequency factor which are valid over the temperatures tested. The apparent rate constant is related to the activation energy as follows:

$$k_o = A_o e^{(-E_o/RT)} \quad (5.14)$$

where  $A_o$  is the apparent frequency factor,  $E_o$  is the apparent activation energy, and  $T$  is the temperature in Kelvins. When diffusional effects are unimportant  $k_o \approx Ae^{(-E/RT)}$ , where  $A$  and  $E$  are the actual frequency factor and activation energy, respectively. Figures 5.9, 5.10, and 5.11 provide plots of  $\ln(k_o)$  versus  $1/T$ . The plot for  $\text{NaNO}_2$  and  $\text{NaNO}_3$  indicate that there may be some curvature in the line as would occur when diffusion becomes important. The plot for  $\text{NaCl}$  has no detectible curvature. This result seems to contradict the evaluation of  $k$  and  $k_m$  from Figure 5.6 and Table 5.2, which indicate that diffusional effects are important. The observed slope in Figure 5.9 may be due to an increase in the mass transfer coefficient at higher temperatures. Table 5.5 provides a summary of the results.

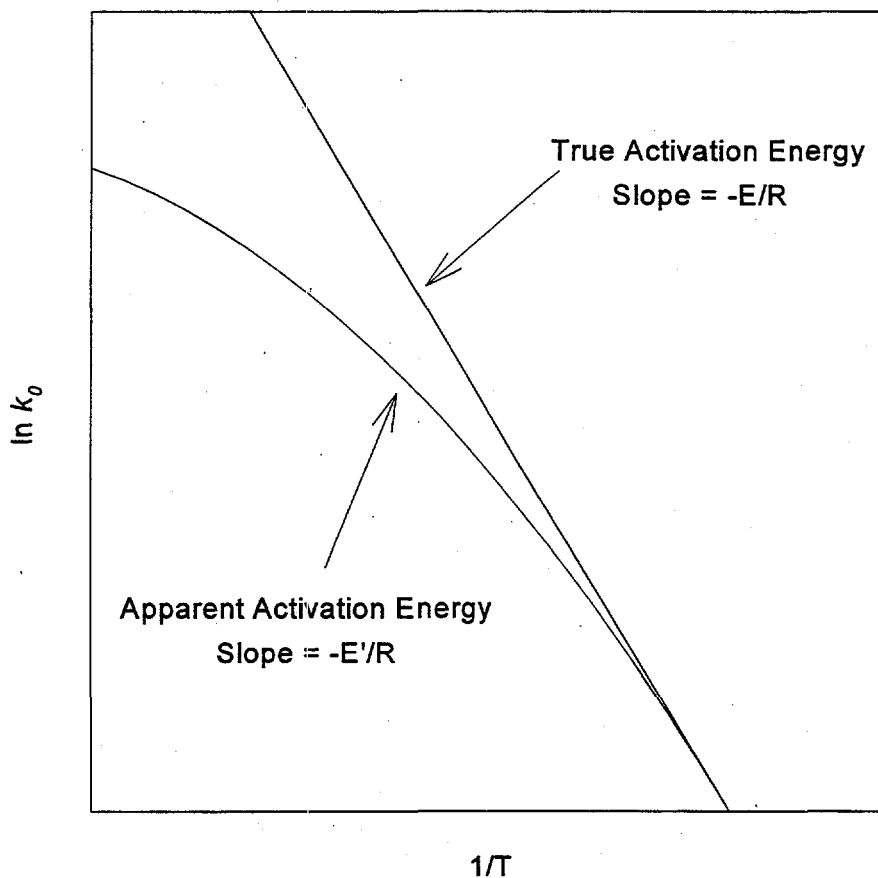


**Figure 5.8.** True and Apparent Activation Energies (Smith 1981)

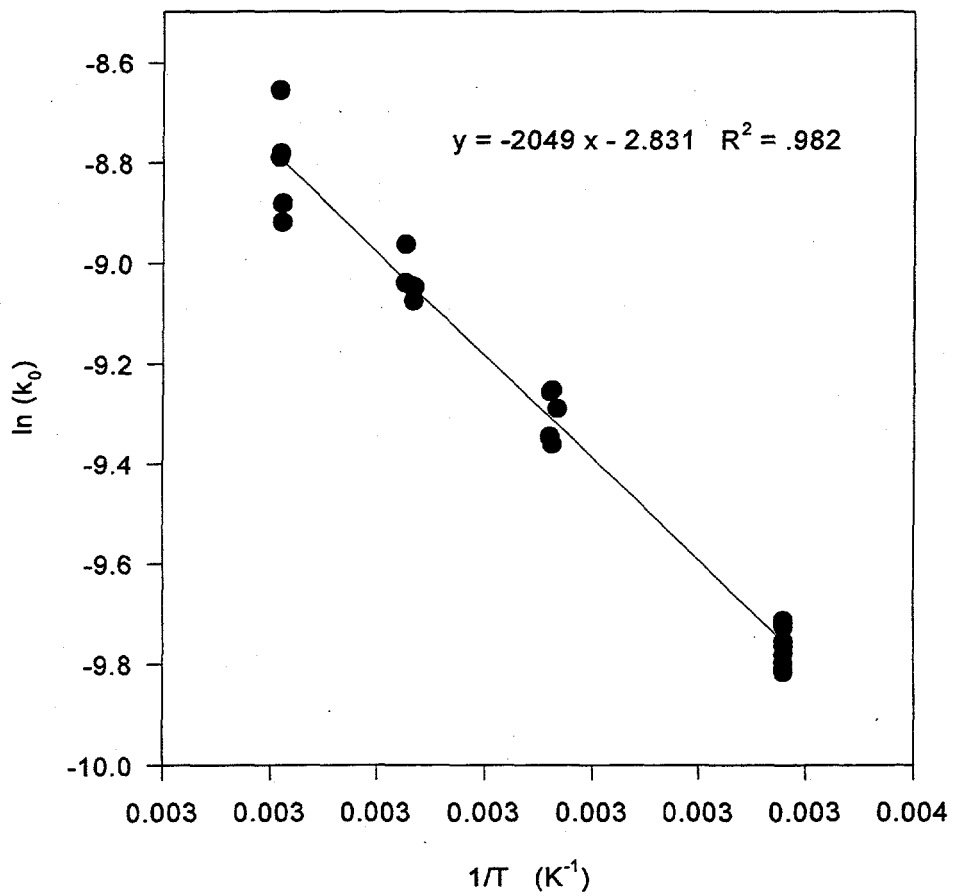


**Figure 5.9.** NaCl Arrhenius Plot

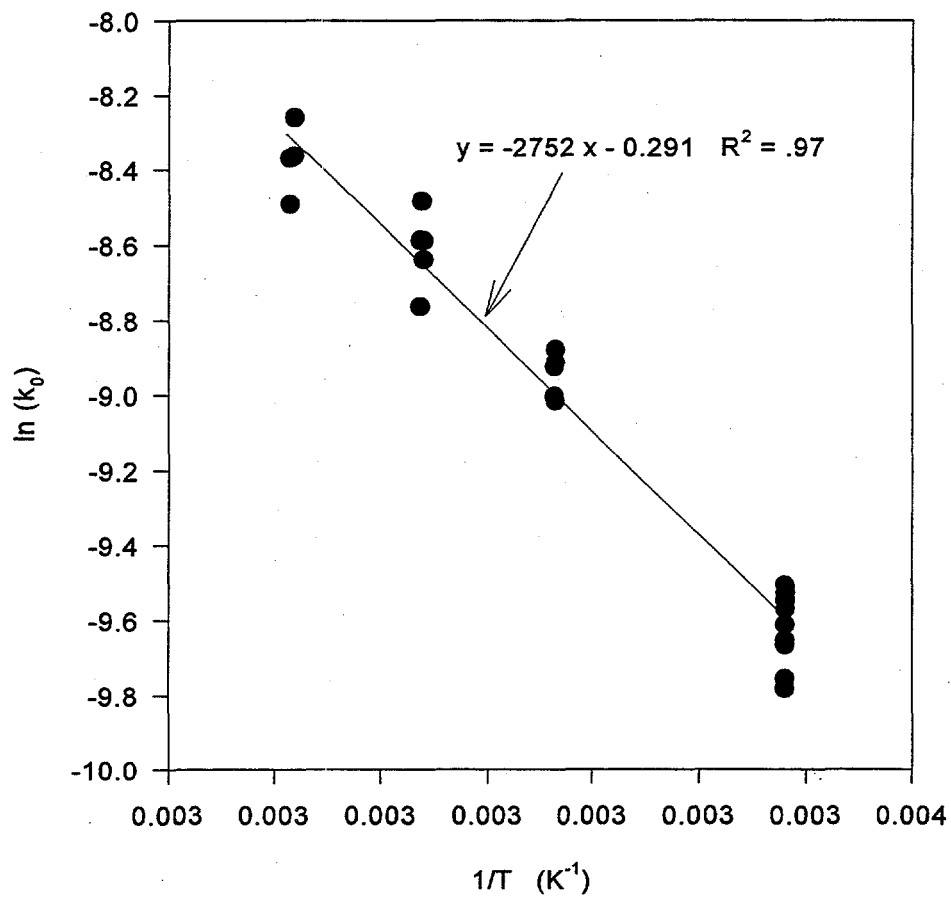


Figure 5.10. NaNO<sub>2</sub> Arrhenius Plot

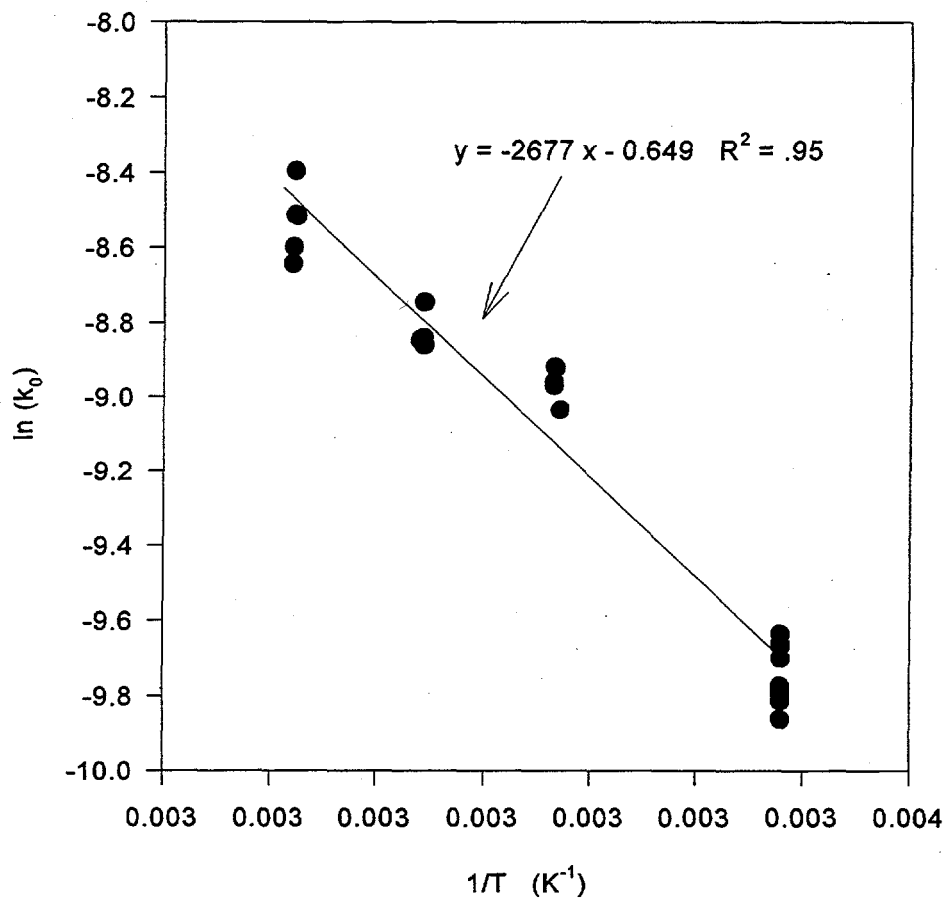


Figure 5.11. NaNO<sub>3</sub> Arrhenius Plot

**Table 5.5. Apparent Activation Energy and Frequency Factors**

Salt	Apparent Frequency Factor, $A_o$ (mole/cm <sup>2</sup> *s)	Apparent Activation Energy, $E_o$ (cal/mole)	Heat of Solution, $\Delta H_{so}$ (cal/mole)
NaCl	0.059	4070	928
NaNO <sub>2</sub>	0.748	5470	3320
NaNO <sub>3</sub>	0.523	5320	4900

Heats of solution are also provided in the table for comparison, since  $E \geq \Delta H$  for endothermic reactions.

### 5.5 Application of Results

The previous sections will help identify under what conditions the dissolution of the considered salts are diffusion or reaction controlled. One may generally use the parameters in Table 5.4 to predict the rate within the test matrix (Na 0-3.75 moles/liter and pH 7-14). The matrix is only good under the falling sphere conditions tested. Outside the matrix or under different mixing conditions one may use the relationship,  $1/k_o = 1/k + 1/k_m [C_s - C_b]$ . The rate constant and mass transfer coefficient, provided in Table 5.2, may be used for conditions outside the test matrix. However, the mass transfer coefficient will have to be evaluated for mixing conditions different from those tested. The rate constant,  $k$ , and the apparent rate (measured) may be used to evaluate  $k_m$  for the conditions of interest, provided  $C_s$  is known.

Temperature dependence can also be accounted for by the equation  $k_o = A_o e^{(-E_o/RT)}$  which is valid under the conditions measured (i.e., a particle falling through water as a solvent with temperature ranging between 20 and 70°C).

It is important to recognize that the mass transfer coefficient can change depending on particle size and fluid flow characteristics. Because of this, these models can best be used to predict relative rates, e.g., rate of dissolution of sodium chloride versus sodium nitrite in similar conditions, rather than absolute rates. Absolute rates can be predicted if the mass transfer coefficient can be estimated. In addition, it is important to note that the sodium concentration in solution was generated by dissolving NaCl in water. The solubility limit of NaCl in water is approximately 6 molar. Extrapolating beyond the test matrix (0 to 3.75 moles Na/liter) may lead to error and is generally not recommended without further testing to verify the models.

The following are examples of how the information can be used.

#### Example 1:

Suppose it is desired to mimic the dissolution time of NaNO<sub>2</sub> using NaCl. From Equation 5.7,

$$t = \rho_{\text{NaNO}_2} r_{\text{NaNO}_2} / k_{\text{NaNO}_2} M_{\text{NaNO}_2} = \rho_{\text{NaCl}} r_{\text{NaCl}} / k_{\text{NaCl}} M_{\text{NaCl}}$$

and substituting physical constants from Table 5.3

$$r_{\text{NaNO}_2}/r_{\text{NaCl}} = 1.18 (k_{\text{NaNO}_2}/k_{\text{NaCl}}).$$

Substituting  $k_0$  for  $k$  and solving for  $k_0$  using parameters from Table 5.2 at pH=7 and  $[\text{Na}] = 0$ , gives

$$r_{\text{NaNO}_2}/r_{\text{NaCl}} = 1.4$$

So to get equal dissolution time, NaCl should have a diameter 70% the size of  $\text{NaNO}_2$ .

As a check on this prediction, approximately 0.1 g of salt was dissolved in 100 g of deionized water. The water was in a beaker and stirred with a stir bar. The diameter ratio using an arithmetic average is 1.5, indicating that the NaCl should dissolve slightly faster than the  $\text{NaNO}_2$ . The results match well with the prediction.

**Table 5.6. Verification of Dissolution Rate Predictions**

Salt	Sieve Range (microns)	Arithmetic Average Size (microns)	Average Dissolution Time (seconds)
$\text{NaNO}_2$	500-589	545	13.0
NaCl	300-425	363	11.9

**Example 2:**

Determine the ratio of dissolution times between  $\text{Na}_2\text{CO}_3 \cdot \text{H}_2\text{O}$  particles in deionized water and  $\text{NaNO}_3$  particles in 5.7 molar  $\text{NaNO}_3$ . It is desired to keep the particle size of the salts equivalent. From Equation 5.7 for  $\text{NaNO}_3$ ,

$$t = \rho r / kM.$$

Using a particle radius of 362 microns and substituting physical constants from Table 5.3

$$t = 9.63 \text{ E-4} * 1/k$$

Since 5.7 molar sodium solution is outside the matrix tested, we use the parameters provided in Table 5.2 to calculate  $k_0$ , which is then substituted for  $k$  in the previous equation.

$$1/k = 1/7.5\text{E-5} + 1/(0.01(0.0105-0.0057))=13,333+20833$$

and  $t = 32.9$  seconds.

For  $\text{Na}_2\text{CO}_3 \cdot \text{H}_2\text{O}$  the same calculation is performed:

$$t = \rho r / kM.$$

and substituting physical constants from Table 5.3

$$t = 6.57 \text{ E-4} * 1/k$$

Substituting  $k_o$  for  $k$  and solving for  $k_o$ , we see we have the choice of using the parameters in Table 5.2 or 5.4 to calculate  $k_o$ .

From Table 5.2,

$$1/k_o = 1/2.1\text{E-5} + 1/(0.007(0.0046-0)) = 78,675$$

From Table 5.4,

$$k_o = 1.3\text{E-5} + 7\text{E-7}, \text{ and } 1/k_o = 72,993$$

$t = 47.9\text{-}51.7$  seconds depending on which value of  $k_o$  used.

The ratio of dissolution times is then,  $t(\text{Na}_2\text{CO}_3 \cdot \text{H}_2\text{O})/t(\text{NaNO}_3) = 1.46\text{-}1.57$ .

Verification:

Approximately 0.1 g of  $\text{Na}_2\text{CO}_3 \cdot \text{H}_2\text{O}$  salt was dissolved in 150 g of room temperature deionized water. The water was in a beaker and stirred with a stir bar. These dissolution rates were compared with dissolving approximately 0.1 g of  $\text{NaNO}_3$  salt in 5.7 molar  $\text{NaNO}_3$  solution at room temperature. The ratio of the average dissolution time was 1.46 which matches the predicted value very well. Note that while the ratio matched well, the predicted dissolution times did not. By varying the rate of stirring the dissolution time can change by a factor of 3 or more. In a case such as this where both salts tested were mass transfer controlled, the mass transfer coefficient must be known to predict actual rates.

**Table 5.7. Verification of Dissolution Time Ratio Prediction**

Salt	Sieve Range (microns)	Average Dissolution Time (Seconds)
$\text{NaNO}_3$	300-425	13.8
$\text{Na}_2\text{CO}_3 \cdot \text{H}_2\text{O}$	300-425	20.2

## 6.0 Conclusions

The methodology used to develop physical tank waste simulants requires a detailed knowledge of the physics involved in the waste retrieval process being tested. Simulants are designed according to which mechanisms and physical properties are expected to be relevant. There is no need to simulate irrelevant properties. Consequently, simulants that are appropriate for testing one process might be inappropriate for another process. The complexity of both the tank wastes and the retrieval processes along with the need to test at large scale using nonhazardous, inexpensive materials present major obstacles to the development of any generally applicable waste simulants.

The simulant development strategy outlined in this report requires commitment and cooperation from both the simulant developers and those who perform waste characterization. Simulant defensibility will improve through an iterative process that involves both process sensitivity testing with simulants and more complete characterization of the relevant waste properties.

The simulant compositions and properties provided in this report can be used to guide future simulant development efforts, but it is inadvisable to use any of the simulants without giving thought to whether the simulant is appropriate.

## 7.0 References

- Aagaard, P. and H. C. Helgeson. 1982. "Thermodynamic and Kinetic Constraints on Reaction Rates Among Minerals and Aqueous Solutions. I. Theoretical Considerations." *American Journal of Science* 282:237-285.
- Bamberger, J. A., D. G. Alberts, C. W. Enderlin, and M. White. 1997. *FY97 Final Report: Borehole Miner - Extendible Nozzle Development for Radioactive Waste Dislodging and Retrieval from Underground Storage Tanks*. PNNL-11730, Pacific Northwest National Laboratory, Richland, Washington.
- Barnes, G. E. 1994. *Waste Dislodging and Conveyance End Effector Development for the INEL HLLW Heel Removal*. INEL-94/0122, Idaho National Engineering Laboratory, Idaho Falls, Idaho.
- Bechtel National, Inc. 1995. *Results of Fall 1994 Sampling of Gunite and Associated Tanks at the Oak Ridge National Laboratory, Oak Ridge, Tennessee*. ORNL/ER/Sub/87-99053/74. Bechtel National, Inc., Oak Ridge, Tennessee.
- Brady, G. S. and H. R. Clauser. 1991. *Materials Handbook*. 13th edition. McGraw-Hill, Inc., New York.
- Carleson, T. E., D. C. Brown, and R. E. Hart. 1987. *Evaluation of the Transport and Resuspension of a Simulated Nuclear Waste Slurry*. PNL-6302, Pacific Northwest Laboratory, Richland, Washington.
- Cussler, E.L. 1984. *Diffusion Mass Transfer in Fluid Systems*. Cambridge University Press, New York.
- Das, B. M. 1983. *Advanced Soil Mechanics*. Hemisphere Publishing Corporation, New York.
- Elmore, M. R., N. G. Colton, and E. O. Jones. 1992. "Development of Simulated Tank Wastes for the U.S. Department of Energy's Underground Storage Tank Integrated Demonstration." SPECTRUM '92 International Topical Meeting on Nuclear and Hazardous Waste Management, Boise, Idaho, August 23 - 27, 1992.
- Fow, C. L., D. McCarthy, and G. T. Thornton. 1986a. *Rheological Evaluation of Simulated Neutralized Current Acid Waste*. PNL-5820, Pacific Northwest Laboratory, Richland, Washington.
- Fow, C. L., D. McCarthy, G. T. Thornton, P. A. Scott, and L. A. Bray. 1986b. *Rheological Evaluation of Simulated Neutralized Current Acid Waste - Transuramics*. PNL-5902, Pacific Northwest Laboratory, Richland, Washington.
- Gauglitz, P. A., S. D. Rassat, M. R. Powell, R. R. Shah, and L. A. Mahoney. 1995. *Gas Bubble Retention and Its Effects on Waste Properties: Retention Mechanisms, Viscosity, and Tensile and Shear Strengths*. PNL-10740, Pacific Northwest Laboratory, Richland, Washington.
- Gibson, R. E. 1953. "Experimental Determination of the True Cohesion and True Angle of Internal Friction in Clays." *Proc. Int. Congr. Soil Mech.*, 3rd., I:126-130.

- Golcar, G. R., J. R. Bontha, J. G. Darab, M. R. Powell, P. A. Smith, and J. Zhang. 1997. *Retrieval Process Development and Enhancements Project Fiscal Year 1995 Simulant Development Technology Task Progress Report*. PNNL-11103, Pacific Northwest National Laboratory, Richland, Washington.
- Hatchell, B. K., J. T. Smalley, and J. C. Tucker. 1996. *Retrieval Process Development and Enhancements Hydraulic Test Bed Integrated Testing Fiscal Year 1995 Technology Development Summary Report*. PNNL-11105, Pacific Northwest National Laboratory, Richland, Washington.
- Hatchell, B. K. 1997 (in press). *Engineering Development of a Lightweight High-Pressure Scarifier for Tank Waste Retrieval*. Pacific Northwest National Laboratory. Richland, Washington.
- Helgeson, H. C., W. M. Murphy, and P. Aagaard. 1984. "Thermodynamic and Kinetic Constraints on Reaction Rates Among Minerals and Aqueous Solutions. II. Rate Constants, Effective Surface Area, and the Hydrolysis of Feldspar." *Geochimica et Cosmochimica Acta*. 48:2405-2432.
- Herting, D. L. 1992. *Laboratory Characterization of Samples Taken in May 1991 from Hanford Waste Tank 241-SY-101*. WHC-SD-WM-DTR-024, Westinghouse Hanford Company, Richland, Washington.
- Hudson, J. D. 1996. *Defining Waste Acceptance Criteria for the Hanford Replacement Cross-Site Transfer System*. PNNL-11146, Pacific Northwest National Laboratory, Richland, Washington.
- Johnson, K. I., M. R. Powell, and O. D. Mullen. 1997 (in press). *Development and Testing of the Cooling Coil Cleaning End Effector*. Pacific Northwest National Laboratory, Richland, Washington.
- Krieg, S. A. 1992. *A Description of the Hanford Single-Shell Tanks and Their Contents*. WHC-SD-TD-TI-001, Rev. 0, Westinghouse Hanford Company, Richland, Washington.
- Kupfer, M. J. 1981. *Preparation of Nonradioactive Substitutes for Radioactive Wastes*. DOE Research and Development Report No. DOE/ET/41900-8 prepared by Rockwell Hanford Operations, Richland, Washington.
- LaFemina, J. P. 1995. *Tank Waste Treatment Science Task Quarterly Report for April - June 1995*. PNL-10764, Pacific Northwest National Laboratory, Richland, Washington.
- Lambe, T. W., and R. V. Whitman. 1969. *Soil Mechanics*. John Wiley and Sons, New York.
- Lea, F. M. 1971. *The Chemistry of Cement and Concrete*. Chemical Publishing Company, Inc., New York.
- Mullen, O. D. 1997. *Engineering Development of Waste Retrieval End Effectors for the Oak Ridge Gunite Waste Tanks*. PNNL-11586, Pacific Northwest National Laboratory, Richland, Washington.
- Nearing, M. A., S. C. Parker, J. M. Bradford, and W. J. Elliot. 1991. "Tensile Strength of Thirty-Three Saturated Repacked Soils." *Soil Sci. Am. J.* 55:1546-1551.
- Powell, M. R., and R. Mahalingam. 1992. "Relationship between Emulsion Drop Size and Solidified Drop (Cell) Size." *Journal of Dispersion Science and Technology* 13(1):13-22.

- Powell, M. R., C. M. Gates, C. R. Hymas, M. A. Sprecher, N. J. Morter. 1995. *Fiscal Year 1994 1/25-Scale Sludge Mobilization Testing*. PNL-10582, Pacific Northwest Laboratory, Richland, Washington.
- Powell, M. R. 1996. *Initial ACTR Retrieval Technology Evaluation Test Material Recommendations*. PNNL-11021, Pacific Northwest National Laboratory, Richland, Washington.
- Powell, M. R., Y. Onishi, and R. Shekarriz. 1997. *Research on Jet Mixing of Settled Sludges in Nuclear Waste Tanks at Hanford and Other DOE Sites: A Historical Perspective*. PNNL-11686, Pacific Northwest National Laboratory, Richland, Washington.
- Reynolds, B. A., E. A. Daymo, J. G. H. Geeting, and J. Zhang. 1996. *Instrument Validation Project*. PNNL-11211, Pacific Northwest National Laboratory, Richland, Washington.
- Rinker, M. W., D. G. Alberts, J. A. Bamberger, B. K. Hatchell, K. I. Johnson, O. D. Mullen, M. R. Powell, and D. A. Summers. 1996. *Tanks Focus Area Retrieval Process Development and Enhancements FY96 Technology Development Summary Report*. PNNL-11349, Pacific Northwest National Laboratory, Richland, Washington.
- Rinker, M. W., D. G. Alberts, J. A. Bamberger, E. A. Daymo, C. W. Enderlin, F. F. Erian, B. K. Hatchell, K. I. Johnson, O. D. Mullen, M. R. Powell, D. A. Summers. 1997. PNNL-11734, Pacific Northwest National Laboratory, Richland, Washington.
- Rodenhizer, D. G. 1987. *Hanford Waste Tank Sluicing History*. Westinghouse Report No. WHC-SD-WM-TI-302, Rev. 0. Westinghouse Hanford Company, Richland, Washington.
- Smith, J.M. 1981. *Chemical Engineering Kinetics*. McGraw-Hill, New York.
- Summers, D. A. 1995. *Waterjetting Technology*. E&FN Spon, an imprint of Chapman & Hall, London.
- Thompson, J. F., A. F. Wellner, and G. D. Thompson. 1993. *Single-Shell Tank Soft Waste Dislodging and Conveying Systems Development Test - Final Report*. WHC-SD-WM-TRP-171, Westinghouse Hanford Company, Richland, Washington.
- van Olphen, H. 1977. *An Introduction to Clay Colloid Chemistry*. John Wiley and Sons, New York.
- Wanner, D. D. 1993. *Justification of Saltcake Simulants*. WHC-SD-WM-TI-545, Rev. 0, Westinghouse Hanford Company, Richland, Washington.
- Weiss, R. L. 1988. *Data Transmittal Package for 241-C-106 Waste Tank Characterization*. SD-RI-TI-205, Rev. 0, Westinghouse Hanford Company, Richland, Washington.
- White, W. A. and E. Pichler. 1959. *Water Sorption Characteristics of Clay Minerals*. Illinois State Geol. Surv., Circ. 266.
- Willingham, C. E. 1994. *Thermophysical Properties of Hanford High-Level Tank Wastes*. PNL-9419, Pacific Northwest Laboratory, Richland, Washington.

Wong, J. J. 1990. *Document for Single Shell Tank Waste Simulant*. WHC-SD-ER-TI-002, Rev. 0.  
Westinghouse Hanford Company, Richland, Washington.

## **Appendix A**

### **Development of a Simulant for SRS Tank 19 Zeolite Heel**

## Appendix A: Development of a Simulant for SRS Tank 19 Zeolite Heel

Development of waste simulants requires a careful evaluation of all available waste characterization data (both quantitative and qualitative) along with a knowledge of which waste properties must be matched and which may be ignored. This often requires that reasoned compromises be made, especially when it is required that the resulting simulant contain only nonhazardous, nonregulated materials. To illustrate the simulant development process, the development of a single simulant is described below.

### A.1 Summary

The available characterization and waste history data for the zeolite heel in Tank 19 were reviewed in an effort to develop a suitable waste simulant. Mechanisms have been identified whereby the zeolite heel strength may have significantly increased since the last waste extraction campaign in 1981. Unfortunately, the extent to which these mechanisms may have occurred cannot be determined from the available data.

Two waste simulants are recommended for sampler and retrieval system testing. The mechanical strength and waterjet resistance of these two simulants are expected to bound that of the Tank 19 solids. The simulants are numbered SRS-KPS-W and SRS-KPS-S. The recommended recipes are

	(SRS-KPS-W) <u>Weak Simulant</u>	(SRS-KPS-S) <u>Strong Simulant</u>
20-50 mesh sand	59.9 wt%	62.6 wt%
kaolin clay	20.1 wt%	14.7 wt%
plaster of Paris	0.0 wt%	6.9 wt%
water	20.0 wt%	15.8 wt%

To prepare these simulants, it is important to mix the ingredients in the proper order. The water and kaolin clay must first be mixed until a uniform slurry is formed. Then the plaster is added while mixing. Once the kaolin/plaster/water slurry is smooth, the sand is added. Care should be taken to minimize the mixing time applied to the simulant after the plaster has been added. The resulting mixture is similar to wet beach sand and must be shoveled or packed by hand into a container for curing. The simulant should be covered while it cures to minimize water loss. Previous testing of plaster-containing waste simulants indicates that the plaster is fully-cured within 24 hours after simulant preparation. Further, the curing reaction proceeds rapidly after 20 to 30 minutes from the time the plaster is mixed with water. It is highly recommended that the simulant be prepared and placed within its curing container in 15 minutes or less. It is permissible to prepare large quantities of this simulant by mixing up several smaller quantities and packing them together.

Characterization data and detailed preparation instructions for each of these simulants are given in the discussion below.

## A.2 Discussion

In July of 1980, a waste retrieval campaign was initiated in Tank 19 at the Savannah River Site. Before retrieval commenced, this tank contained roughly 1058 kgal of salt, 13 kgal of spent zeolite, and 12 kgal of sludge. The principal goal of this retrieval effort was to remove the salt. The sludge and zeolite are to be removed as part of a future campaign.

Water was added to Tank 19 to dissolve the salt. The salt dissolution rate was increased through the use of jet mixer pumps, which mix the waste slurry during salt dissolution. Two mixer pumps were used during this salt retrieval campaign. The salt was removed in four batches. Each salt removal "batch" consisted of adding a quantity of pH-adjusted water to the tank and then mixing the waste for up to several weeks (until the solution became saturated with salt). The resulting salt solution was then pumped from the tank and the next retrieval batch subsequently started. Through the four successive salt extractions, the waste remaining in the tank was reduced to a heel of solids consisting of roughly 13 kgal of solid salt, 13 kgal of zeolite, and 7 kgal of sludge. The final extraction (fourth) was prematurely halted because of mechanical problems with the mixer pumps (broken shaft). The tank supernate was pumped out following the last extraction such that only 55 kgal of salt solution remained. The salt solution remaining in the tank apparently contained 2.3 M nitrate, 0.96 M hydroxide, and <0.1 M nitrite, although this is not clear in the report describing these operations (Goslen 1986).

The remaining heel was photographed and sampled. A "3-liter" sampler was used to take the solid sample. This device grabbed roughly a 3-liter quantity of solids from near the heel surface. The 3-liter sampler did not sample very far down into the bulk of the pile of solids, which is roughly 4 ft high and spanning the tank in an hour-glass shape. Thus, the sample might not be representative of the bulk of the Tank 19 heel (dissolution during the final salt extraction may have removed more salts from near the heel surface than from deep within the heel). The solid sample was separated into water, soluble solids, and insoluble solids. The weight percent water, which was presumably determined by weight loss on drying, was reported to be 19 wt%. The insoluble solids amounted to roughly 56% of the sample mass, and the soluble solids made up the remaining 25%. The insoluble solids were analyzed via an elemental analysis technique. The soluble solids were presumably separated from the insoluble solids by diluting the solid sample with water (dilution factor is not known). The resulting solution was then analyzed to determine the concentrations of various anions and cations. The relevant concentration data are given in Table A.1.

After the solid heel was sampled and photographed, approximately 141 kgal of water was added to the tank to ensure that hydrostatic pressure from groundwater did not cause the tank bottom to buckle upward. This brought the total waste volume to about 230 kgal. After several years it was estimated that the roughly 196 kgal of tank supernate was composed of 193 kgal of water and 3 kgal of dissolved salt. It is not clear how this estimate was made.

The October 1995 Tank Chemistry Report for Tank 19 gives the results of a recent grab sample of tank supernate. Apparently only anion analyses were performed on this sample. The reported concentrations are nitrate = 1.70 M, nitrite = 1.49 M, hydroxide = 0.86 M, sulfate = 0.1 M, and carbonate = 0.56 M. The current tank waste volume is reported to be nearly 280 kgal. Apparently some liquid has been added to this tank since the *Tank 19 Salt Removal* report (Goslen 1986) was prepared (i.e., waste volume has increased by 50 kgal). Further, the nitrite concentration in the supernate has increased from

Table A.1. Tank 19 Residual Solids Data (from DPSP-84-17-7)

Soluble Solids (mols/liter of sample)		Insoluble Solids (wt%)	
NO <sub>3</sub> <sup>-</sup>	1.61	Aluminum	22.9
NO <sub>2</sub> <sup>-</sup>	0.003	Silicon	8.82
OH <sup>-</sup>	0.028	Iron	1.66
SO <sub>4</sub> <sup>2-</sup>	0.90	Manganese	0.32
CO <sub>3</sub> <sup>2-</sup>	not meas.	Mercury	0.067
Ca <sup>2+</sup>	1.1	Unidentified	22.2
Na <sup>+</sup>	0.4		

less than 0.1 M to 1.49 M. It seems likely that approximately 50 kgal of concentrated sodium nitrite solution was added to the waste probably for corrosion control, although no documentation of such an addition has been found.

If no such nitrite solution occurred, then many questions are generated. First, where did the additional waste volume come from? Second, where did the additional nitrite come from? The data in Goslen (1986) show that nitrite was a very low fraction of the total waste volume during all phases of Tank 19 retrieval. Clearly the nitrite did not dissolve out of the waste heel. Several arguments can be made to support this assertion, but they will not be made unless it is determined that nitrite solution was not added to Tank 19 since 1986. It is possible, although highly unlikely, that the nitrite formed by the radiolysis of nitrate anions. Undoubtedly *some* of the nitrite formed this way, but it is thought that this is only a small fraction of the total nitrite now in Tank 19.

The solid sample taken before the ballast water was added was reported to contain some solid nitrate salts (see table above). The exact amount present in the solid heel is uncertain because it is unlikely that the solid sample (taken near the heel surface) was representative of the whole solid heel. Regardless, the assertion that the heel contained significant nitrate is supported by the fact that the current tank supernate contains roughly 247 kgal of 1.70 molar nitrate (equals 1580 kmol nitrate) while the 55 kgal of 2.3 molar nitrate (apparently) that remained in the tank following the fourth extraction contained only 480 kmol of nitrate. Approximately 1580 - 480 = 1100 kmol of nitrate has been removed from the Tank 19 heel and is now present in the supernate. It is not clear how the "gallons of salt" estimates were made by Goslen (1986), but the crystalline volume of 1100 kmol of sodium nitrate is nearly 11 kgal of salt. If the 33 kgal estimate for the heel volume in 1981 was correct, then it is certain that an appreciable amount of solid nitrate salt has dissolved from the Tank 19 heel (unless nitrate has been added to the tank since 1981).

Based on the known high solubility of most nitrate salts, it seems unlikely that significant quantities of solid nitrate remains within the Tank 19 heel. The removal of the nitrate salts from the heel is expected to have decreased the volume fraction solids in the heel from what it was following the fourth waste extraction in 1981. This fact, however, does not imply that the heel has no appreciable remaining mechanical strength with which it can resist impinging waterjets.

To develop a simulant for the Tank 19 waste heel, it will be necessary to estimate the mechanical strength (e.g., shear strength, tensile strength) and dissolution properties of the waste heel. The amount of soluble salt solids remaining in the heel are likely to be small because so much of the salt has apparently already dissolved into the ballast water. Thus, it is appropriate to neglect the dissolution properties of the heel for the purposes of simulant development (this is conservative with respect to waste mobilization rate).

The waste heel may still exhibit some resistance to the impinging waterjet, however. At high pH (like in Tank 19 where pH = 14), zeolite particles may undergo phase change reactions and/or dissolution/precipitation reactions which serve to bind the particles together at their contact points. Similar reactions may take place between sludge particles. One driving force for the bonding together of particles is described by the Kelvin effect of surface curvature on solubility (Hunter 1995). The Kelvin effect, which is also known as Ostwald ripening, increases the solubility in regions of high solid curvature (i.e., the surface of small salt particles or the pointed edges of larger particles) and decreases salt solubility in regions of high liquid surface curvature (i.e., where particles touch). Over time, ions dissolving from low surface curvature regions will migrate and "fill in" the high surface curvature regions. The result is that particles become bound together at their contact points. Another driving force for strength development is the continual dissolution and subsequent precipitation that will occur as the result of temperature cycling (i.e., daily and/or seasonal changes in the waste temperature).

Whether the Kelvin effect can account for appreciable strength development in the Tank 19 heel cannot be determined without considerable effort. Zeolite and sludge solubility rate data at high pH would need to be gathered as part of such an effort. It is not known whether this type of data are available in the literature or if tests would need to be performed. Further, it is not clear whether the surface curvature between the sludge and/or zeolite particles is large enough to produce a significant change in solubility. Typically the Kelvin effect is not significant until the length-scale of the curvature is smaller than about one micron. Regardless, the immediate need for a Tank 19 simulant does not allow a protracted research and development effort. It is conceivable that zeolite and sludge binding at contact points is relatively insignificant in the Tank 19 waste, but this cannot be stated with certainty.

Tests have been conducted with zeolites exposed to moderately high pH (10.9) and high salt concentration (but not saturated) for up to 1 year and no evidence of strength development was reported.<sup>(a)</sup> This implies that the dissolution/precipitation of zeolite solids may be negligible. However, the pH in Tank 19 is higher than that used in the study, and high pH is known to accelerate dissolution and phase changes in zeolites (Sherman 1977). Further, the Tank 19 solids have been exposed to this higher pH for much longer than 1 year (actually about 15 years).

Another possible strength development mechanism for the Tank 19 waste heel is the formation and interconnection of salt crystals. High solubility salts (e.g., sodium nitrate) are thought to have been largely removed from the tank heel via dissolution, so these salts would not increase the heel strength. Low solubility salts, however, may undergo slow dissolution/precipitation reactions that bind particles and salt crystals together. The principal low-solubility salts thought to be present in the Tank 19 heel are

---

(a) Bray, L. A. and L. L. Burger 1986. *Zeolite Storage Behavior Final Report*. WVST 86/58 JRC. Letter report prepared for West Valley Nuclear Services Co., Inc., by Pacific Northwest Laboratory, Richland, Washington.

calcium sulfate and calcium carbonate. Calcium nitrate is unlikely to be present in significant amounts as its solubility is considerably higher than either the carbonate or sulfate. Any calcium cation produced by the dissolution of calcium nitrate will be quickly scavenged by a carbonate<sup>(a)</sup> or sulfate anion to form a low solubility precipitate. The shift to less soluble calcium salts may, over time, tend to bind the solids together into a monolithic mass provided that the amount of calcium present is sufficient to do so.

It is postulated that the insoluble solids of the Tank 19 heel (i.e., sludge and zeolite particles) are bound together by a combination of interstitial calcium salt crystals and bonding at the particle contact points. The extent to which each of these mechanisms operates must be estimated. Unfortunately, sufficient data are not available to defensibly make this assessment. One approach is to assume that all of the strength development in the Tank 19 heel is due to calcium salt dissolution/precipitation.

If it is assumed that the calcium salts are responsible for any zeolite heel strength development, then a *rough* estimate of the zeolite heel strength can be made. The solid sample taken from Tank 19 in 1981 indicated that the calcium concentration in the waste was about 1.1 moles per liter of waste heel. Making assumptions about the packing fraction in the waste heel and the sludge shear strength allows a simulant to be formulated.

First, the zeolite packing fraction in Tank 19 must be estimated. The zeolite solids placed into Tank 19 are reported to have been sized to between 20 and 50 mesh.<sup>(b)</sup> Tests with sand in this size range revealed that loosely packed sand has a void fraction of about 0.45. Vibrating the sand was found to decrease the void fraction to about 0.40. Because the zeolite heel was presumably deposited by the settling of particles during mixer pump operation, the zeolite would be expected to consolidate to somewhere between the loosely and tightly packed void fractions. Based on this, the zeolite void fraction would be expected to lie between 0.4 and 0.45.

However, two factors may have resulted in higher void fractions. First, the interstitial liquid contains micron-sized sludge particles. The sludge particles both increase the apparent viscosity of the interstitial fluid and have the potential to act like a weak glue between adjacent zeolite particles. Both of these effects tend to hamper the settling of zeolite particles into a tightly packed configuration like that expected from zeolite particles settling in water (low viscosity and no sludge particles). The second factor that may have increased the void fraction is the dissolution of interstitial salt. As mentioned above, significant quantities of nitrate salts may have dissolved out of the Tank 19 heel into the supernate since the heel was formed. If this occurred, then the void fraction has increased (the dissolving salt crystals leave only supernate/sludge mixture in their place).

For the purposes of simulant development, the void fraction in the Tank 19 heel is assumed to be about 0.50; that is, the zeolite solids are assumed to occupy roughly 50% of the heel volume. The remaining volume is sludge, salt, and supernate. A void fraction of 0.5 is higher than that expected based solely on sand settling tests (0.4 to 0.45), but it was selected in an effort to account for the effects of

---

(a) Note that carbonate anion is slowly and continuously added to the waste supernate by the dissolution of carbon dioxide from air into the supernate.

(b) Memorandum from J. R. Fowler and R. M. Wallace to M. J. Plodinec dated December 2, 1980. "CRC Zeolite in SRP Waste." DPST-80-488.

dissolving salt crystals and interstitial sludge. There is no clear basis for determining how much higher than 0.4 to 0.45 the void fraction should be assumed to be. The actual void fraction could be higher or lower than 0.5, but this cannot be determined from the data available.

The rheological properties of the sludge are also relevant to simulant development. It is assumed that a sludge/supernate/salt mixture fills the voids between the zeolite particles. The sludge is reported to be composed of micron-sized metal hydroxide particles. The rheological properties of the sludge are strongly dependent on the particle size and shapes as well as on the volume fraction of sludge solids in the mixture. The sludge present within the Tank 19 heel was presumably contained within the dissolved saltcake and was freed when the saltcake was dissolved by the four successive extractions. The sludge solids subsequently settled in the center of the tank along with the zeolite and undissolved saltcake.

The sludge is expected to be relatively unconsolidated because it is exposed to only a small consolidating pressure. Sludge with high shear strength has been found in Hanford tanks with deep sludge layers. The strongest sludge is usually near the tank floor. This is to be expected as the overburden pressure will squeeze interstitial liquid from the sludge thereby resulting in a higher volume fraction of sludge solids. The Tank 19 sludge probably has not been exposed to significant consolidating pressure as the zeolite particles are likely packed tightly enough that the interstitial liquid and sludge do not provide support to the zeolite particles (the zeolite particles rely mostly on other zeolite particles for support).

Metal hydroxide sludge that is relatively unconsolidated will have a low shear strength (interstitial salt crystal and interparticle bonding effects excluded). Kaolin clay, which has a particle size distribution similar to that of some metal hydroxide sludges, will consolidate only to about 45 to 50 wt% (for a layer roughly 1.5-m thick). The shear strength of a 50 wt% kaolin clay (in water) slurry is quite low (less than 100 Pa). Based on this, it is expected that the sludge/supernate mixture occupying the space between zeolite particles in Tank 19 also has a low shear strength - probably akin to that of a  $\leq 50$  wt% kaolin/water mixture.

For the purposes of developing a Tank 19 zeolite heel simulant, it will be assumed that a 50 wt% kaolin/water slurry is representative of the sludge. Based on the observed settling and consolidation behavior of kaolin clay, this is probably a reasonable assumption. It is unlikely that the sludge in Tank 19 would have consolidated to a shear strength considerably higher than 100 Pa. Further, the shear strength of the sludge is of only minor importance in terms of the bulk strength of the Tank 19 zeolite simulant, which is determined largely by the curing of plaster of Paris as described below.

Goslen (1986) gives the calcium ion concentration in the Tank 19 heel solids as 1.1 moles per liter of sludge. As described earlier, it is possible that the low-solubility calcium salts (chiefly sulfate and carbonate) have undergone dissolution and reprecipitation reactions to form salt crystals that now bind the zeolite particles together. A conservative approach is to assume that all of the calcium sulfate present in the waste heel undergoes such reactions. This is the approach that will be used to select the calcium sulfate concentration in the Tank 19 zeolite heel simulant.

The total calcium ion concentration in the heel sample taken in 1981 was 1.1 moles calcium per liter of sample. The sulfate ion concentration was reported to be 0.90 moles per liter of sample.

Therefore, it is expected that the heel sample contained about 0.90 moles per liter of  $\text{CaSO}_4 \cdot 2\text{H}_2\text{O}$  and about 0.2 moles per liter of some other calcium salt, which was probably carbonate.<sup>(a)</sup>

To simulate the presence of the calcium salt crystals, DAP Durabond™ Plaster of Paris has been selected. According to DAP representatives, this product is roughly 80 wt% calcium sulfate hemihydrate ( $2\text{CaSO}_4 \cdot \text{H}_2\text{O}$ ) and 20 wt% calcium carbonate. This is very near the estimated ratio of calcium sulfate to calcium carbonate expected in Tank 19 based on the heel sample taken in 1981. The plaster of Paris will undergo a hydration reaction and bind the insoluble kaolin and sand particles together. This reaction is expected to proceed to completion within about 24 hours. It is expected that the strength development provided by the curing plaster will be as great or greater than that expected in the Tank 19 heel (provided that the heel has a total calcium concentration of about 1.1 moles/liter of heel).

The Tank 19 simulant contains enough plaster of Paris in it so that the concentration of calcium ion is about 1.1 moles per liter of simulant. Whether the actual average calcium ion concentration in the Tank 19 heel is about 1.1 moles/liter is not known. This is dependent upon whether the sample taken in 1981 was representative of the whole. Since the sample was taken near the heel surface, it is possible that some of the calcium salts may have been leached away during the final extraction. This would imply that the actual average concentration may be higher than 1.1 moles per liter of waste. It cannot be determined whether this is the case based on the data available.

A simulant recipe can be generated based on the assumptions listed above, which are: 1) the zeolite solids occupy 50% of the heel volume, 2) the sludge present between the zeolite particles is rheologically similar to a 50 wt% kaolin/water slurry, 3) the total calcium concentration is about 1.1 moles per liter of simulant with about 80 wt% of the calcium salts being sulfate, and 4) the calcium salts in Tank 19 have undergone dissolution/precipitation reactions that resulted in some bulk strength development and this strength development is similar to that obtained from the curing of plaster of Paris (at 1.1 moles calcium per liter of simulant).

To simulate the zeolite particles, ideally 20 to 50 mesh Linde AW-500 zeolite particles would be used. This material is relatively expensive, however, so an alternative has been selected. Coarse sand between 20 and 50 mesh will be used to simulate the zeolite particles. The sand particles have a higher density than the zeolite particles, but this is unlikely to be significant with respect to bulk simulant strength,<sup>(b)</sup> which is relevant to both the simulant's waterjet resistance and to the efficacy of a mud-snapper waste sampling device. The sand particles being used for scoping tests have a particle density of  $2.65 \text{ g/cm}^3$ . The density of wet zeolite particles is approximately  $1.7 \text{ g/cm}^3$  (based on a measurement of Linde AW-500 zeolite). The skeleton density of zeolite is higher, but it is the particle density that is relevant here.

---

(a) If the sulfate ion in the heel sample was actually associated with some other, more soluble cation (e.g., sodium), the calcium nitrate present would be expected to react with the sodium sulfate to produce dissolved sodium nitrate and calcium sulfate precipitate. Similarly, the calcium cations will be scavenged by carbonate anions from either the sulfate or nitrate calcium salts because of the low solubility of calcium carbonate.

(b) Note that tests to evaluate the retrieval rate of this simulant need to address the higher settling rate of the sand compared to zeolite.

Employing the four simulant recipe assumptions listed above, a set of equations can be developed describing the fraction of water, kaolin clay, sand, and plaster of Paris needed. These equations are

$$W_s = (\phi_z) \left( \frac{2.65}{\rho} \right)$$

$$W_p = \frac{(0.133 \text{ kg/mol})(C_p)}{\rho}$$

$$W_k = W_w - \frac{22}{145} \left( \frac{(0.133 \text{ kg/mol})(C_p)}{\rho} \right)$$

$$W_w = 0.5 \left[ 1 - \frac{2.65\phi_z}{\rho} - \frac{124}{145} \left( \frac{(0.133 \text{ kg/mol})C_p}{\rho} \right) \right]$$

$$\rho = \left( \frac{\phi}{\rho} + \left[ W_w - 0.149 \left( \frac{0.133C_p}{\rho} \right) \right] \left( 1 + \frac{1}{2.65} \right) + \frac{1.16}{2.40} \left( \frac{0.133C_p}{\rho} \right) \right)^{-1}$$

where  $W_s$ ,  $W_p$ ,  $W_k$ , and  $W_w$  are the weight fractions of sand, plaster of Paris, kaolin clay, and water, respectively. The volume fraction sand is  $\phi_z$  (which is estimated to be 0.50), the total calcium ion concentration is  $C_p$  moles calcium per liter of simulant, and  $\rho$  is bulk density of the simulant.

Solving these equations simultaneously while employing  $\phi_z = 0.5$  and  $C_p = 1.1$  moles/liter yields a Tank 19 zeolite heel simulant recipe of 62.6 wt% sand, 14.7 wt% kaolin clay, 6.9 wt% plaster of Paris, and 15.8 wt% water. Once cured, this simulant recipe is expected to yield a material with a mechanical strength equal to or greater than that of the Tank 19 heel (provided that the heel calcium concentration is not appreciably higher than 1.1 moles per liter of waste). The equations above are solved for several different assumed zeolite volume fractions and calcium concentrations. The results are presented in Table A.2.

Simulant recipes for various plaster concentrations at both 0.5 and 0.45 sand volume fractions are shown. As detailed above, it is expected that the zeolite volume fraction is approximately 0.5 in the tank, but it may be as low as 0.45 or lower. Similarly, the calcium concentration in the tank was measured at 1.1 moles per liter of waste heel, but sampling errors may have biased this measurement either low or high. Finally, it is plausible that the calcium salts in the Tank 19 heel have not undergone the dissolution/precipitation reactions to the full possible extent as is implicitly assumed by the use of

Table A.2. Tank 19 Zeolite Simulant Recipes

$\phi_z$	$C_p$ (mole/l)	Sand (wt %)	Kaolin (wt %)	Plaster (wt %)	Water (wt %)	Density (g/cm <sup>3</sup> )
0.5	0	64.6	17.7	0.0	17.7	2.051
0.5	0.55	63.6	16.2	3.5	16.7	2.084
0.5	1.1	62.6	14.7	6.9	15.8	2.116
0.5	2	61.1	12.4	12.3	14.3	2.170
0.45	0	59.9	20.05	0.0	20.05	1.991
0.45	0.55	58.9	18.5	3.6	19.0	2.024
0.45	1.1	58.0	16.9	7.1	18.0	2.056
0.45	2	56.5	14.5	12.6	16.4	2.110

plaster of Paris as a calcium salt simulant. If this is the case, then it may be appropriate to use a smaller amount of plaster of Paris in the simulant. Unfortunately, whether this is the case cannot be determined without testing a relatively undisturbed sample of the Tank 19 heel.

To prepare these simulants, it is important to mix the ingredients in the proper order. The water and kaolin clay must first be mixed until a uniform slurry is formed. Then the plaster is added while mixing. Once the kaolin/plaster/water slurry is smooth, the sand is added. Care should be taken to minimize the mixing time applied to the simulant after the plaster has been added. The resulting mixture is similar to wet beach sand and must be shoveled or packed by hand into a container for curing. The simulant should be covered while it cures to minimize water loss. Previous testing of plaster-containing waste simulants indicates that the plaster is fully-cured within 24 hours after simulant preparation. Further, the curing reaction proceeds rapidly after 20 to 30 minutes from the time the plaster is mixed with water. It is highly recommended that the simulant be prepared and placed within its curing container in 15 minutes or less. It is permissible to prepare large quantities of this simulant by mixing up several smaller quantities and packing them together.

The performance of the Savannah River Site "mud-snapper" was evaluated using three simulants.<sup>(a)</sup> These simulants are given in the table above as  $\phi_z = 0.5, C_p = 1.1$ ;  $\phi_z = 0.5, C_p = 2$ ;  $\phi_z = 0.45, C_p = 0.0$ . The mechanical strengths of the  $\phi_z = 0.5, C_p = 2$  and  $\phi_z = 0.45, C_p = 0.0$  simulants are expected to bracket the strength of the waste in Tank 19. The intermediate strength simulant ( $C_p = 1.1$ ) might be considered a "representative" simulant as it is based on the measured calcium ion concentration. However there is just too much uncertainty in the extent to which reactions may have bonded the Tank 19 heel into a solid to assess whether any simulant is "representative."

---

(a) The "mud snapper" is a spring-loaded sampling device. Its jaws open and close like those of a clam.

Shear strength measurements on these three simulant recipes were made. The strongest simulant ( $\phi_z = 0.5$ ,  $C_p = 2$ ) has a shear strength in excess of 92 kPa (13 psi), which is the upper measurement limit of our shear vane. The shear strength of the  $\phi_z = 0.5$ ,  $C_p = 1.1$  simulant was found to be  $39 \pm 7$  kPa (5.6 psi). The shear strength of the weakest simulant,  $\phi_z = 0.45$ ,  $C_p = 0.0$ , was measured at  $1.2 \pm 0.1$  kPa (0.17 psi).

The mud-snapper sludge sampler was used to sample each of the three simulants. The spring tension was adjusted such that about 3.4 in. of the spring was visible when the mud-snapper was closed. The sampler was dropped into each simulant from a height of 1 foot (in air). The amount of material recovered by the sampler was observed.

The sampler recovered very little of the hardest simulant. Recovery was on the order of 5 to 10 g of solids. From the medium-strength simulant the sampler recovered approximately 50 to 80 g of solids (roughly the size of a golf ball). The sampler recovered a full-load of the weakest simulant. In fact, the amount captured exceeded the sampler volume by about 20% (the sampler did not fully close because the close packing of the relatively large sand particles prevented the sampler from closing completely).

### A.3 References

Goslen, A. O. 1986. *Tank 19 Salt Removal*. DPSP-84-17-7, Savannah River Laboratory, Aiken, South Carolina.

Hunter, R. J. 1995. *Foundations of Colloid Science: Volume I*. Clarendon Press, London. p. 98.

Sherman, J. D. 1977. "Ion Exchange Separations with Molecular Sieve Zeolites." Presented at the 83rd National Meeting of the American Institute of Chemical Engineers, Houston, Texas. March 20-24, 1977. Union Carbide Corporation, New York.

## Distribution

**No. of  
Copies**

**Offsite**

2 DOE/Office of Scientific and  
Technical Information

**Onsite**

3 **DOE Richland Operations Office**

M. J. Glasper, K8-50  
B. M. Mauss, K8-50  
J. A. Frey, K8-50

2 **Numatec Hanford**

P. D. Gibbons, H6-12  
L. B. McDaniel, H6-12

40 **Pacific Northwest National Laboratory**

K. M. Airhart, K5-22 (10)  
J. A. Bamberger, K7-15  
W. F. Bonner, K9-14  
T. M. Brouns, K9-04  
J. L. Buelt, P7-41  
E. A. Daymo, P7-43  
C. W. Enderlin, K7-15  
F. F. Erian, K7-15  
J. G. H. Geeting, P7-28  
G. R. Golcar, P7-43 (3)  
B. K. Hatchell, K5-26  
K. I. Johnson, K5-26  
O. D. Mullen, K5-26  
M. R. Powell, P7-43 (8)  
M. W. Rinker, K5-22  
P. A. Scott, K9-46  
J. A. Yount, K5-26  
Technical Report Files (5)